68-15,935

KENT, Gerald I., 1941-

THEORETICAL AND EXPERIMENTAL INVESTIGATION OF PLASMA FLUTE MODES IN A NON-UNIFORM ELECTRIC FIELD.

The City University of New York, Ph.D., 1968
Engineering Mechanics

University Microfilms, Inc., Ann Arbor, Michigan

THEORETICAL AND EXPERIMENTAL INVESTIGATION OF PLASMA FLUTE MODES IN A NON-UNIFORM ELECTRIC FIELD

by

GERALD I. KENT

A dissertation submitted to the Graduate Faculty in Engineering in partial fulfillment of the requirements for the degree of Doctor of Philosophy, The City University of New York.

1968

This manuscript has been read and accepted for the University Committee in Engineering in satisfaction of the dissertation requirement for the degree of Doctor of Philosophy.

May 10, 1968
date

Chairman of Examining Committee

May 13 1968
date

Executive Officer

Prof. M. Ettenberg

Prof. H. E. Hart

Prof. M. L. Pei

Prof. J. R. Steven

Prof. N. C. Jen, Chairman
Supervisory Committee

The City University of New York

ACKNOWLEDGMENTS

For his guidance, effort, and encouragement during the research and writing of this thesis I am deeply indebted to my mentor Professor Norman C. Jen.

The guidance of Professor Francis F. Chen, Visiting Professor, throughout the work is also gratefully acknowledged. Several useful discussions with the members of my Doctoral Committee, Professors M. Ettenberg, H. Hart, M. L. Pei, and J. R. Steven have been most helpful. The comments of Dr. H. W. Hendel (Princeton Plasma Physics Laboratory) on the first draft are appreciated.

I would like to thank both the City University and the United States Air Force Office of Scientific Research for the financial support given to me personally and to the Magnetohydrodynamics Laboratory of The City College without which this work could not have been done. The financial aid and services provided by The City College and the Department of Civil Engineering are gratefully acknowledged.

TABLE OF CONTENTS

LIST OF FIGURES

NOMENCLATURE

B	magnetic field
C	integration constant
D	integration constant
e	charge of the electron
E	electric field
F	surface of discontinuity
g	effective gravitational acceleration
i	imaginary unit = $(-1)^{\frac{1}{2}}$
k	wave number
m	azimuthal mode number
n	number density
r	radial position coordinate
t	time
T	$= r^3 \overline{\omega} (\rho \overline{\omega} + \frac{\gamma}{r} \rho')$
v_{th}	thermal speed of ions
V_o	zero order drift velocity
x	cartesian coordinate
y	cartesian coordinate
z	cartesian coordinate

α normalized density

β particle pressure to magnetic pressure ratio

γ $= \frac{m}{2} \frac{v_{th}^2}{\Omega}$

δ relative thickness of region 2 in 3 region theory

Δ difference operator

ϵ small value of r

θ azimuth angle coordinate

ρ mass density

ϕ potential

ψ eigenfunction

ω frequency

Ω cyclotron frequency of ions

ABSTRACT

The flute mode in a plasma with non-uniform electric fields is studied experimentally and theoretically. Experiments were performed with low-beta alkali metal plasmas produced in a Q-machine. The flutes propagate azimuthally and have maximum amplitude near the plasma column edge where a large radial electric field, E_r, exists. The $E_r \times B$ drift velocity produces an instability similar to the Kelvin-Helmholtz instability. A solution to a differential equation including finite Larmor radius effects, formulated by Rosenbluth and Simon, is presented. Consideration of adjacent regions undergoing rigid body rotations and having constant density leads to an expression for the oscillation frequencies and a stability criterion.

Theoretical results show that velocity shear is the mechanism which drives the instability, but centrifugal effects are also destabilizing. Finite Larmor terms stabilize short wavelengths as for the gravitational flute instability.

If the experiment is interpreted in light of the present theory, the oscillation frequencies, stability conditions and radial amplitude distributions compare favorably.

CHAPTER 1

INTRODUCTION

In the field of controlled fusion research, one of the major problems is understanding the flute mode in a non-uniform electric field. The flute mode is characterized by low frequency propagation around the plasma column with no propagation along the magnetic field. Until now, the lack of a theoretical solution to this problem has made it difficult to interprete experiments and as a result, this instability has not been well understood.

Recently, a theory has been formulated by Rosenbluth and Simon,[1] but the differential equation found was not solved. In the present work, a model based on measurements in a Q-machine is used to find a solution to the differential equation. This solution is then used as a guide to perform a complete experiment which leads to an understanding of flute mode in a non-uniform electric field.

In previous works[2-9] low frequency oscillations in Q-machines have been described. In some of these experiments[8,9] the maximum relative amplitude of the wave occurred where large radial electric fields have been measured. In a Q-machine the change of sheath conditions between the hot plate and the relatively cool aperture limiter produces radial electric fields and the instabilities which

form in this region have been called edge oscillations.[10] In other experiments[2-7] the oscillations have been identified as drift waves and will not be considered here. Both the theoretical and experimental work pertinent to the problem of the flute mode in a non-uniform electric field is reviewed below.

1.1 Review of Experimental Work

Two experiments in which the electric field could be varied have been reported. Hartman and Munger[8] varied the electric field by introducing a temperature gradient on the ionizer plate. With the temperature highest at the center of the plate, coherent oscillations were observed with azimuthal mode $m=2$ being the lowest mode observed. As the magnetic field was increased, higher modes became dominant. The wave amplitude peaked at the edge of the column. A standing wave was observed in the longitudinal direction. The authors found that the shear in the $E_r \times B$ velocity is essential for the excitation of the observed wave.

The second experiment (without theory) where electric fields could be varied has been carried out recently by Enriques, Levine and Righetti.[9] The ionizer plate was formed from a disk and a separated annulus: A potential difference could be applied between both sections producing a non-uniform electric field. With this configuration an edge oscillation was observed, which destabilized for radial electric

fields above a threshold value. From the experiment, the authors conclude that the non-uniformity in the electric field is important in exciting the wave which is the same conclusion reached by Hartman and Munger.[8]

It will be shown in Chapter 4 that shear in the drift velocity is predicted to lead to low frequency oscillations of the type observed in Q-machines near the edge of the plasma column. Since the experimental work done here has shown that the observed oscillation is a flute mode, the pertinent theory will be reviewed below.

1.2 Review of Theoretical Work

The theory of the flute instability has been derived from the two-fluid magnetohydrodynamic equations by Kadomtsev[11] for the case when the instability is driven by an effective gravitational force field. The analysis showed the differential drifts between ions and electrons responsible for exciting the instability. The difference in drifts is caused by the mass difference of the two species. Results showed that for the gravitational force in the direction of decreasing density the plasma is unstable. It becomes apparent that any affect which influenced the particle drifts would affect stability of the plasma. The inclusion of finite Larmor radius (FLR) phenomena was shown to affect stability.[12]

Rosenbluth et al,[12] starting with the equations of kinetic theory and taking FLR effects into account, showed that the flute instability could be stabilized for sufficiently short wavelengths. In this analysis it was assumed that the Larmor radius was small compared with the characteristic radial length of the system. Mikhailovskii[13] included all values of Larmor radius, the results differing only slightly from the previous work. The case for mode one is different than that for the higher modes. Mode one corresponds to a displacement of the plasma as a whole producing a perturbed electric field which is uniform in space. This means that FLR effects are not important here. It has been shown[14] that the flute azimuthal mode $m=1$ is always unstable.

The above results can also be derived from the so called guiding center approximation.[15] In this method the zero and first order particle drifts are written down from physical considerations and then these are used in the equations of continuity to find the perturbed densities. The perturbed densities can then be substituted into Poisson's equation to yield the instability frequencies and the stability criterion. Here the FLR effects are taken into account explicitly by using the averaged electric field which a particle experiences in a gyration and by relating the guiding center density to the particle density.

Until recently, the work on flute modes assumed that no zero order electric fields existed. However, inclusion of non-uniform electric fields is important since these fields usually exist in experimental

systems. The analysis for a flute mode in a non-uniform electric field has been carried out by Rosenbluth and Simon.[1] Their work used the Vlasov equation as a starting point to develop a set of hydrodynamic equations which includes both FLR and non-uniform electric field effects. From the resulting set of equations an eigenvalue problem for stability is formulated, but no solution has been reported. The same problem has been formulated from the guiding center approximation by Stringer and Schmidt,[16] resulting in the differential equation given in Ref. 14.

1.3 Summary

The purpose of this thesis is to understand the flute mode which appears as edge oscillations observed in Q-machines. This is accomplished by carrying out a complete set of experiments in a Q-machine which have been guided by the solution of the Rosenbluth and Simon equation describing a flute mode in a non-uniform electric field.

In this chapter the experimental work on edge oscillations in a Q-machine has been reviewed along with the theory relevant to flute modes.

Chapter 2 contains a description of the experimental apparatus. In Chapter 4 the eigenvalue problem formulated in Ref. 1 will be solved for conditions found in Q-machines. A comparison of the experiment with the theory appears in Chapter 5. The conclusions of this dissertation are summarized at the end of Chapter 5.

CHAPTER 2

EXPERIMENTAL APPARATUS

Since the introduction of Q-machines[17] in 1960 a number of these devices have been built and operated both in this country and abroad.[2-9] The Q-machine has the advantage of producing a steady, relatively quiescent, fully ionized plasma as opposed to older methods such as steady or pulsed discharges producing partially ionized gases. A great part of the Q-machine and its auxiliary equipment at the MHD Laboratory at The City College has been designed and constructed by the author over the past few years. The Q-machine is the main apparatus in the Laboratory and may be used for a number of different types of experiments in plasma physics including studies of oscillations, confinement, ionization and plasma turbulence. Since a good deal of effort was devoted to the actual construction of the apparatus, a detailed description is given.

2.1 General Description of the Q-machine

In a Q-machine an electron gun is used to heat a plate onto which an alkali metal vapor is sprayed. The metal vapor is ionized by surface ionization on the hot plate ($T \simeq 2300^{o}K$), which also supplies electrons by thermionic emission. The resulting plasma is confined by a uniform magnetic field perpendicular to the surface of the ionizer

plate. Making the field perpendicular to the hot plate as done here has the advantage of reducing temperature gradients on the plate and making the column into a right circular cylinder. The electron gun and the plasma column are contained in a vacuum chamber whose walls are water-colled to keep the background of neutrals at a low level (10^{-6} torr.). The machine may be operated double-ended (hot plate at each end) in which case a stationary plasma is produced or single-ended (one plate replaced by a cold collector) thus producing a plasma which drifts from the hot plate with the ion thermal speed. In Fig.2-1, the external structure of the Q-machine is shown. The vacuum chamber can be seen at both ends of the ten water-colled solenoids which provide the magnetic field. In the background, the power supplies for the electron gun are shown. Figure 2-2 is a schematic of the Q-machine showing single-ended operation.

2.2 Elements of the Q-machine

1. Electron Gun

(a) Construction: The purpose of the electron gun is to heat the ionizer plate to sufficiently high temperatures to ionize the potassium vapor and at the same time produce neutralizing electrons by thermionic emission. The gun is constructed similar to a vacuum tube diode in that its elements are a filament type emitter biased negative with respect to the plate. The circuit is shown in Fig.2-3. The major

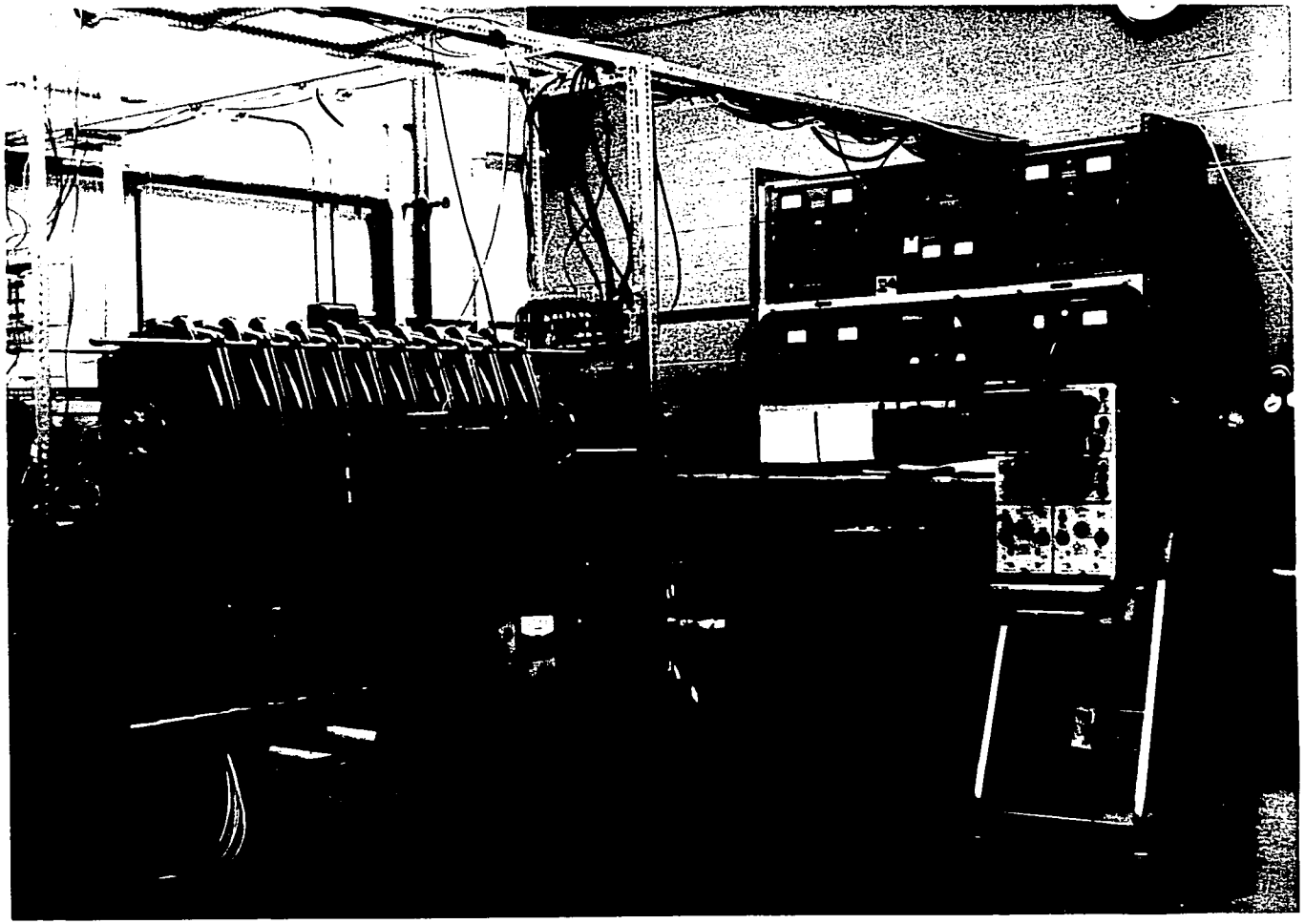

Fig. 2-1 Photograph of Q-machine

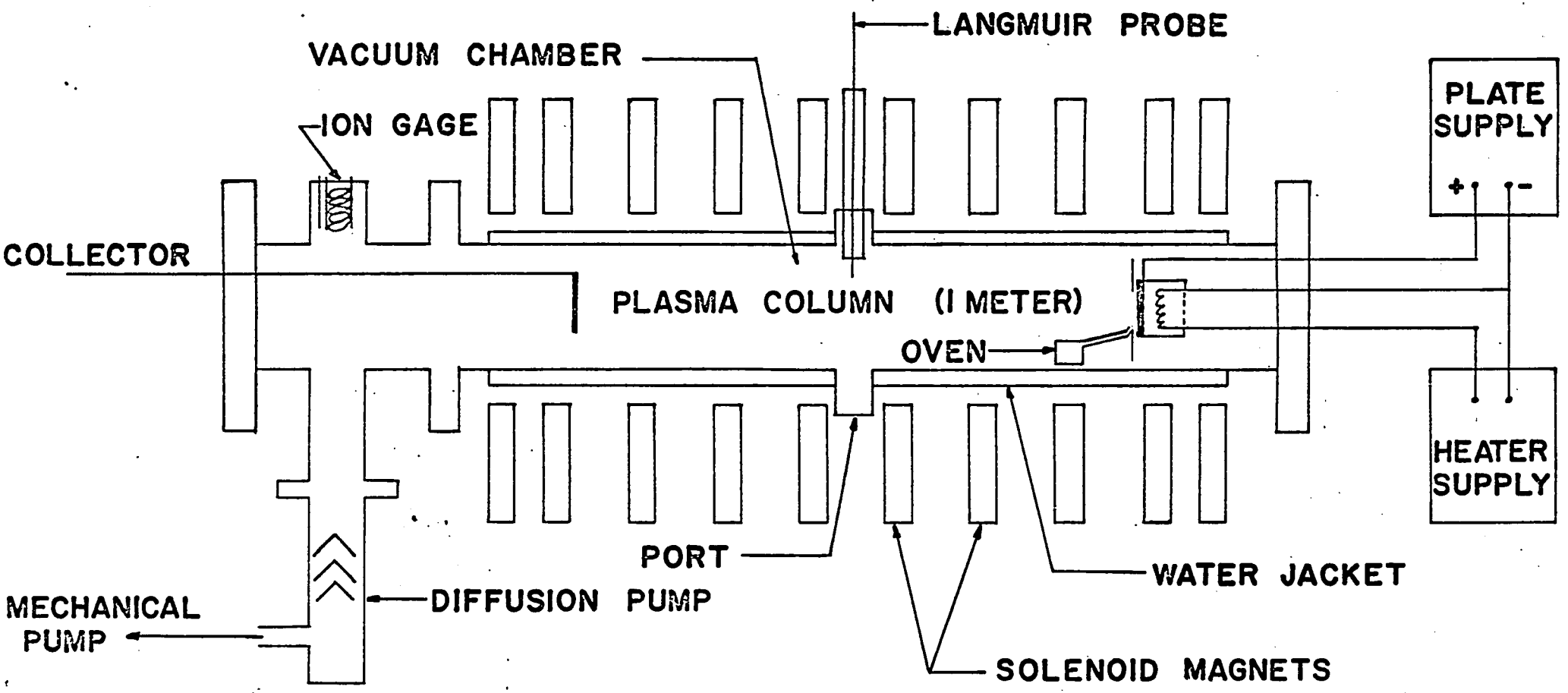

Fig. 2-2 Schematic of Q-machine

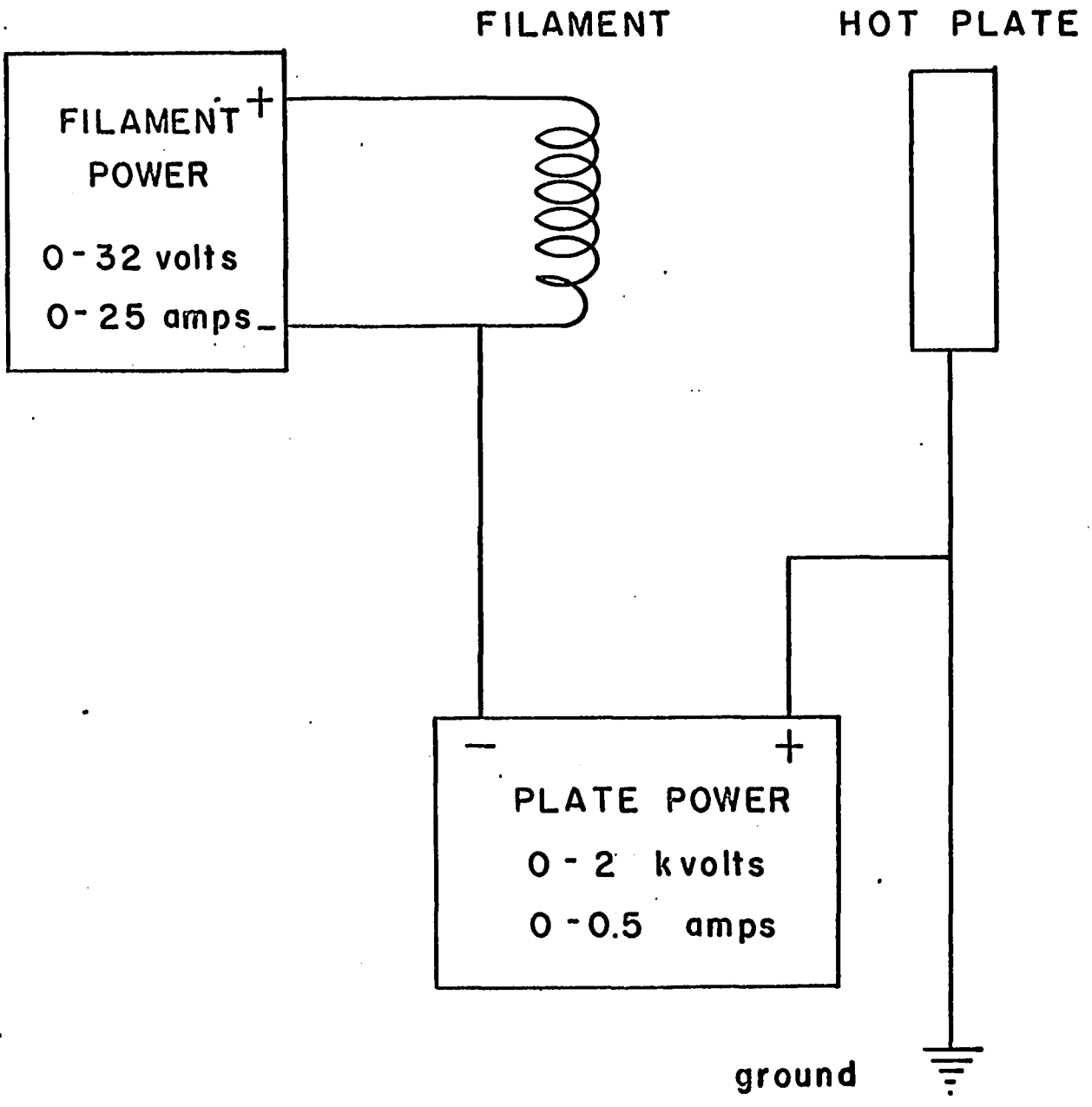

Fig. 2-3 Filament-Cathode circuit

difference between Q-machine and diode is that the Q-machine plate is operated at high temperatures (2300°K). The electron gun structure is shown in Fig.2-4. The upper figure shows a partial top view so that the tungsten plate is visible through the aperture limiter. In the lower figure a side view shows the supporting rings (stainless steel) and the outer shield (tantalum). A schematic drawing (Fig.2-5) shows the positions of the cathode (hot plate), filament, shields and the input power leads for the filament.

The tungsten filament is wound around alumina ceramic pins (Fig.2-6). The pins are held in a boron nitride support. The inner tantalum shield is mounted on the support as shown. The purpose of the shields is to limit radiation losses from both the filament and the hot plate and at the same time to keep stray particles away from the gun to allow more stable operation.

(b) Operation: Theoretically, the gun may be operated in the space charge limited regime or in the temperature limited regime. In space charge limited operation the current voltage characteristic follows the Langmuir-Childs "three halves power" formula. In temperature limited operation electrons emitted by the filament are accelerated to the plate. Operation of the gun, however, is neither strictly space charge nor temperature limited: the observed mode of operation does not exactly agree with the Langmuir-Childs model. In their model, one type of particle with zero initial velocity is accelerated through the

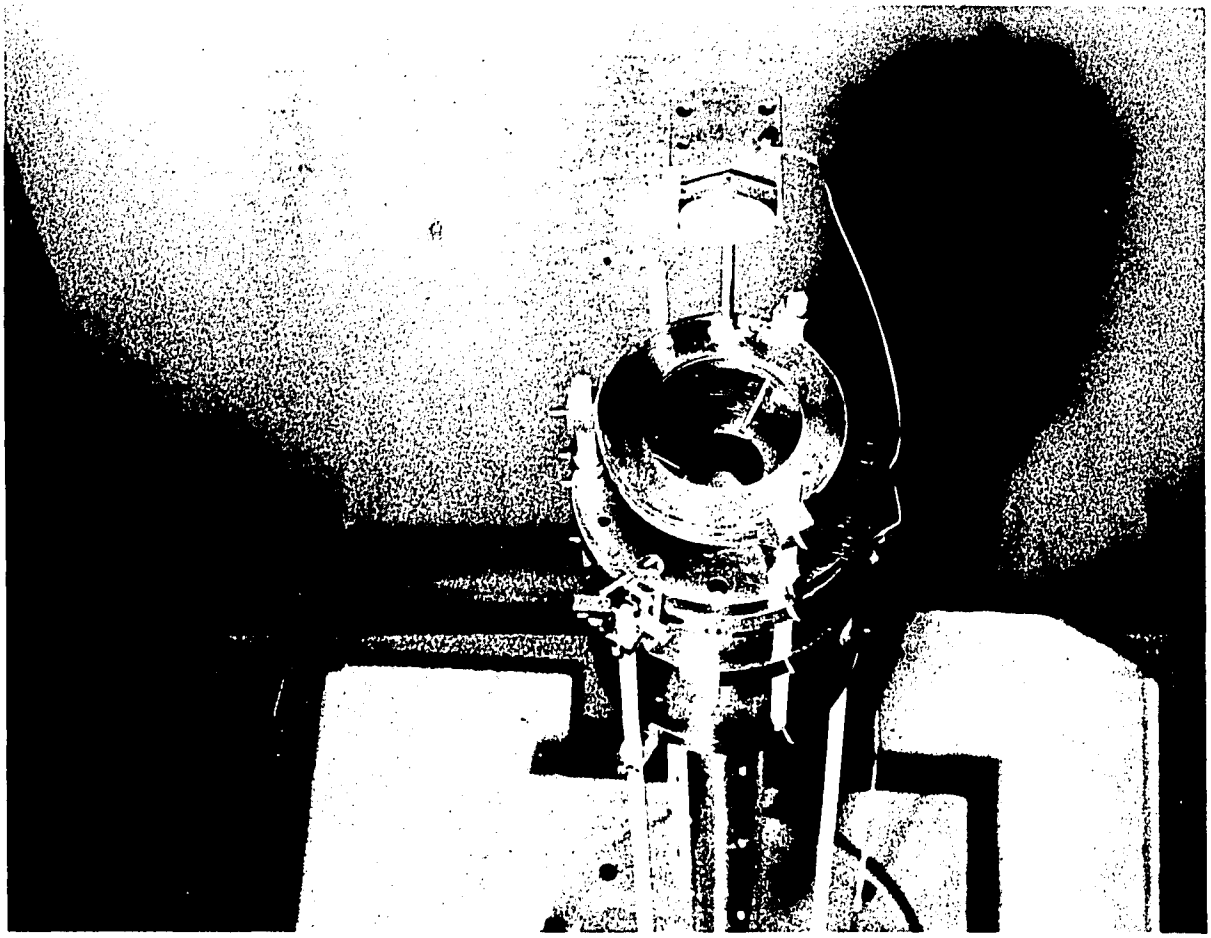

Fig. 2-4 Electron gun assembly

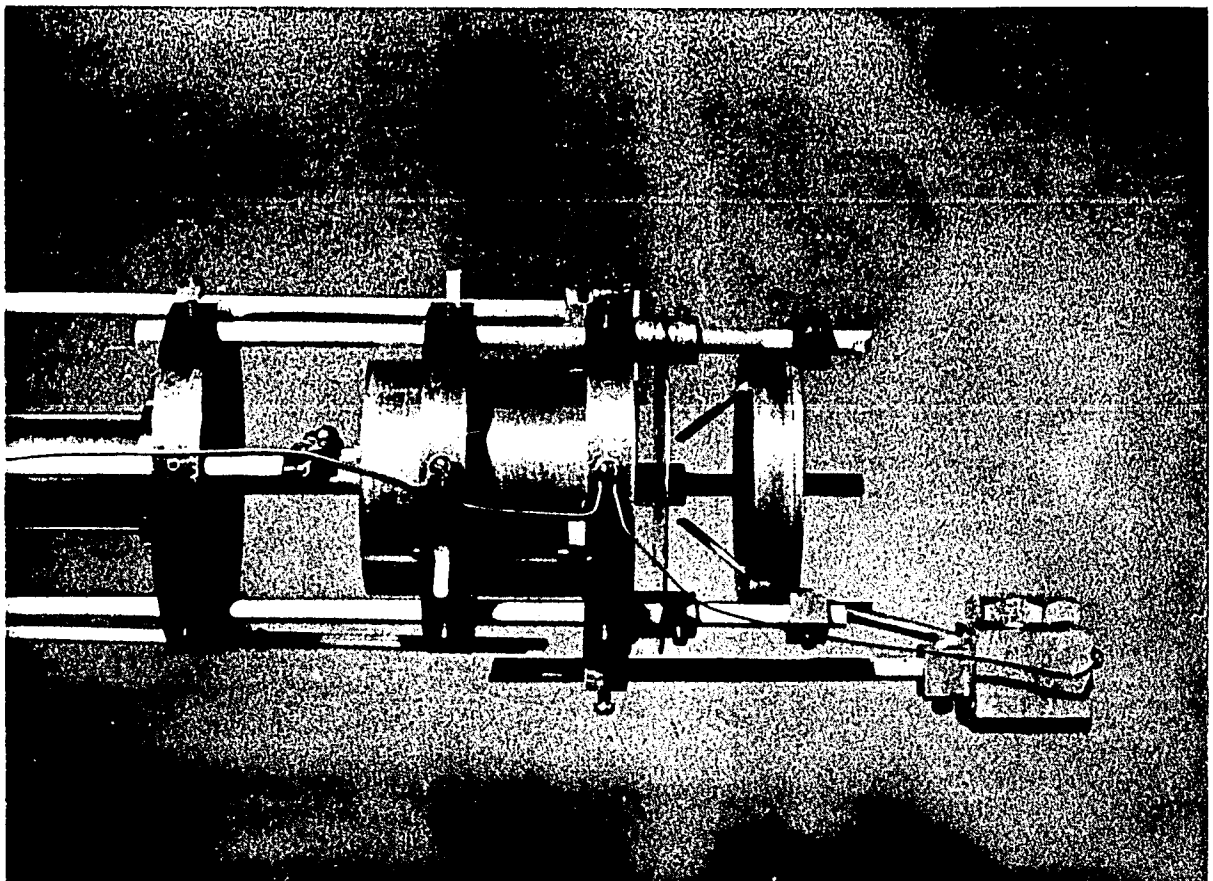

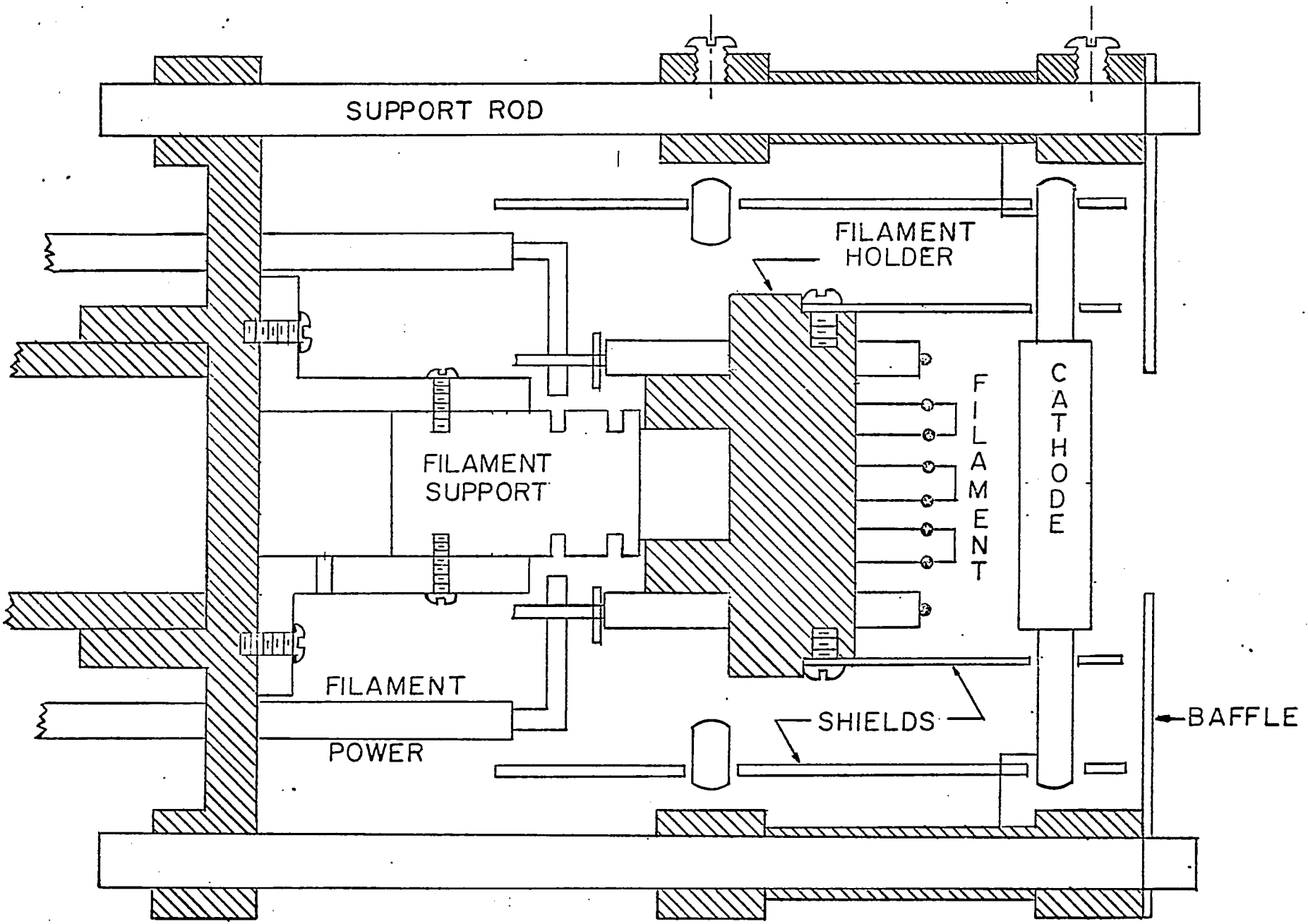

Fig. 2-5 Schematic of electron gun

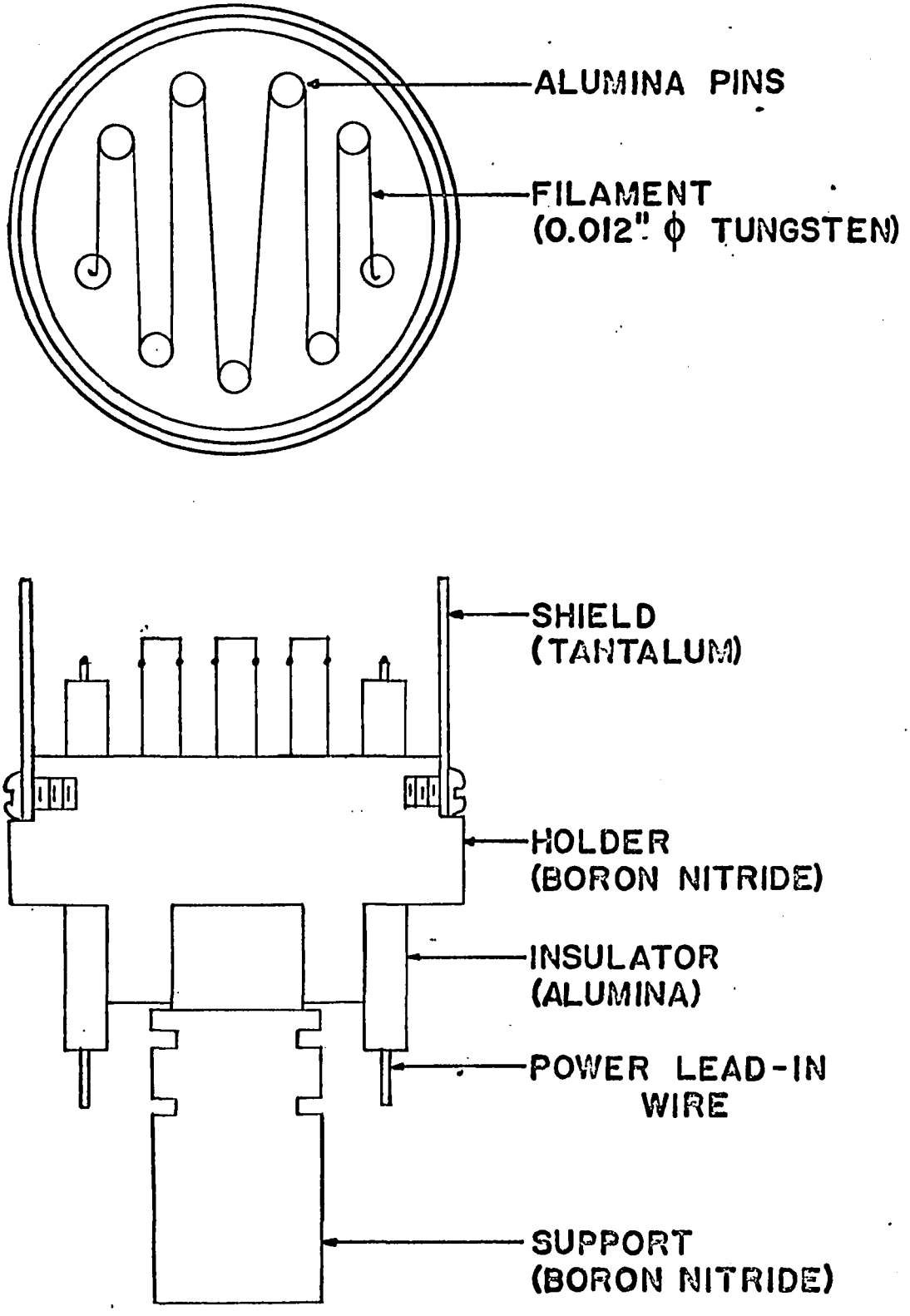

Fig. 2-6 Filament structure

space charge region. In the present case there exists the probability of ions being generated. This means strict adherence to the above formula should not be expected. Some typical operating characteristics of the electron gun are shown in Fig.2-7, along with the applicable portion of the Langmuir-Childs law. It is obvious that the observed current collected by the plate is higher than that predicted by the Langmuir-Childs law when the pressure is high, but for low pressure the Langmuir-Childs law is followed quite well.

When operating in the space charge limited regime the temperature of the hot plate varies linearly with the input power (Fig.2-8). This is convenient for adjusting the plate temperature especially when the plate is obscured from view by diagnostic equipment and the optical pyrometer cannot be used.

(c) Design Considerations: The materials used in construction of the gun will be subjected to temperatures of the order of 2500°K near the filament and plate, but considerably less elsewhere. Tungsten has been used for both the filament and the plate because of its high melting point (3600°K) and high emission properties. The work function of the ionizer plate must be larger than the ionization potential of the alkali metal to be ionized: the work function of tungsten is -4.5 volts while the ionization potential of potassium is -4.31 volts.

The ionizer plate is supported by three tungsten pins (Fig.2-5) held in a stainless steel ring. The temperature of the ring is about

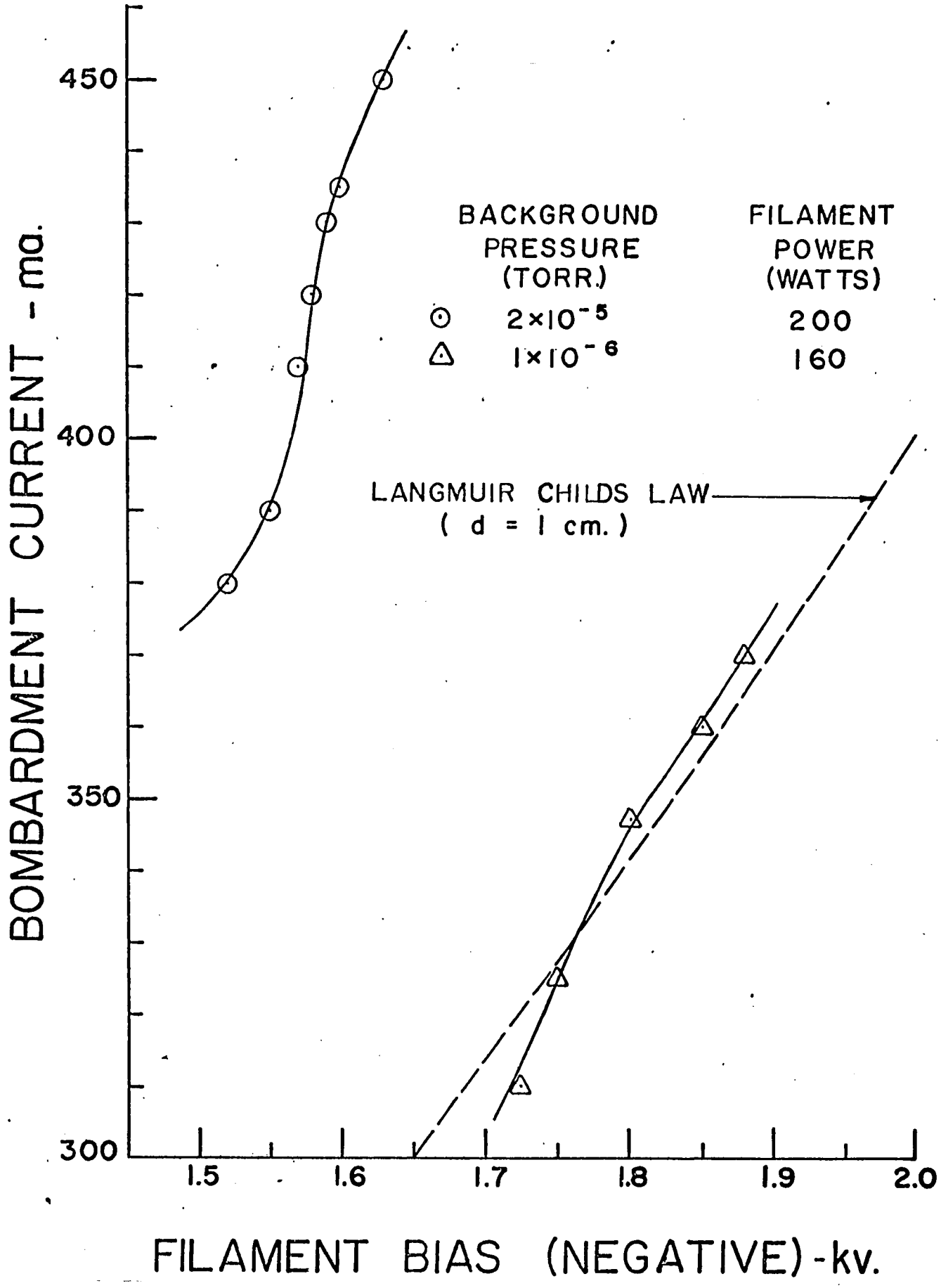

Fig. 2-7 Electron gun characteristics

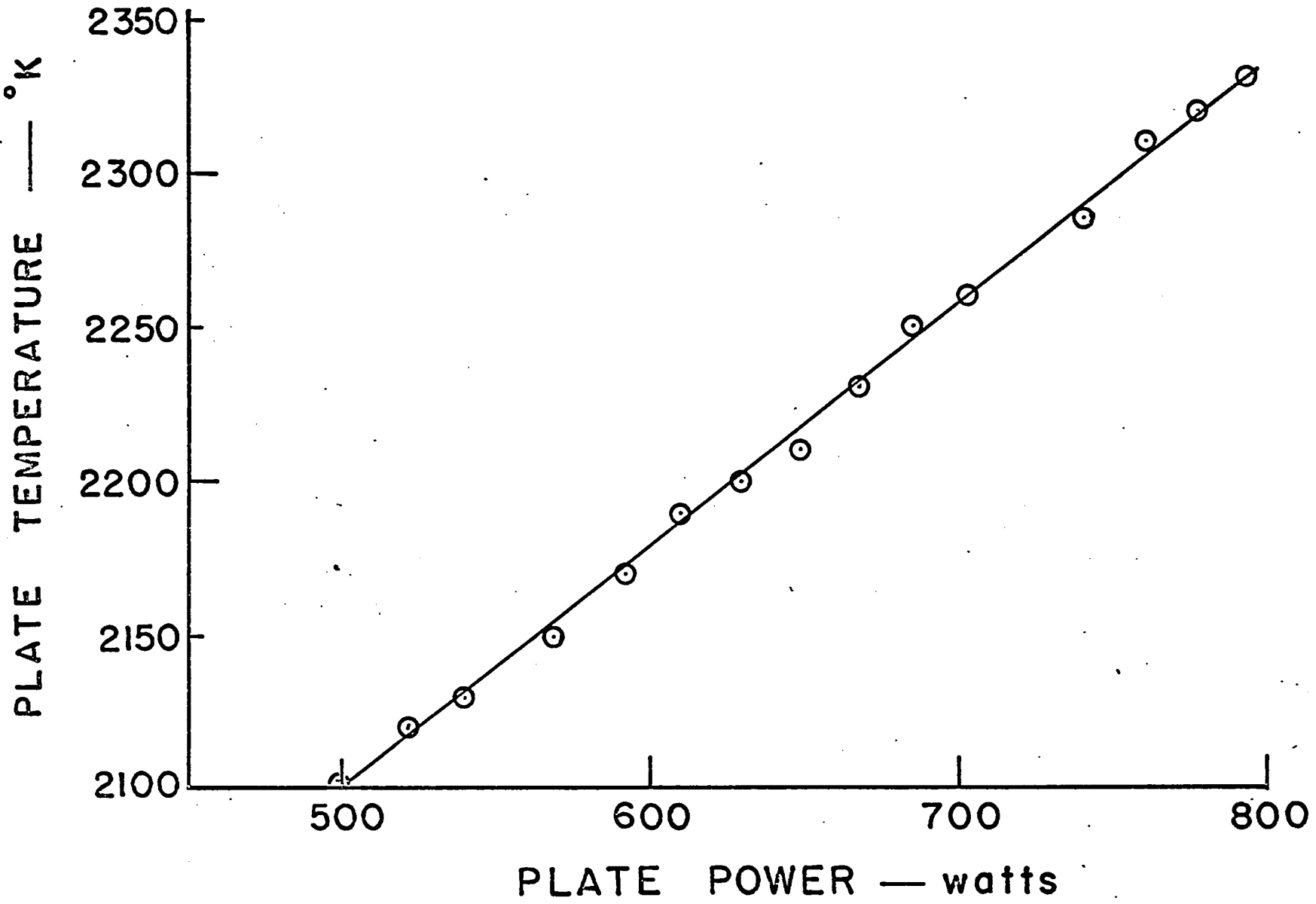

Fig. 2-8 Plate temperature vs plate input power

750°K during operation, so that evaporation is negligible.

For the filament, atomic film emitters were rejected because of the possibility of interaction with the potassium. Tantalum was tested because its emission is slightly higher than that of tungsten at the same temperature and in the annealed form tantalum is much easier to work than tungsten. Unfortunately the tantalum filament test showed excessive evaporation and also permanent deformation due to the magnetic field.

When designing and operating high voltage (1 - 2 kv), high current (0.4 - 0.5 amp) electron beams in a residual gas, it becomes necessary to consider the effect of ion production by the beam, which can affect the operation and life of the filament.

The current-voltage characteristic for the 0.012 inch diameter tungsten filament used in the electron gun is shown in Fig.2-9. The slope of the characteristic, which represents the resistance of the filament, is seen to increase with age in the operating region. This is a result of ion bombardment which makes the filament diameter smaller thus making the resistance higher. Examination of the filament after failure shows a rough surface which is further evidence of ion bombardment.

The production of ions increases with beam current and background pressure[18,19] so to minimize the effects of ion bombardment one should operate at as low a pressure possible and with as small a

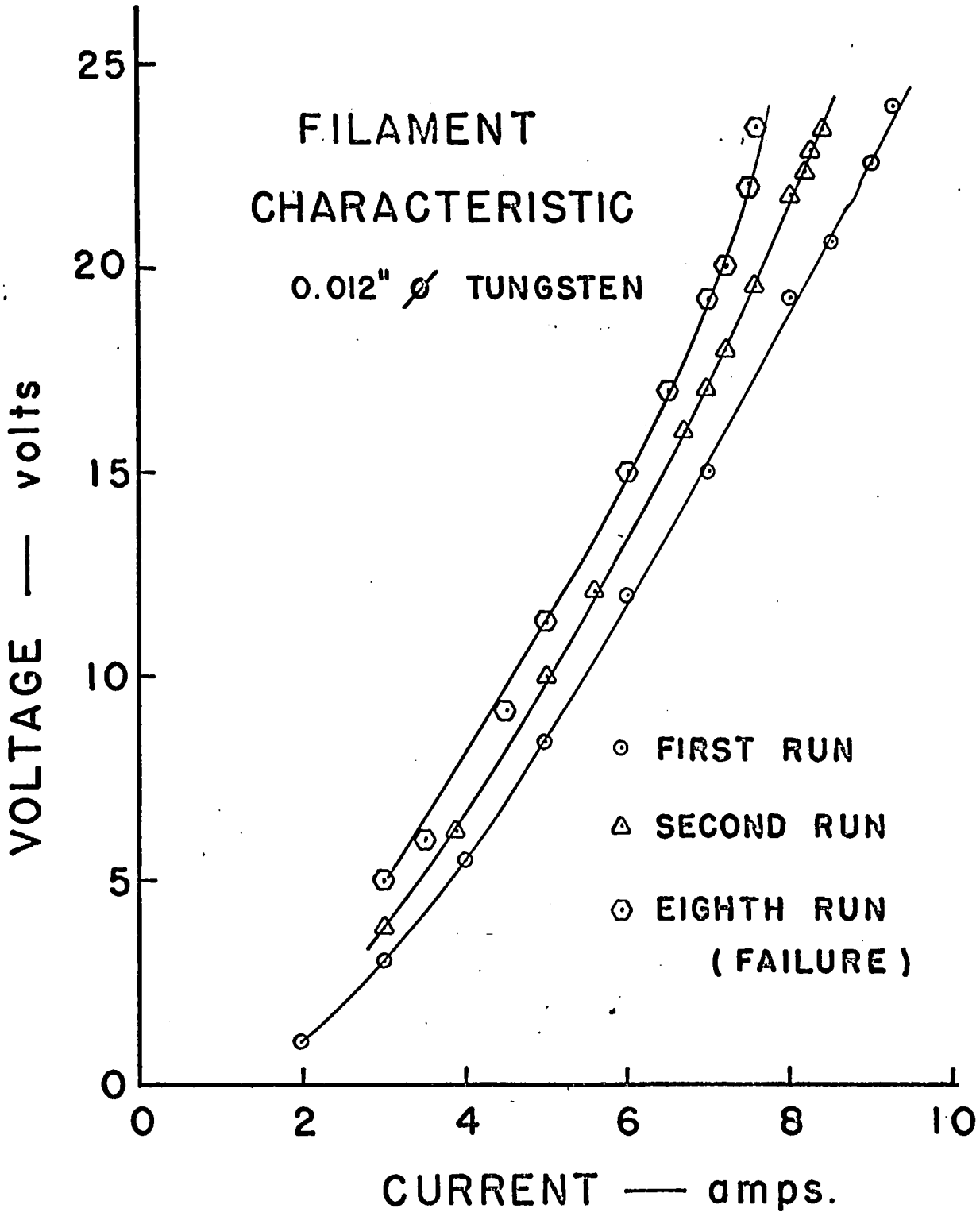

Fig. 2-9 Filament characteristics

beam current as possible. Due to the steepness of the emission curve any small increase in filament power greatly increases the emission. By operating at low filament temperature the effect of instability is minimized.

Finally, the filament is powered by direct current (1% ripple) in order to eliminate mechanical vibrations. The bombardment current is also direct current.

2. Atomic Beam Source

Potassium neutrals are supplied to the hot plate from an oven which feeds a manifold fitted with three "nozzles" (Fig.2-10). The nozzles spray the potassium vapor evenly over the hot plate. This structure is fabricated from stainless steel with silver-soldered joints. The oven is thick walled to prevent temperature variations outside from changing the conditions within the oven.

The flux of neutral particles is controlled by a heater filament placed at the base of the oven. This filament is tungsten and is insulated from the oven by an alumina ceramic sleeve. A copper water jacket is provided at the base of the oven to prevent evaporation of the potassium in the oven during the pump-down and outgassing stages. The oven cooling provides more flexibility for controlling the neutral flux.

Sufficient heat is radiated to the manifold and nozzles to prevent potassium from condensing before reaching the ionizer plate.

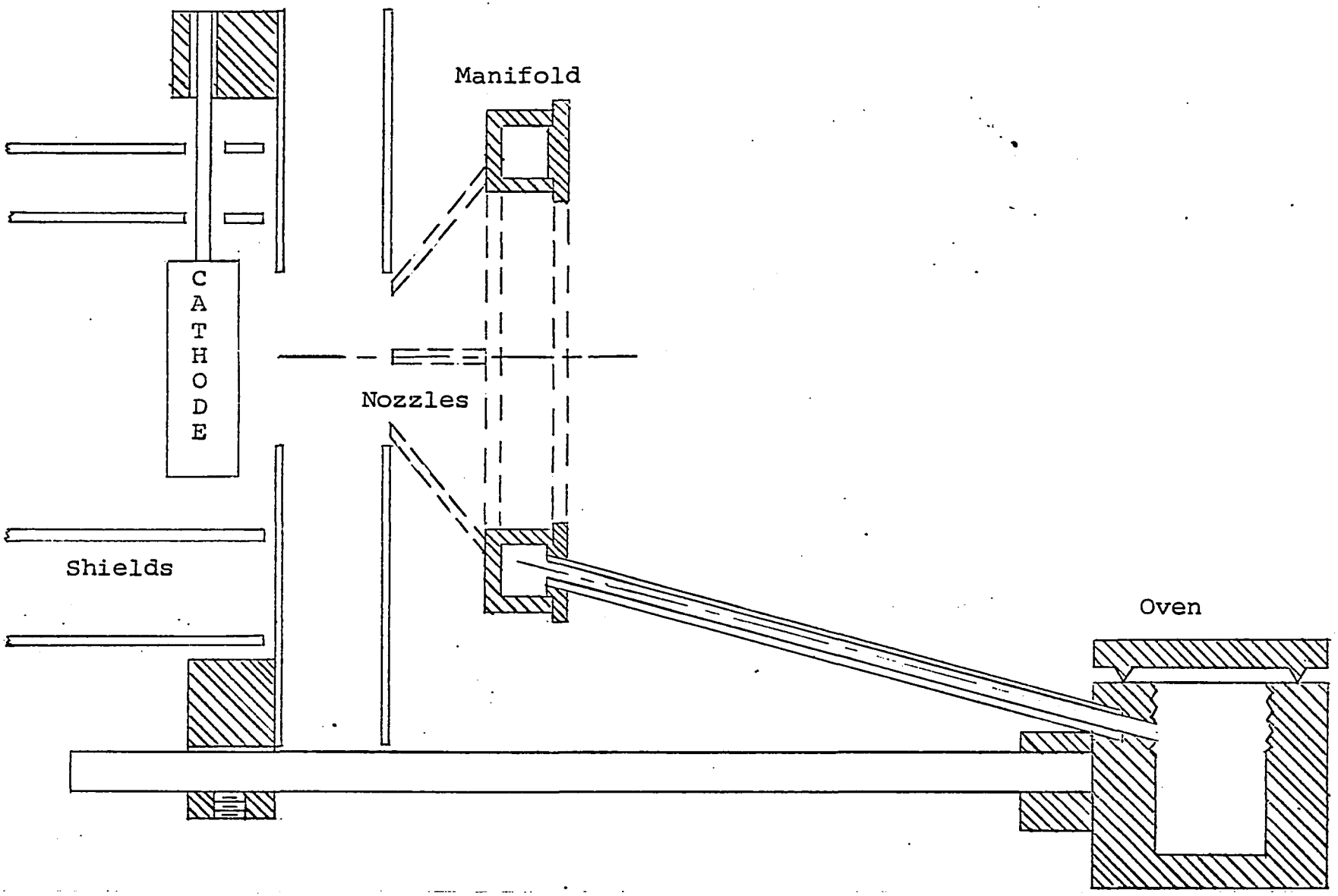

Fig. 2-10 Oven and manifold

For some experiments the manifold was removed and potassium neutrals were sprayed from a single nozzle, influencing the results negligibly.

3. Auxiliary Equipment

(a) Vacuum Chamber: The electron gun, oven and manifold are mounted on a flange. This electron gun assembly seals the end of the vacuum experimental chamber which is stainless steel tube $4\ ^3/_4$" I.D. $\times\ 4\ ^1/_2$ ft. long. Vacuum seals use viton "O" rings. The outside of the chamber is water-cooled by a system of copper tubes soldered parallel to the axis and the water flows in alternate directions to keep the temperature of the chamber uniform.

(b) Vacuum System: The vacuum pumping system consists of a two stage roughing pump (10 cu.ft./min. at 0.1 microns) in series with a 4" diameter diffusion pump (750 liters/sec.); a water-cooled chevron-ring baffle mounted above the diffusion pump serves to prevent oil vapor from the pumps entering the experimental chamber. Background pressures to 10^{-8} torr. are obtained in the system as monitored by a nude inverted Bayard-Alpert type Ionization gauge.

(c) Magnetic Field: The magnetic field is supplied by ten water-cooled solenoids with a seven inch diameter air core into which the vacuum chamber is placed. The spaces between the solenoids allow access to the probe ports and chamber windows. Power for the solenoids is supplied by a rectifier whose maximum output is 200 kilowatts at

1,000 amperes of current. With this system fields of up to 10,000 gauss and of varying configuration may be produced. In normal operation of the Q-machine, a field which is uniform over 50 cm. of length is used.

The spacing of the solenoids for the uniform field configuration has been calculated by superimposing the field due to one solenoid which is moved along the axis. This is allowable since the equations governing magneto-statics are linear. The resulting field which has been measured with Hall probes is seen to be uniform over a longitudinal distance of 50 cm. within 2% (Fig.2-11). The radial variation of the magnetic field is seen to be almost uniform over the $4\frac{3}{4}$ inch diameter of the experimental chamber. These results are similar to those reported elsewhere on the same type of apparatus.[21]

2.3 Plasma Probes

The probes used are Langmuir probes which consist of a wire inserted in the plasma (Fig.2-12). The wire is insulated exposing only a small portion at the tip (1 mm) to the plasma. The tip of the wire then can be used to collect the plasma particles. Such a probe has the advantage of relatively good spatial resolution, something which even more sophisticated techniques such as microwave measurements lack. At the same time, however, the Langmuir probe has the disadvantage of having to be physically inserted into the plasma. In a magnetic

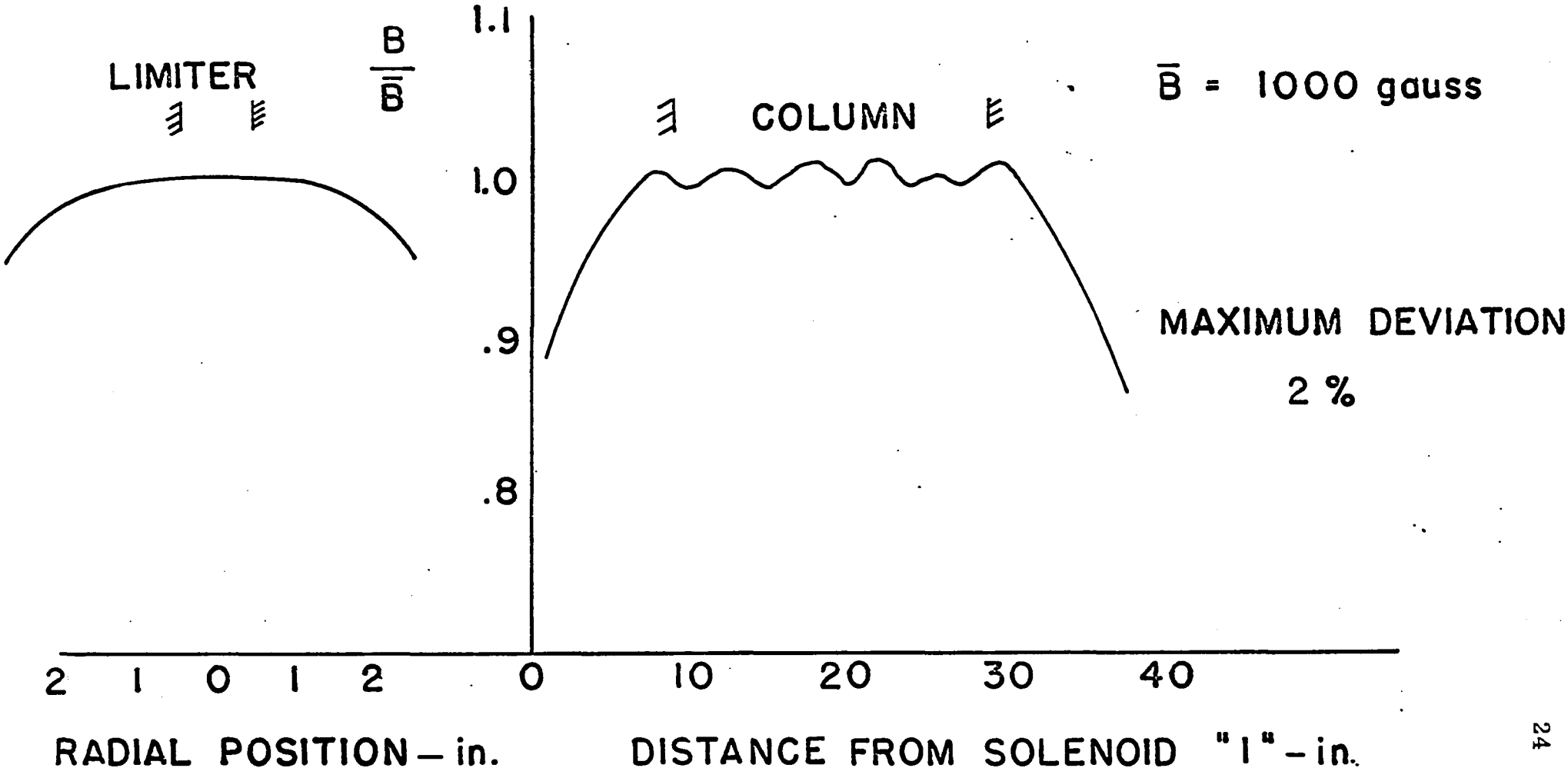

Fig. 2-11 Magnetic field

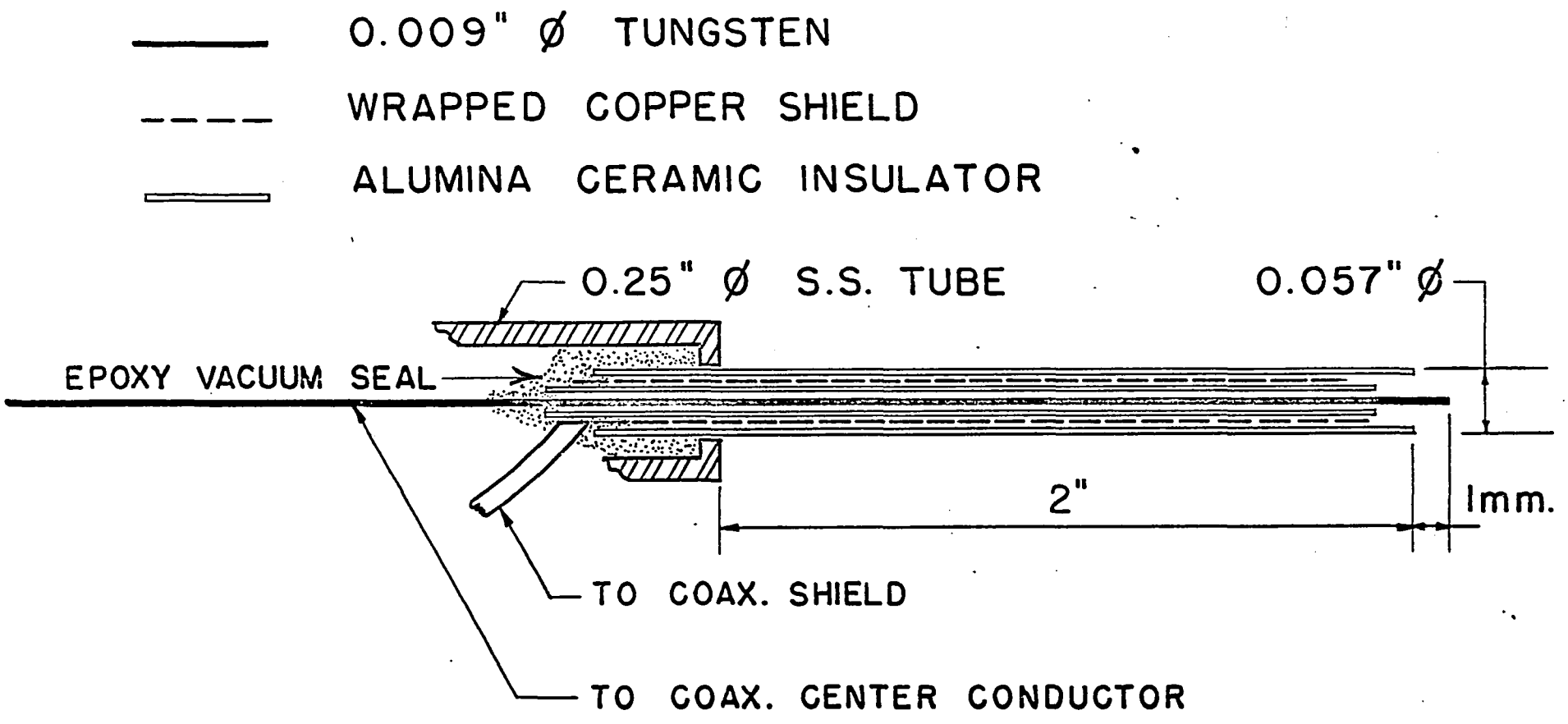

Fig. 2-12 Probe detail

field the perturbation is limited if the probe diameter is smaller than the ion Larmor radius.[20] Probe theory[20] comprises an entire branch of plasma physics and poses some formidable problems: no complete theory for a Langmuir probe in magnetic field exists. It is fortunate though, that the elementary theory suffices in most cases. Now a qualitative description of the theory is given.

With reference to Fig.2-13 (actual data), which depicts a so-called probe characteristic, it is seen that when the probe is biased sufficiently negative with respect to the plasma, almost all the electrons are repelled and the current collected is due mainly to ions; this is called the ion saturation current (region A). In this region all ions which move towards the probe as a result of their thermal motions are collected by the probe and some are accepted by the sheath. As the potential becomes more positive, fewer electrons are repelled and a point is reached at which the electron current exactly equals the ion current to the probe hence the net probe current vanishes; this point is called the floating potential. In region B some of the ions are repelled and the electron current to the probe becomes more positive until the potential is sufficiently positive to repel all the ions and attract all electrons which move to the (effective) probe because of their random velocities (Region C); this is electron saturation current.

The slope of the curve in Region C is due to sheath which builds up around the probe. Usually the sheath thickness can be

Dec. 12 66

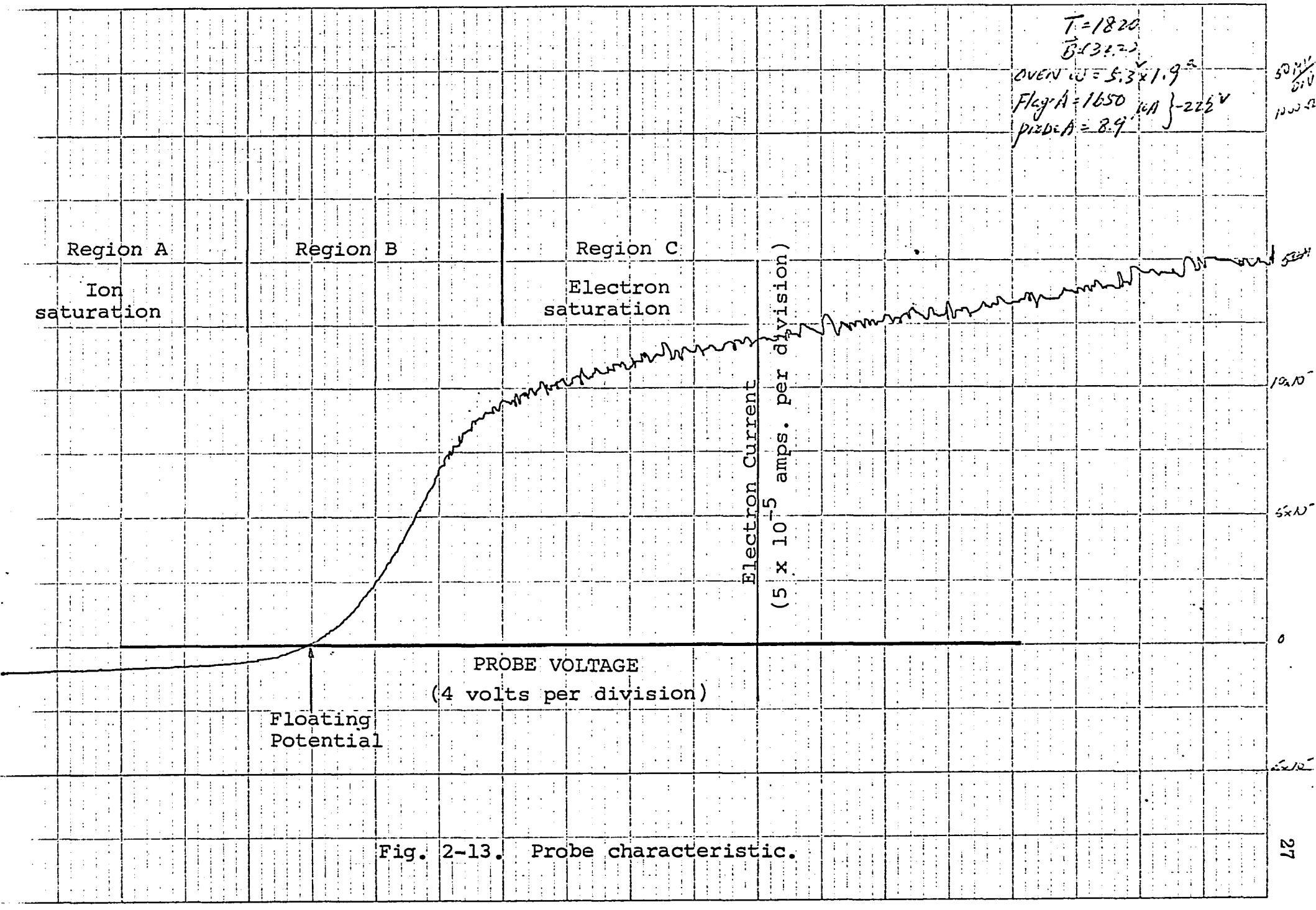

Fig. 2-13. Probe characteristic.

neglected, but as the potential is increased the sheath size increases and therefore creates a larger effective probe area which accounts for the increase of electron current with voltage.

In actual use the probe current is measured by an electrometer and the probe voltage by a vacuum tube voltmeter. The outputs of these meters are used to drive the X and Y axes of a chart recorder all shown in Fig.2-14. The characteristic of Fig.2-13 was recorded in this manner.

Because the ion current saturates rather fast for moderate negative voltages, it is used to calculate the plasma density. In the elementary theory it is assumed that all the ions which strike the probe because of their thermal motions are collected. For a Maxwellian distribution the ion saturation current is given by

$$I_{sat.} = \frac{1}{2} n e \left(\frac{2kT}{\pi M}\right)^{\frac{1}{2}}$$

where n is the number density, e is the electric charge, k is Boltzmann's constant, T is the temperature and M is the ion mass. Densities calculated in this way are generally accurate within a factor of two, but this is sufficient for the present purposes, since the phenomena studied is independent of the absolute magnitude of the density.

In order to study instabilities, the probes have been shielded (Fig.2-12) to reduce the spurious noise. Ion density oscillations are

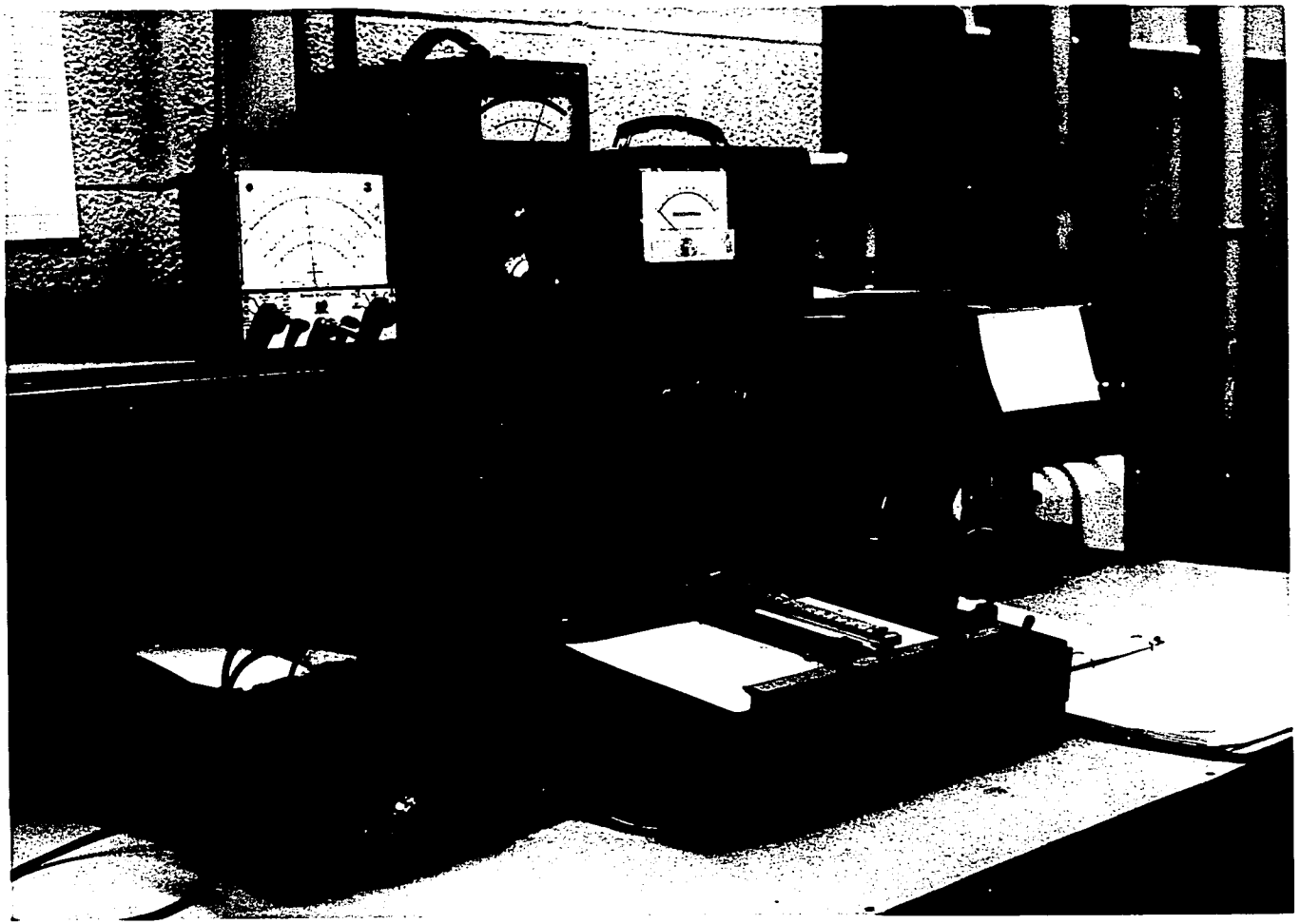

Fig.2-14. Instrumentation.

observed by biasing the probe to collect ion current and letting this current pass through a 1000 ohm resistor, measured with Tektronix 555 Dual-beam oscilloscope using a type 1A7 vertical pre-amplifier. The output of the 1A7 is then connected to a spectrum analyzer which provides a continuous display in the frequency domain.

2.4 Summary

In this chapter the experimental apparatus and Langmuir probe diagnostic techniques have been described. The Q-machine produces a relatively quiescent fully ionized plasma well suited for the study of plasma instabilities due to the low level of background noise. In the Q-machine the change in sheath conditions between the hot plate and the relatively cool aperture limiter creates a jump in potential at the edge of the plasma column.

CHAPTER 3

EXPERIMENT

The aim of the experiment was to determine the parametric dependences of an observed, self-excited oscillation. The parameters are magnetic field, density, temperature and column length. In order to determine the wave it is necessary to measure its phase velocities by measuring the longitudinal and azimuthal components of the propagation vector, k, and the frequency, ω. In the next paragraph a general qualitative description of the observed wave is given including radial amplitude dependence and in the remainder of this chapter the specific measurements made are described.

3.1 General Description of the Wave

The wave appeared with varying degrees of coherence for magnetic field strengths ranging between 500 and 5200 gauss, for ionizer plate temperatures from 2000 to 2400^{o}K, and for densities of 5×10^{8} to 5×10^{10} ions per cubic centimeter. Probe measurements were corroborated by densities computed from the ion current drawn by the cold collecting plate which terminates the plasma column. A typical frequency spectrum is shown in Fig.3-1. The spectrum shows a dominant mode with a frequency of 9 kHz. and harmonics whose frequencies are integral multiples of that of the dominant mode. The first

SPECTRUM

of

OSCILLATIONS

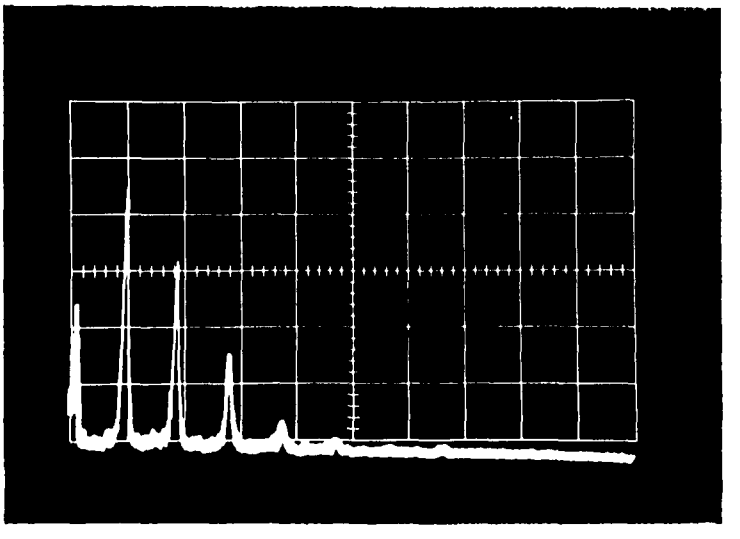

f — 10 kHz. / div.

Fig. 3-1 Frequency spectrum

peak at the left of the spectrum is the zero marker. Depending on operating conditions either spectra with one dominant mode, multi-mode spectra, or noisy spectra could be produced; noisy spectra being produced more easily at higher magnetic fields. The wave was observed for plasma columns with a high degree of azimuthal symmetry and for columns which were strongly asymmetric.

Two typical density and floating potential profiles are shown in Fig.3-2. The step-like falloff in the density profile in Fig.3-2b is the striking difference between the two profiles. This is caused by the annular manifold (Fig.2-10) used to supply neutrals to the ionizer plate. In Fig.3-2a the manifold was removed and only one tube was used to carry the neutrals from the oven to the hot plate. The wave was observed for both configurations.

3.2 Determination of Flute Character of the Wave

In order to determine whether the observed oscillation is a flute mode it is necessary to measure the propagation vector component parallel to the magnetic field, $k_{\parallel}$ ($k_{parallel}$). Here, a flute mode is defined as a wave with $k_{\parallel} = 0$. The drift modes, which are instabilities driven by the pressure gradient, can have $k_{\parallel} \approx 0$. It has been shown theoretically[22] and verified experimentally[7] that drift modes occur with a small, but finite, $k_{\parallel}$. This leads to difficulties in interpreting the results of the measurement of $k_{\parallel}$, but as will be shown below the

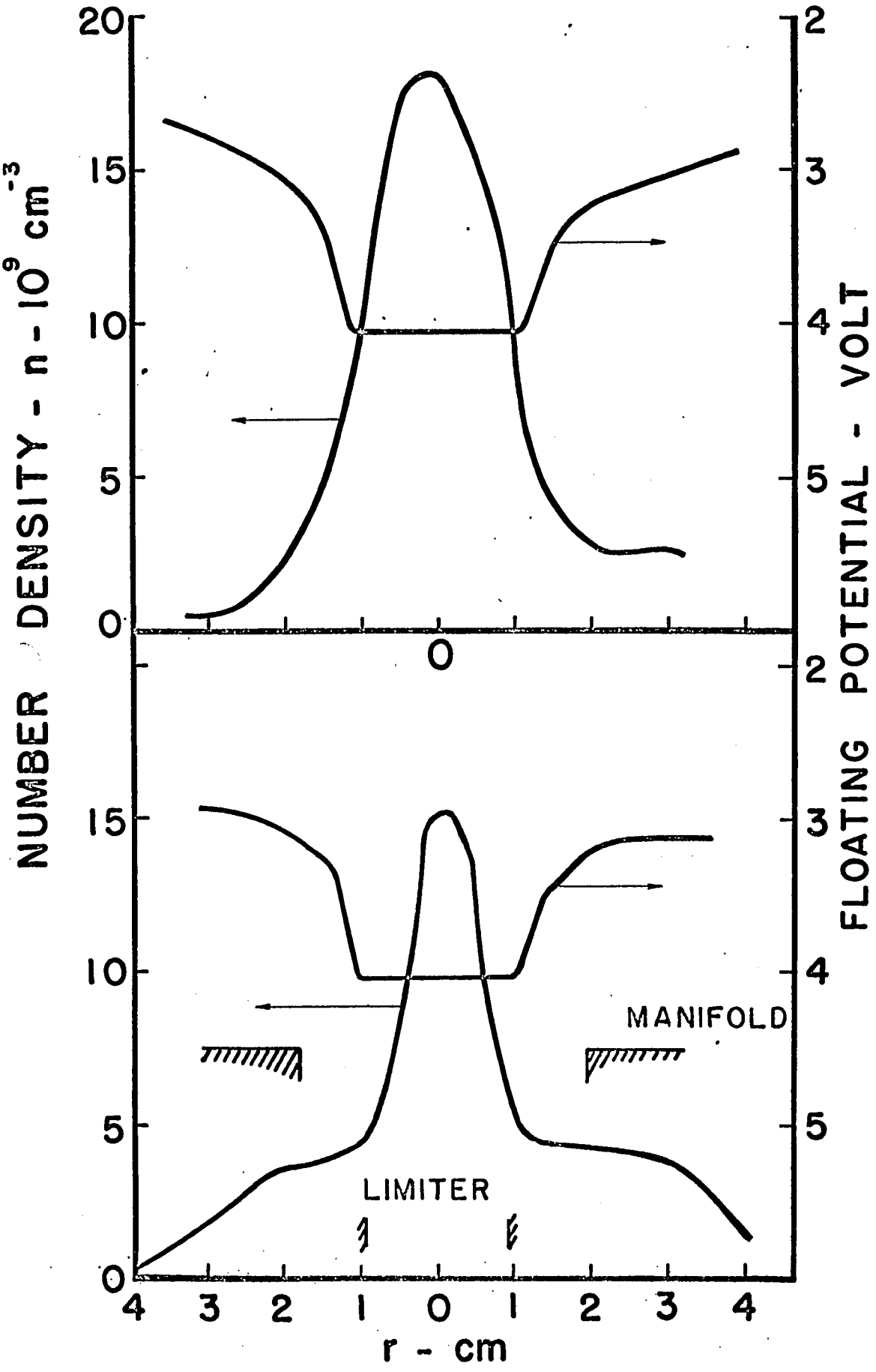

Fig. 3-2 Density and potential profiles

longitudinal wavelength of drift modes is much smaller than that for the present instability.

The longitudinal wave number, $k_{\parallel}$, was measured by means of a probe which could be moved along the magnetic field and rotated across the field along a predetermined arc. In order to find $k_{\parallel}$ it is necessary to find the phase shift between the probe wave form at different known longitudinal positions with respect to a fixed "trigger" probe. If t is the measured phase shift and z is the distance the probe has been moved then equating the phase velocity $\omega/k_{\parallel}$, to the velocity computed from the phase shift, z/t, gives $k_{\parallel} = \omega t/z$. Since here one is looking for small $k_{\parallel}$ it is necessary to align the probe accurately along the same magnetic field line. The method used to do this is described below.

With a point chosen at the edge of the column the ion saturation current drawn by the probe could be used to indicate if the probe, once moved longitudinally, was still on the same field line. Since at the edge of the column the density gradient is very steep, there is almost no error due to reading the current. The only source of error is a possible misalignment of the chamber with respect to the magnetic field. Both the coils and the chamber, however, have been aligned by methods of optical tooling which limits any misalignment to less than 0.1 mm off axis over 100 cm. of length along the axis. Using these figures one estimates the maximum experimental error in $k_{\parallel}$ to be

1×10^{-2} cm^{-1}. The error comes from a shift of the plasma column with respect to the axis of the probe. This means that when the probe is positioned by the method described above it may not be at the same azimuth as before, hence the observed phase shift would have a contribution due to the azimuthal propagation of the wave which creates an error in the measurement of the longitudinal propagation. The measurement of the longitudinal propagation is shown in Fig.3-3. The trigger probe is fixed in position and acts only as a reference signal. Using the average phase shifts between the trigger signal and the movable probe one calculates $k_{\parallel} = 6.12 \times 10^{-3}$ cm^{-1} over a distance of 20.55 cm. From this value of $k_{\parallel}$ one finds the corresponding longitudinal wavelength $\frac{2\pi}{k_{\parallel}}$, to be 1.02×10^{3} cm. which is more than 20 times the length of the apparatus. When the uncertainty is added to the measured $k_{\parallel}$ the corresponding $\lambda_{\parallel}$ is still 8 times the length of the apparatus. Drift modes usually occur with longitudinal wavelengths of the order of 2 times the length of the apparatus.[7]

The constancy of the amplitude of the waveforms in Fig.3-3 allows only a standing wave whose length is much greater than that of the apparatus.

The wave dependence on $k_{\parallel}$ can also be measured by changing the length of the plasma column; if the longitudinal propagation depends on the column length then a frequency shift will be observed when the length is changed. In the single-ended operation of the Q-machine

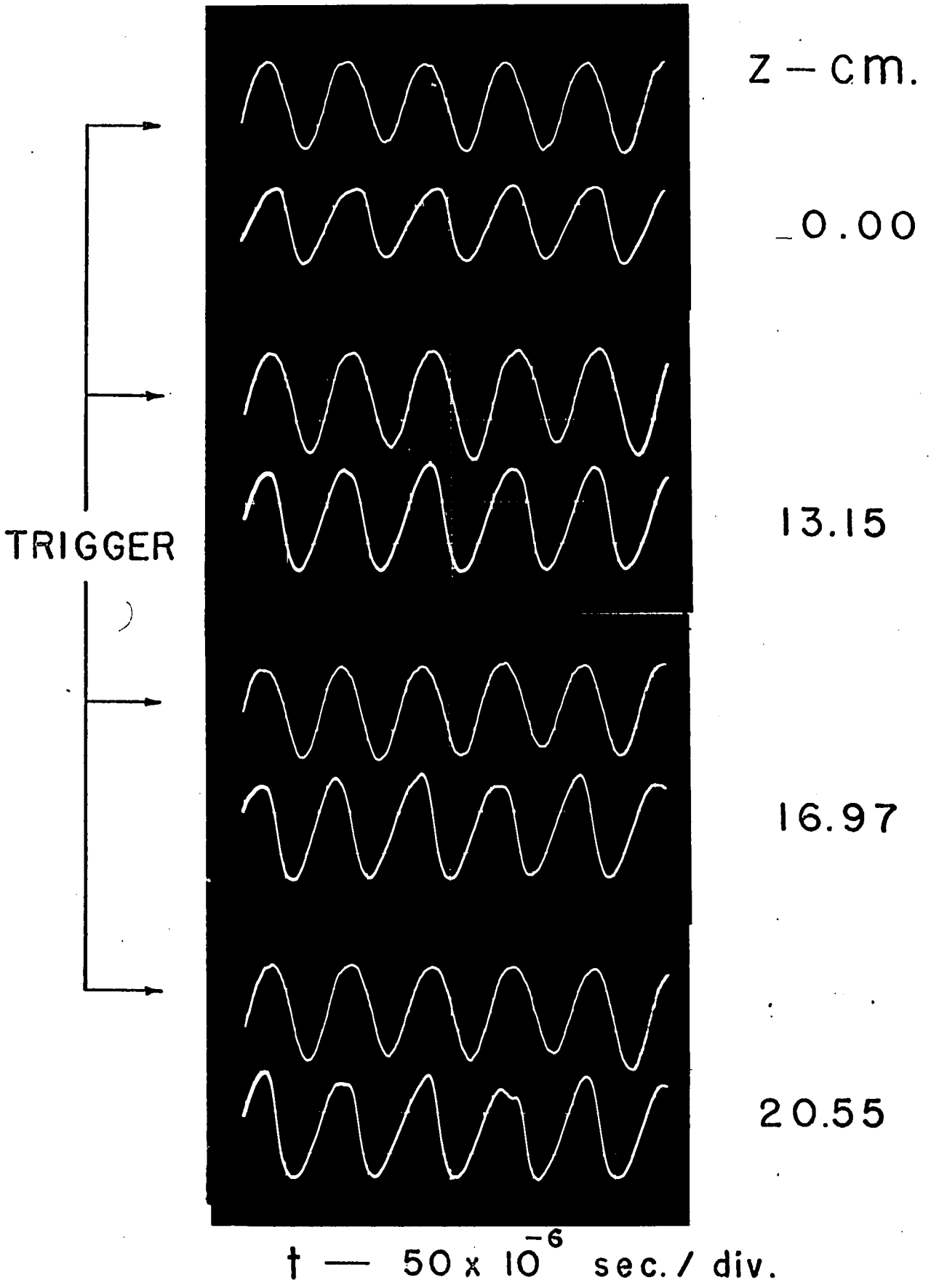

Fig. 3-3 Measurement of $k_{\|}$

this is easily done by moving the cold collecting plate along the axis of the chamber. In the present experiments, when the collecting plate was used to change the column length by 50% neither the amplitude nor the frequency of the wave changed a measureable amount.

3.3 Determination of Edge Oscillation

An edge oscillation in a Q-machine is defined here as a wave whose maximum amplitude occurs at the edge of the plasma column. In the present experiment the relative amplitude peaked sharply at the edge of the column (Fig. 3-4) indicative of an edge oscillation. The curve in Fig. 3-4 has been obtained by connecting the oscilloscope output of the probe signal to an a-c voltmeter whose d-c output was used to drive the Y axis of an X-Y recorder. The X axis of the recorder is connected to a linear potentiometer which provides a voltage proportional to the position of the radial probe. The resulting plot is then normalized by dividing by the density at each point. The relative amplitude curve in Fig. 3-4 has been plotted from 50 calculated points.

3-4 Radial Propagation

A similar measurement was performed to see if the wave propagated in the radial direction. For this measurement there was no problem in placing the probe since the radial probes can be set with a maximum error of 0.25 mm. radially and are constructed to go through

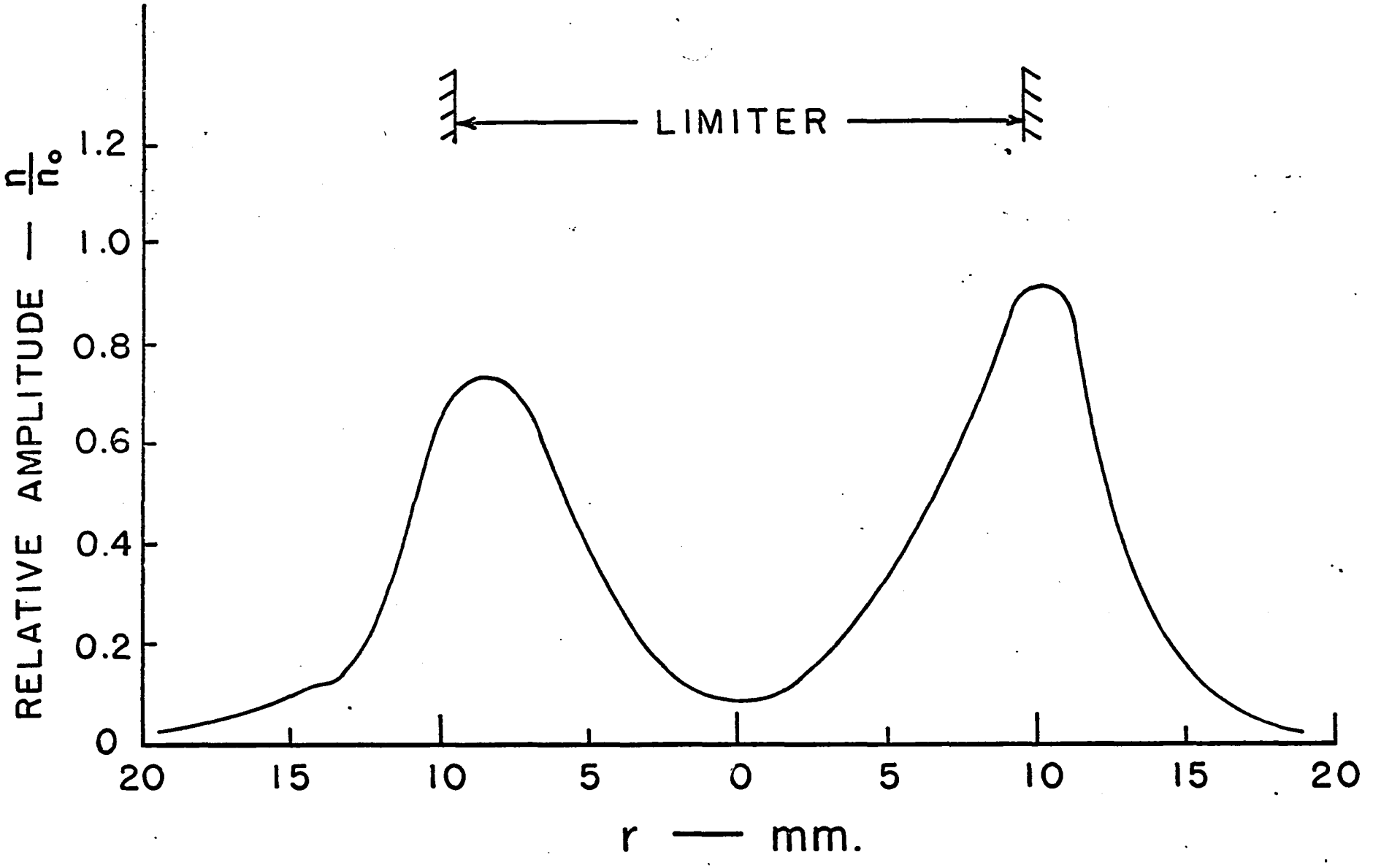

Fig. 3-4 Relative wave amplitude vs radial position

the center of the column within a millimeter. The results showed no propagation in the radial direction (Fig. 3-5).

3.5 Azimuthal Propagation

The measurement of azimuthal mode numbers is similar to that for $k_{\parallel}$ except now the two probes must be placed at some known angle θ instead of some distance z. In this case the phase velocity is $2\pi r/mT$ where T is the period of the wave and m is the azimuthal mode number and now the velocity measured by the phase shift is $r\theta/t$ where θ is the angle between the probes so that $m = 2\pi t/\theta T$. In general, the two probes must be in the same plane perpendicular to the magnetic field for this measurement. It has already been shown that $k_{\parallel} \approx 0$ which means that the wave propagates in the same way at each cross section of the column hence it is not necessary to have the two probes in the same plane. One of the radial probes was used with the probe shown in Fig.3-6 to measure mode numbers. Several mode numbers were measured, but in many cases multi-mode or noisy spectra made these measurements difficult. In some cases one was able to observe the shift in modes by watching the frequency spectrum while the magnetic field was changed very slowly, but in other cases it was difficult to know which mode one observed. Figure 3-7 shows measurements of modes three and four. Notice that the waveforms in the measurement of mode three were taken on single sweep mode of

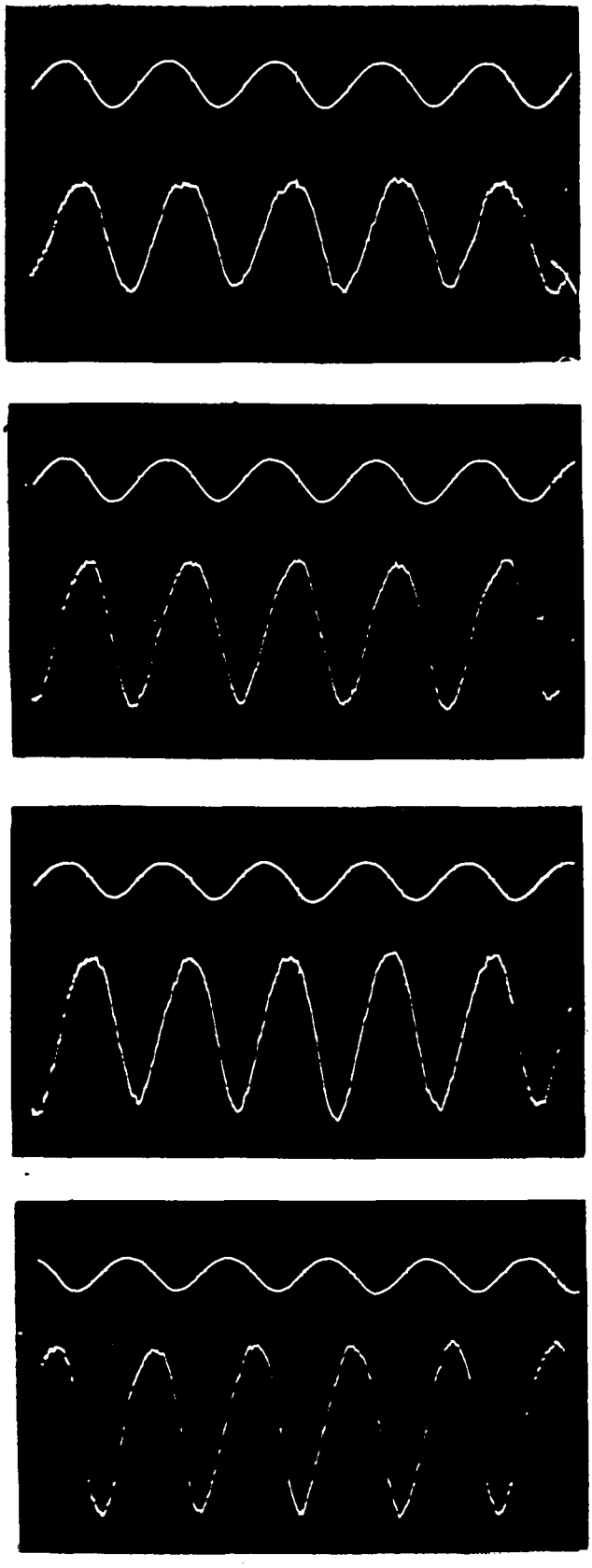

Fig. 3-5 Measurement of k_r

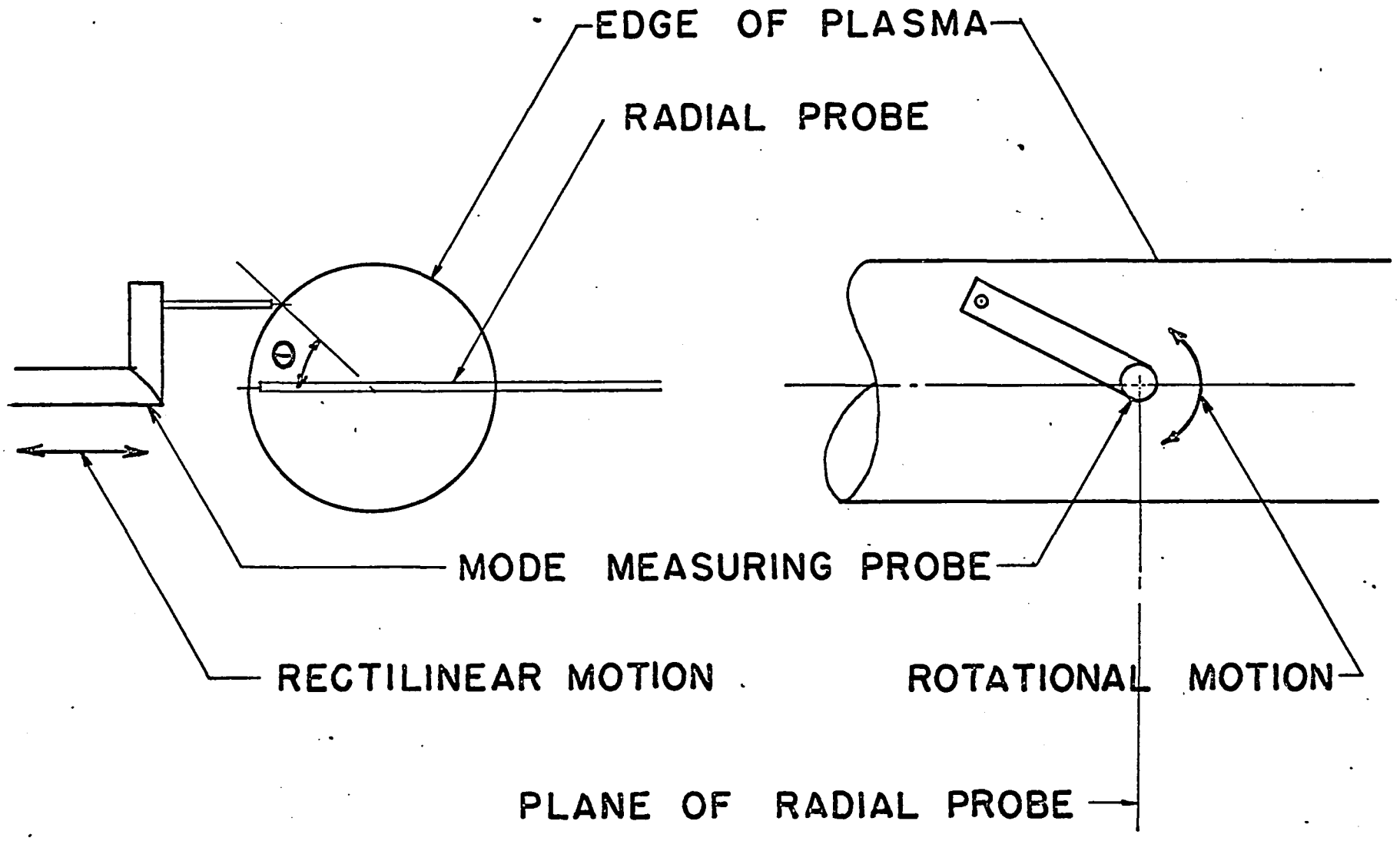

Fig. 3-6 Mode measurement probe

MODE 3

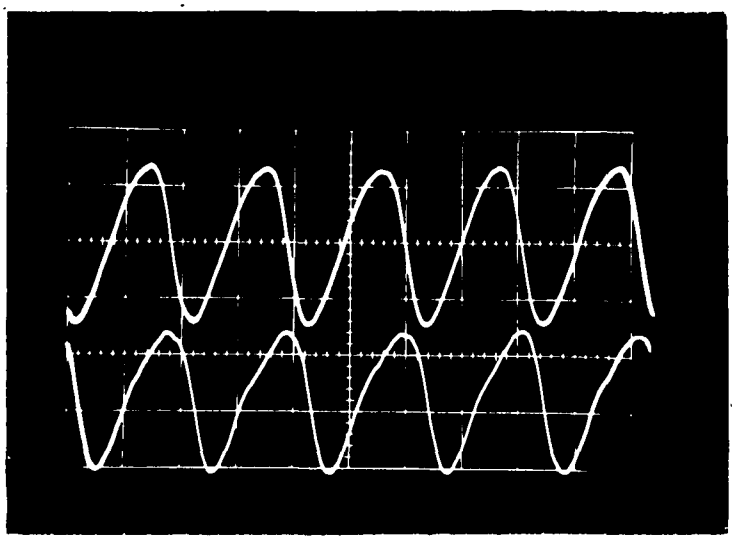

MODE 4

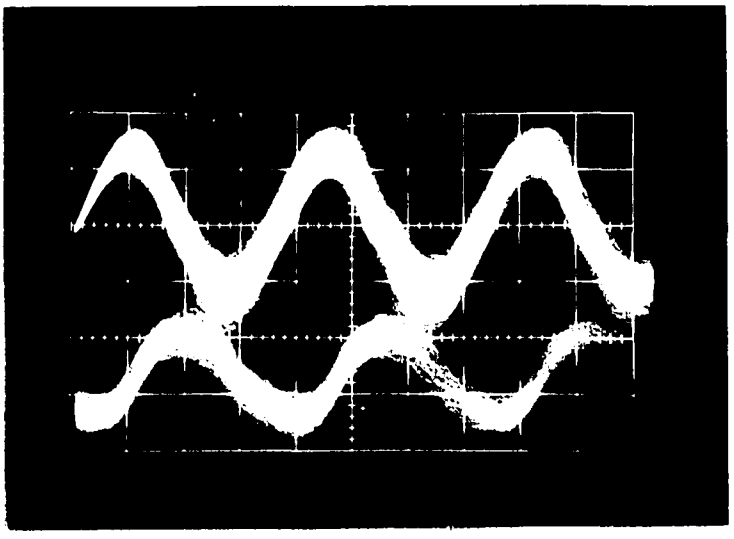

t — 50×10^{-6} sec./ div.

Fig. 3-7 Mode measurement

the oscilloscope while those for mode four show multiple sweeps. The use of the multiple sweep measurement was necessitated by the presence of higher and lower modes than mode four which distort the waveform and make phase shift measurements meaningless. Using multiple sweeps averages these undesirable effects.

3.6 Wave Properties Depending on the Collecting Voltage

The wave appeared unchanged when the cold collecting plate was allowed to float electrically as opposed to being biased negatively to collect ions. When the collecting plate was grounded the wave still destabilized, but with high background noise and modified spectrum. Finally when the collector was biased to collect electrons the oscillations disappeared into the background noise.

3.7 Mode Amplitude Dependence on Magnetic Field

Measurements of mode amplitude were made from the spectra and normalized to the background density. These relative amplitudes are plotted against $B/(\alpha_1 - \alpha_2)$ Fig. 3-8 where α_1 and α_2 depend on the density inside and outside the column. In the theory section the normalization $(\alpha_1 - \alpha_2)$ will be discussed. This dependence on B is similar to that of Ref. 7, but it will be shown that the two phenomena are different from the physical point of view.

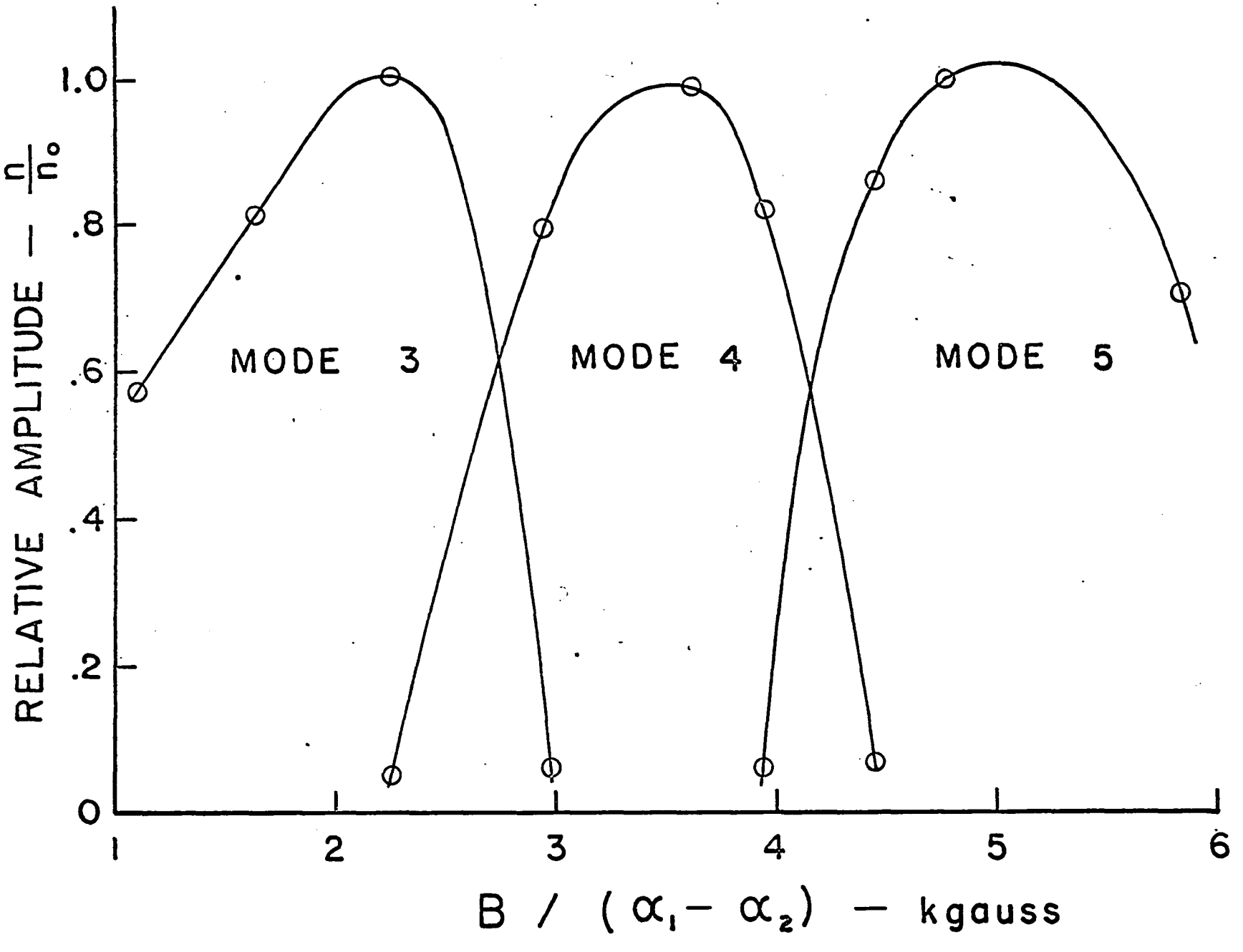

Fig. 3-8 Mode amplitudes

3.8 Frequency Dependence and High Magnetic Field Behavior

In Fig.3-9 the wave frequency normalized by its respective mode number is plotted versus $B/(\alpha_1 - \alpha_2)$. This figure shows that the frequency of a particular mode decreases for increasing B. As the magnetic field is increased, higher modes appear (Fig.3-8) and then the frequency of the highest dominant mode becomes constant. When the field is increased further, the narrow line character of the spectrum disappears as the last mode observed is stabilized (Fig.3-10). The resulting spectrum shows low level noise having a maximum amplitude near the frequency of the stabilized mode (16 kHz. in the case shown). Accompanying the spectral change is a change in the density profile (Fig.3-11). It has been found that when the frequency spectra are comprised of discrete modes the data is reproducible from one run to the next, but when the spectra are noisy reproducibility is poor.

3.9 Study of Electrode Assembly Configuration Effects

The affect of the boundary conditions at the electrode assembly end of the plasma column has been studied. The aim of this study was to find whether the "scraping off" of plasma by the aperture limiter affected the observed oscillation. Three different configurations were examined (Fig.3-12). Case A corresponds to a thin plate which was fitted around the hot plate and mounted flush to it; cases B and C are similar except in case B a collar made of thin tantalum sheet was

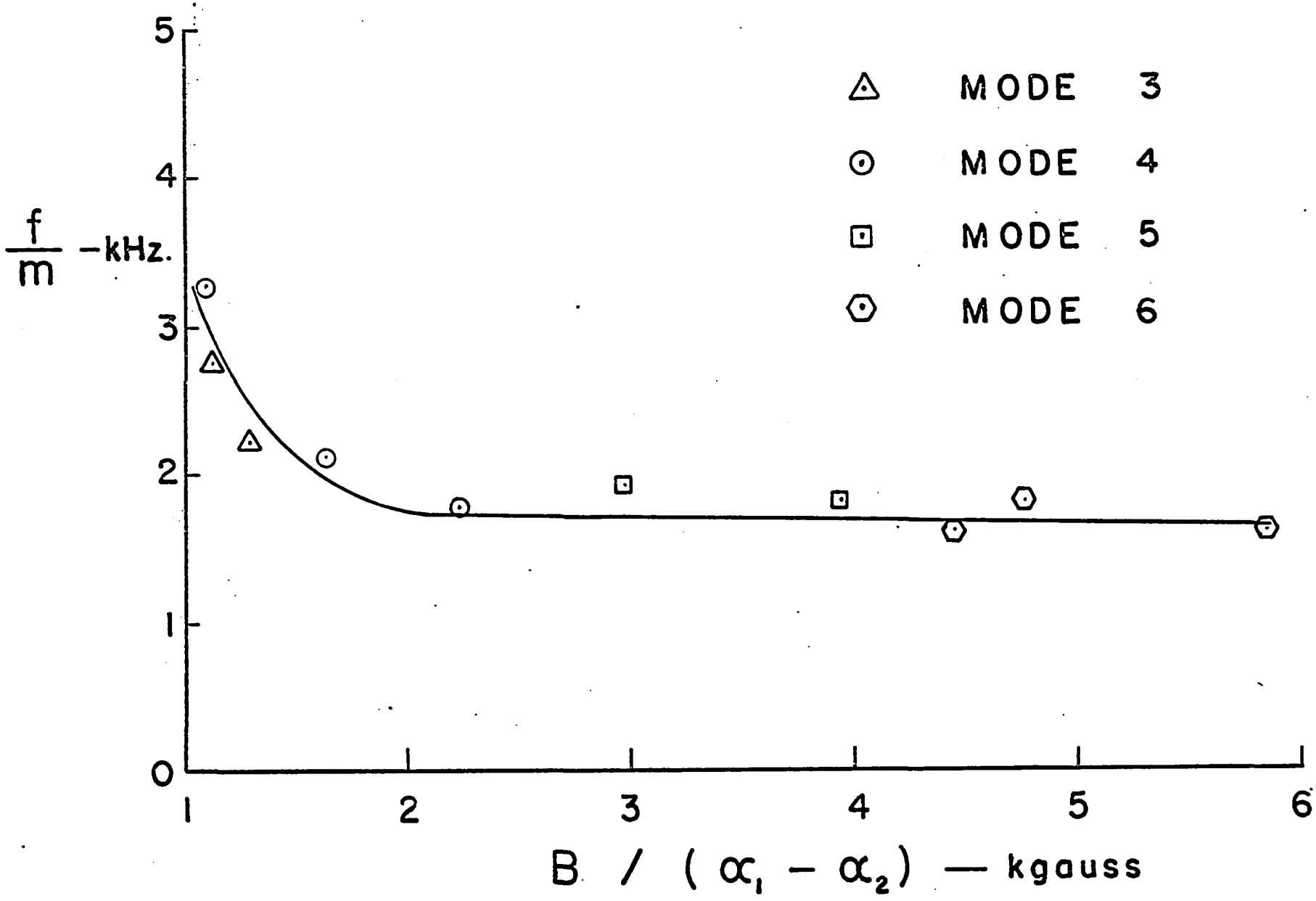

Fig. 3-9 Frequency dependence on magnetic field

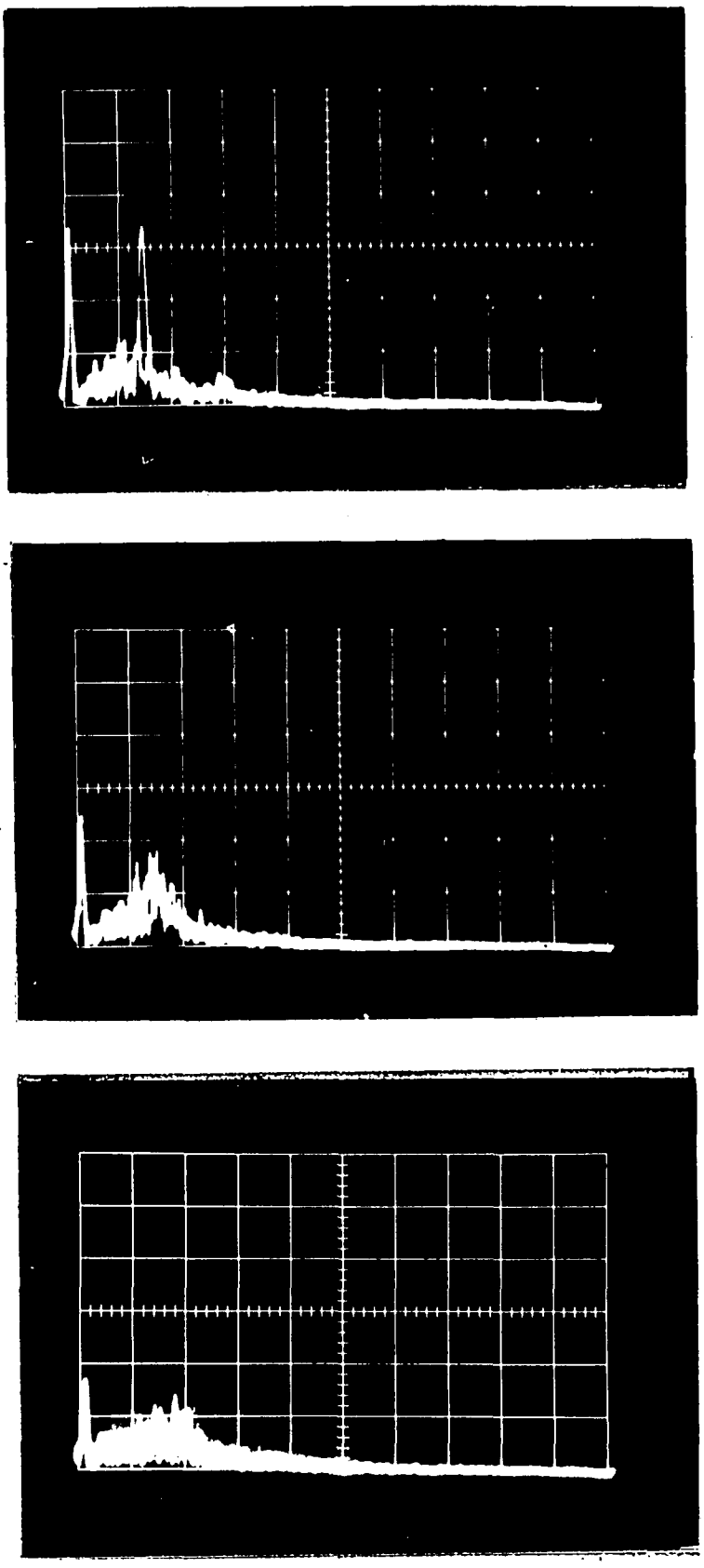

Fig. 3-10 High magnetic field spectra

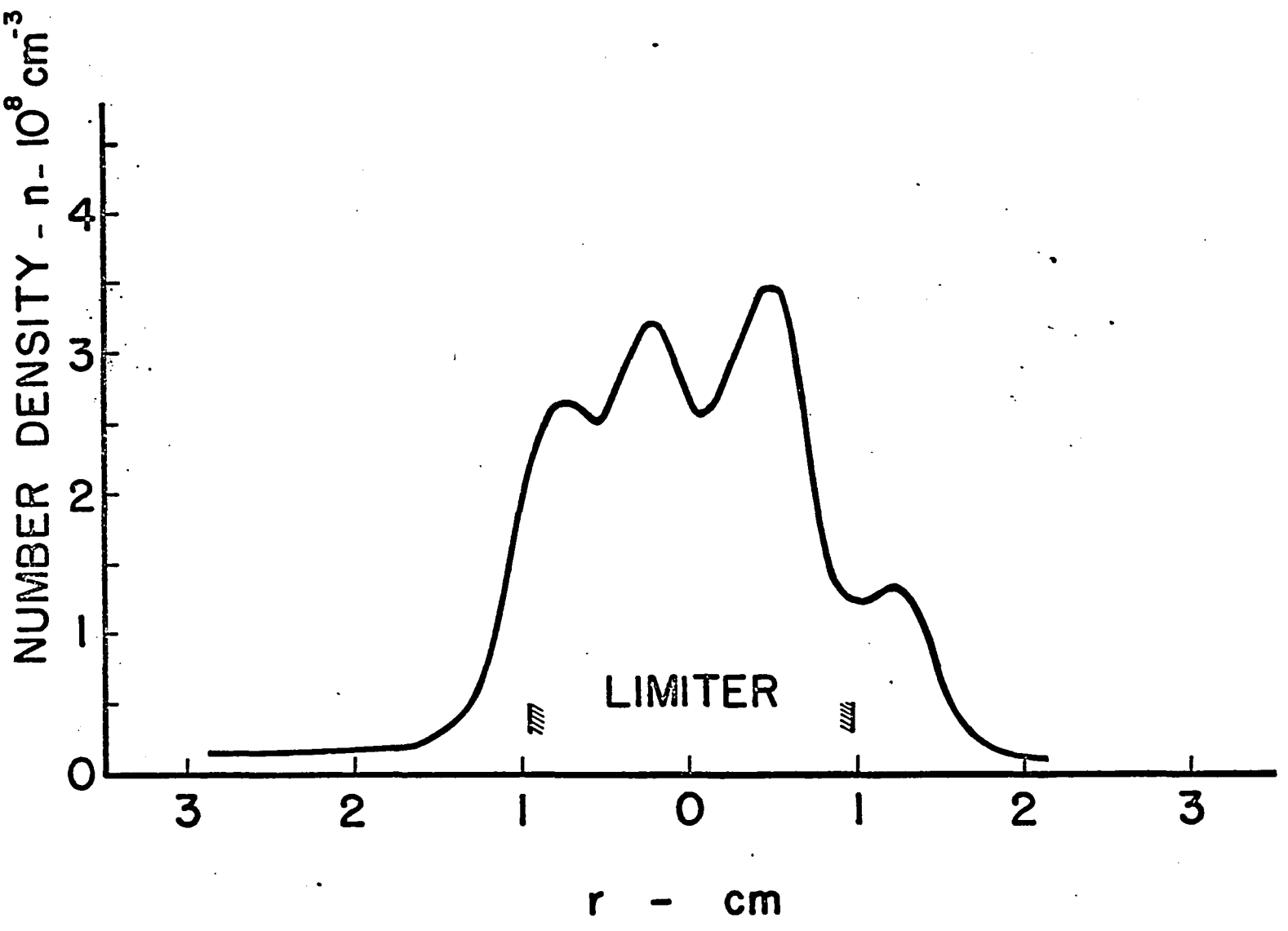

Fig. 3-11 Density profile with feedback

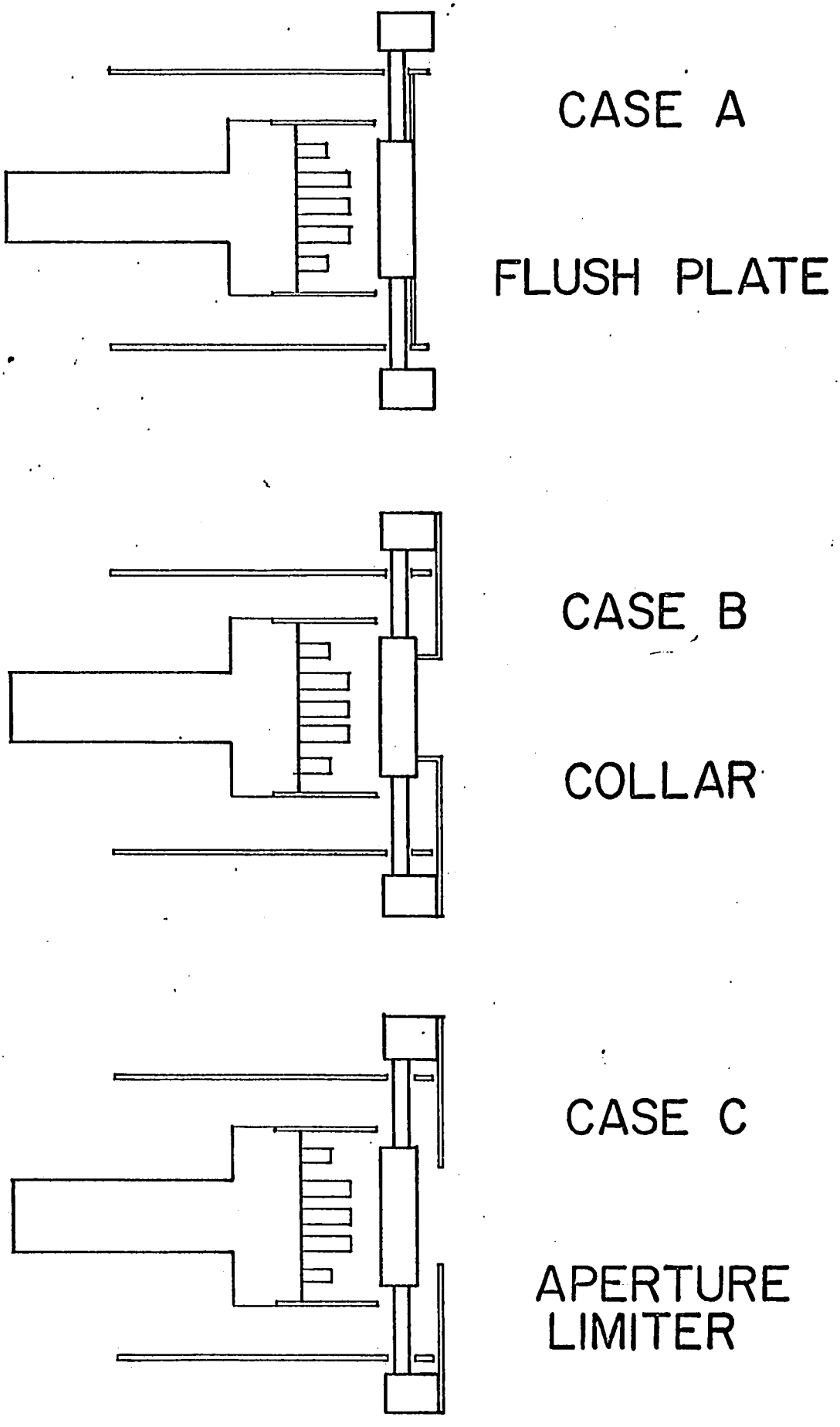

Fig. 3-12 Electrode assembly configuration

welded inside an ordinary aperture limiter. Case C is the ordinary aperture limiter usually used in Q-machines to create the plasma column. It should be noted that these tests were performed with the annular manifold in place; the manifold has an inside diameter of 38 mm. and an outside diameter of 63.5 mm. In Figs. 3-13 and 3-14 the density profiles are shown for cases A and B respectively. Comparison of these profiles with that of Fig.3-2 (case C) shows that the changes in boundary conditions made here do not affect the density distribution significantly. The only difference is due to the change in column diameter. In case A the column was limited by the size of the hot plate which has a 25.4 mm. diameter, in case B the inside diameter of the collar configuration was 22.2 mm and the aperture limiter in case C had a diameter of 19.05 mm.

The oscillation spectra which correspond to cases A and B are also shown in Figs. 3-13 and 3-14. Comparing these spectra to that shown in Fig.3-1 shows that the oscillations have not been affected by the change in boundary conditions. From this data it can be concluded that the mechanical "scraping off" of particles is not responsible for exciting the observed oscillations.

3-10 Summary

In this chapter an oscillation observed in a Q-machine has been described. The wave was observed for magnetic fields between

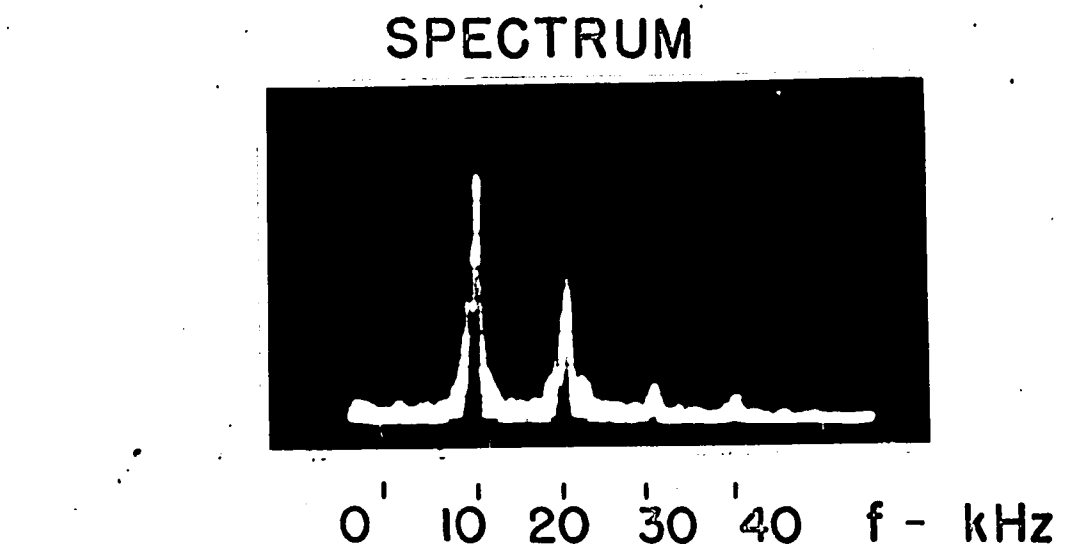

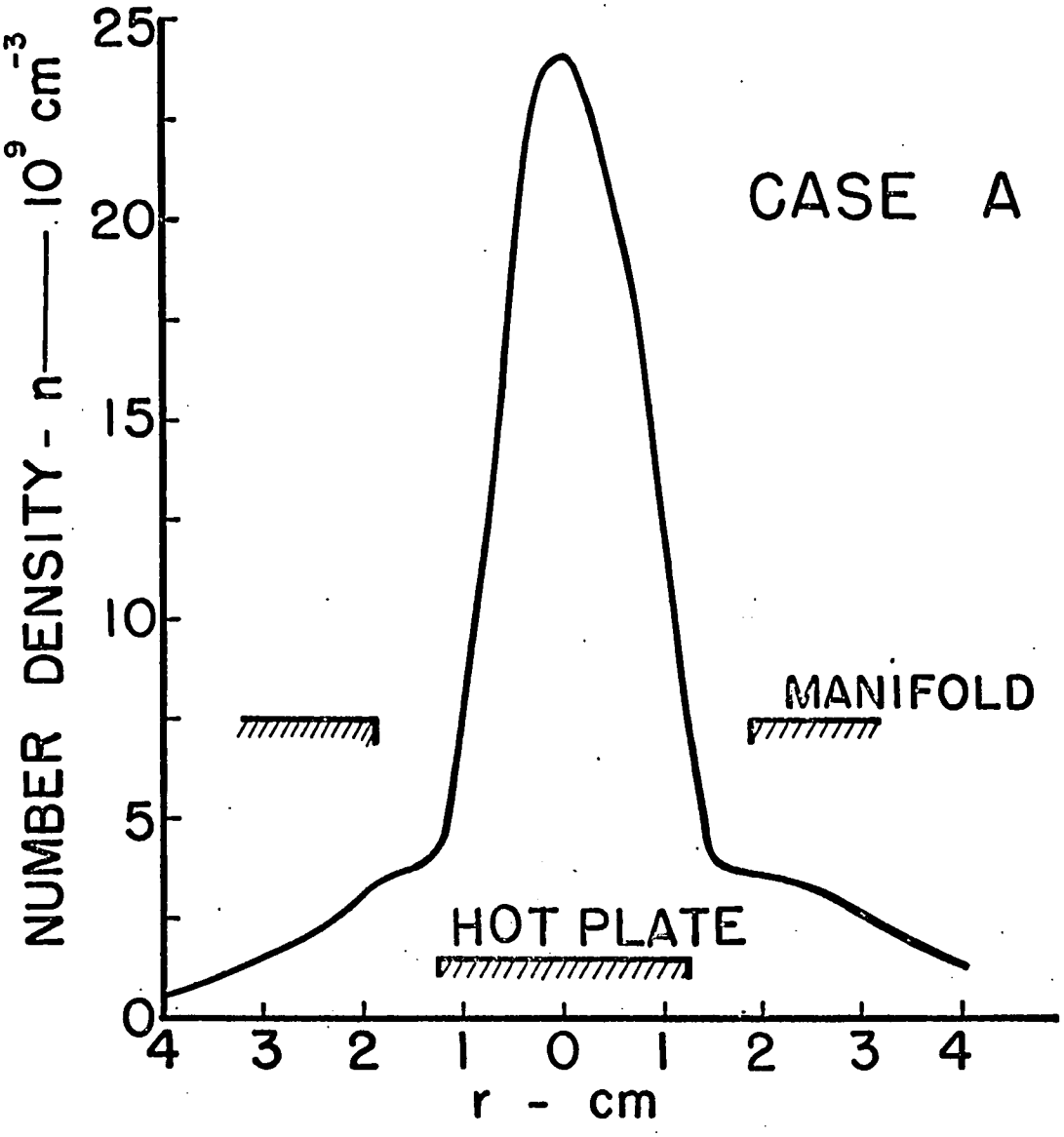

Fig. 3-13 Density profile and spectrum (case A)

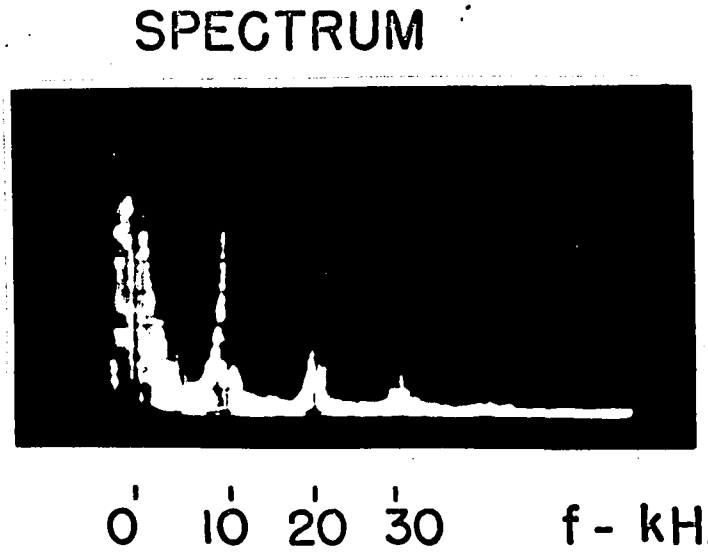

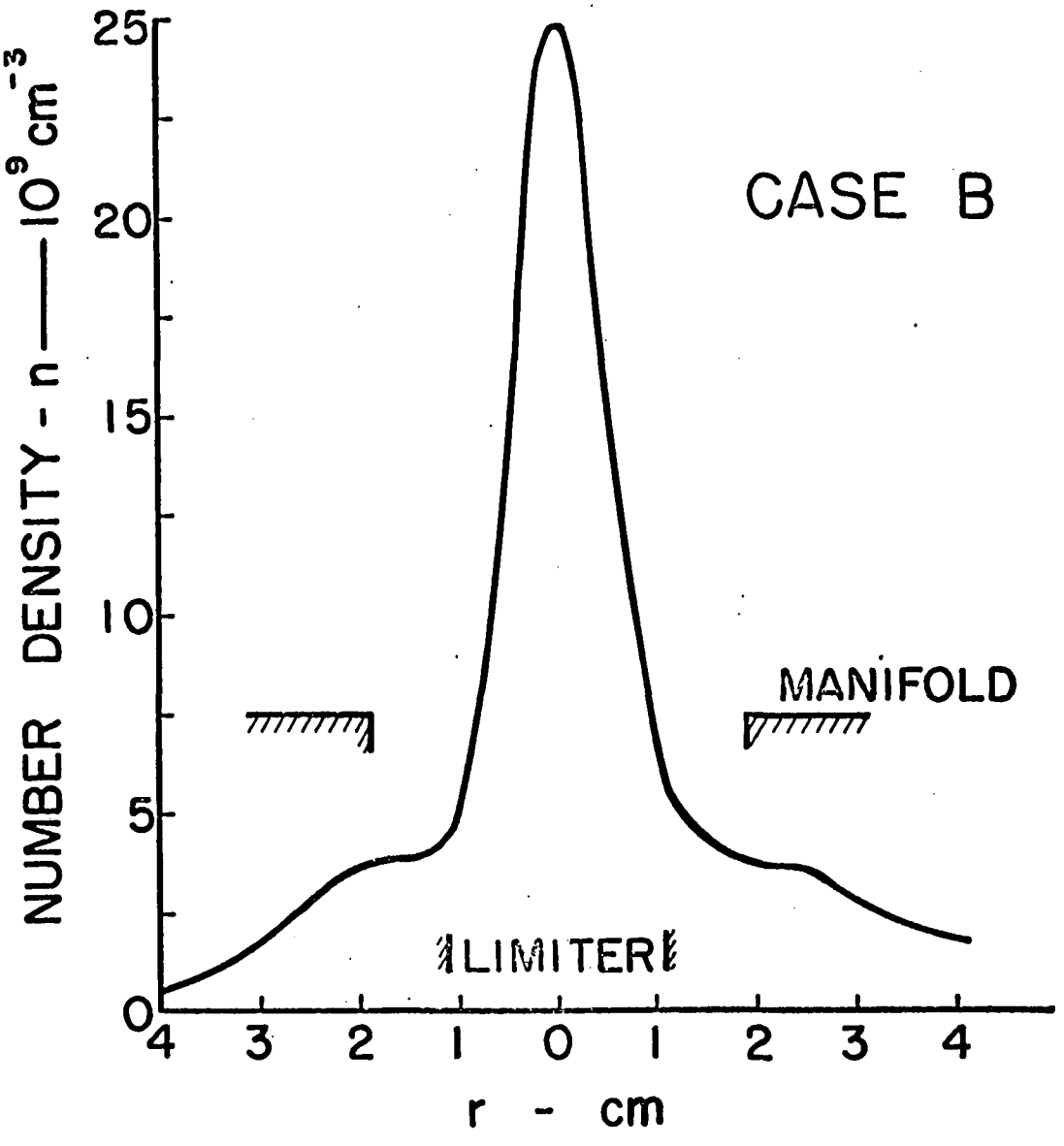

Fig. 3-14 Density profile and spectrum (case B)

500 and 5200 gauss, for cathode temperatures from 2000 to 2400°K and for densities ranging from 5×10^8 to 5×10^{10} particles per cu.cm. The following important properties have been measured:

1. $k_{\parallel} \approx$ zero.
2. The maximum amplitude of the wave peaks sharply at the edge of the plasma column.
3. The wave propagates azimuthally.
4. There is no radial propagation.
5. The dominant mode observed depends on $B/(\alpha_1 - \alpha_2)$ with higher modes being present for larger values of this parameter.
6. The frequency of an observed mode decreases for increasing $B/(\alpha_1 - \alpha_2)$.
7. The wave is not excited by the mechanical "scraping off" of particles by the aperture limiter.

Edge oscillations observed in Q-machines have not yet been explained theoretically. In the next chapter the equation for the flute-type instability in a non-uniform electric field is solved. The solution presented is the first known solution of this equation and it will be shown in Chapter 5 that this theory describes the experimental observations.

CHAPTER 4

THEORY

In an ordinary fluid there are two well known types of instabilities:

1. The Rayleigh-Taylor instability which may occur whenever a heavy fluid is supported by a light fluid against gravity.
2. The Kelvin-Helmholtz instability which may occur whenever two adjacent layers of fluid move with different velocities thereby producing shear in the velocity.

The analog of these two instabilities in the MHD regime has been known for some time.[23] In an MHD fluid the ratio of particle pressure to magnetic pressure, β, is of order unity, hence perturbations in the density create perturbations in the magnetic field; in low β plasmas, the zero order magnetic field remains unperturbed. In the case of Rayleigh-Taylor instability the magnetic field places the lighter fluid, while in the case of Kelvin-Helmholtz instability there exists shear in the velocity. For low-β plasmas the flute mode corresponding to Rayleigh-Taylor instability is called a gravitational flute, while the mode corresponding to Kelvin-Helmholtz instability is called a flute mode in a non-uniform electric field. The non-uniform radial electric field produces velocity shear through the resulting

$E_r \times B$ drift.

In both types of flutes a destabilizing drift is produced by a force field (either an effective gravity or an electric field). In the case of the gravitational flute the problem has been solved, but for the flute instability in a non-uniform electric field no solution is available. In this chapter a solution for the flute mode in a non-uniform radial electric field is presented and the driving mechanism of flute modes is described.

4.1 Description of Plasma Flute Modes

For the flute mode including FLR effects, the resulting dispersion relation is given by:[15]

$$\omega^2 + \omega k \left[\frac{g}{\Omega} + \frac{v_{th}^2}{2\Omega} \frac{n'}{n_o} \right] + g \frac{n'}{n_o} = 0$$

where ω is the frequency, k is the wave number, g is the effective gravitational force, v_{th} is the thermal speed of the ions, n_o is the zero order density and where primes denote derivatives with respect to the position coordinate. If the Larmor radius, v_{th}/Ω, is zero the dispersion relation takes the simpler form:

$$\omega^2 + \omega k \frac{g}{\Omega} + g \frac{n'}{n_o} = 0$$

This expression may be derived from the two-fluid MHD equations without FLR effects.[11] A further simplification results if one assumes the phase velocity of the wave ($\frac{\omega}{k}$) to be much greater than

the gravitational drift ($\frac{g}{\Omega}$):

$$\omega^2 = -g \frac{n'}{n_o} \quad ,$$

showing that the plasma is unstable whenever gravity acts in the direction of decreasing density. Now the driving mechanism will be described.

Consider a plane geometry configuration, Fig.4-1. The effective gravitational force acts in the negative x-direction, the density gradient in the y-direction and the magnetic field in the z-direction. Since the gravitational force depends on particle mass, its affect on the electron motion is neglected: it produces only a zero order ion drift. FLR effects will be considered later. Due to the charge separation produced by the differential drifts of ions and electrons in the gravitational field a perturbed electric field forms which, in turn, gives rise to electric and inertial drifts. These drifts move plasma in region 1 (Fig.4-1) toward the y-z plane from below and move plasma in region 2 toward the y-z plane from above. In region 1 the drifts tend to cancel the charge separation causing the drifts but in region 2 the effect is to increase the charge build-up. Since charge brought in from region 2 comes from a source of higher density (due to the density gradient) than that of region 1, the space charge is increased. When the drift due to the gravitational field is of the same order as the phase velocity of the wave shortwave perturbations will be damped,

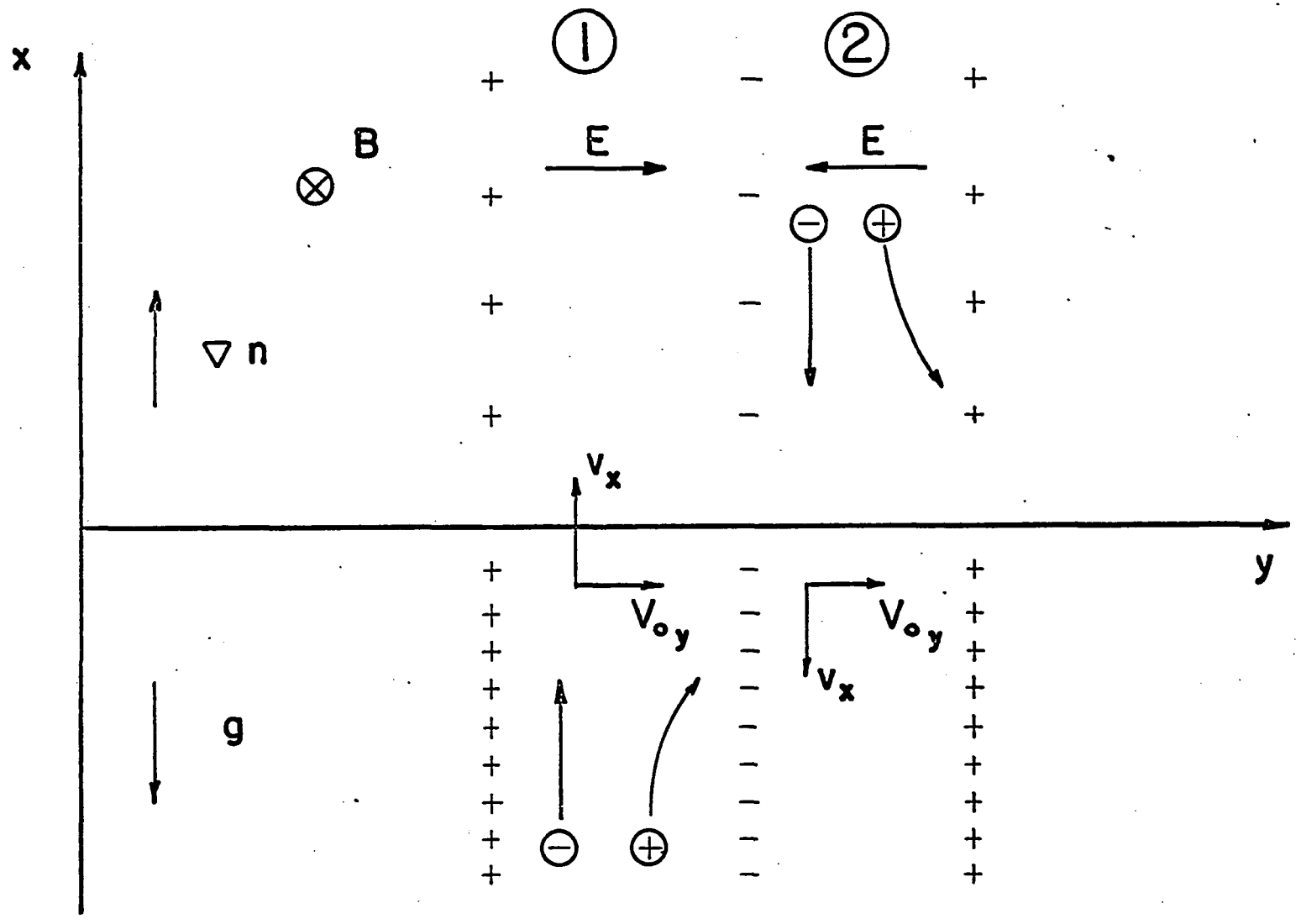

Fig. 4-1 Description of flute mode

as can be understood from the following argument. The gravitational drift carries space charge in the direction of increasing y, so that in time the direction of the electric fields in the two regions will be reversed. This tends to cancel the space charge in both regions. For short wave lengths there is not enough time for the charge to build up between changes in the direction of the electric field and these wavelengths are damped. In the case of long wavelengths there is sufficient time for the charge to build up: residual space charge from one period is enhanced during the next period. This causes instability through a growing wave (overstability) and is shown quantitatively from the stability condition for this case:[14]

$$k^2 \geq 4 \frac{\Omega^2}{g} \frac{n'}{n_o}$$

When FLR effects are considered the stability condition becomes[15]

$$\frac{k^2}{\Omega^2} \left(g + \frac{v_{th}^2}{2} \frac{n'}{n_o} \right)^2 \geq 4 g \frac{n'}{n_o}$$

in which an additional term depending on the Larmor radius has entered. Physically, the effect of this term is to speed up the wave in the y-direction thereby enhancing the damping due to gravitational drift.

The flute instability just described is well understood, but when non-uniform electric fields are included in the analysis the problem is not easily solved. This problem is discussed in the next

section.

4.2 Flute Instability in a Non-uniform Electric Field

When the effects of the non-uniform electric field are considered the flute instability is analogous to the Kelvin-Helmholtz instability of a fluid: the velocity shear is the driving force. As for the gravitational flute instability FLR effects play an important part in determining both the real part of the frequency and the stability of a given mode. The eigenvalue problem formulated by Rosenbluth and Simon[1] for cylindrical geometry takes the form of a differential equation:

$$(T\psi')' + \left[\frac{(1-m^2)}{r^2} T + r^2 \omega^2 \rho'\right] \psi = 0$$

$$\psi = \frac{E_\theta}{\bar{\omega}}, \quad \bar{\omega} = \omega + \frac{m}{r} V_o \tag{1}$$

$$T = r^3 \bar{\omega} \left(\rho \bar{\omega} + \frac{\gamma}{r} \rho'\right), \quad \gamma = \frac{m}{2} \frac{v_{th}^2}{\Omega}$$

where E_θ is the perturbed electric field in the θ direction, V_o is the zero order drift velocity in the θ direction, ω is the frequency, m is the mode number, ρ is the density and where v_{th} is the thermal velocity of the ions. The equation is linear, of second order, has variable coefficients which may be complex, and is singular.

4.3 Solution of the Eigenvalue Problem

The geometry corresponding to the equilibrium configuration for which Eq. (1) will be solved is shown in Fig.4-2. The constant and uniform magnetic field acts in the z-direction. A zero order electric field acts in the negative r-direction producing a zero order drift velocity in the θ direction. It is assumed that the density, ρ, and the zero order rotation, $\frac{V_o}{r}$, are constant in two adjacent regions, but suffer a jump discontinuity at $r = r_s$, as shown in the lower part of Fig.4-2.

In each of the two regions where ρ and $\frac{V_o}{r}$ are constant Eq. (1) becomes

$$\psi'' + \frac{3}{r}\psi' + \frac{(1-m^2)}{r^2}\psi = 0 \tag{2}$$

which is of Euler-Bernoulli form and has as its solution

$$\psi = Cr^{m-1} + Dr^{-m-1} \tag{3}$$

For $m > 1$ the boundary conditions require that ψ vanish at r equal to zero and infinity. The case $m = 1$ must be treated separately. If the region $0 \le r \le r_s$, is called region "1" and the region $r_s \le r$ is called "2" then application of the boundary conditions in each region yields from Eq. (3)

$$\begin{aligned} \psi_1 &= C_1 r^{m-1} \qquad 0 \le r \le r_s' \\ \psi_2 &= D_2 r^{-m-1} \qquad r_s \le r \end{aligned} \tag{4}$$

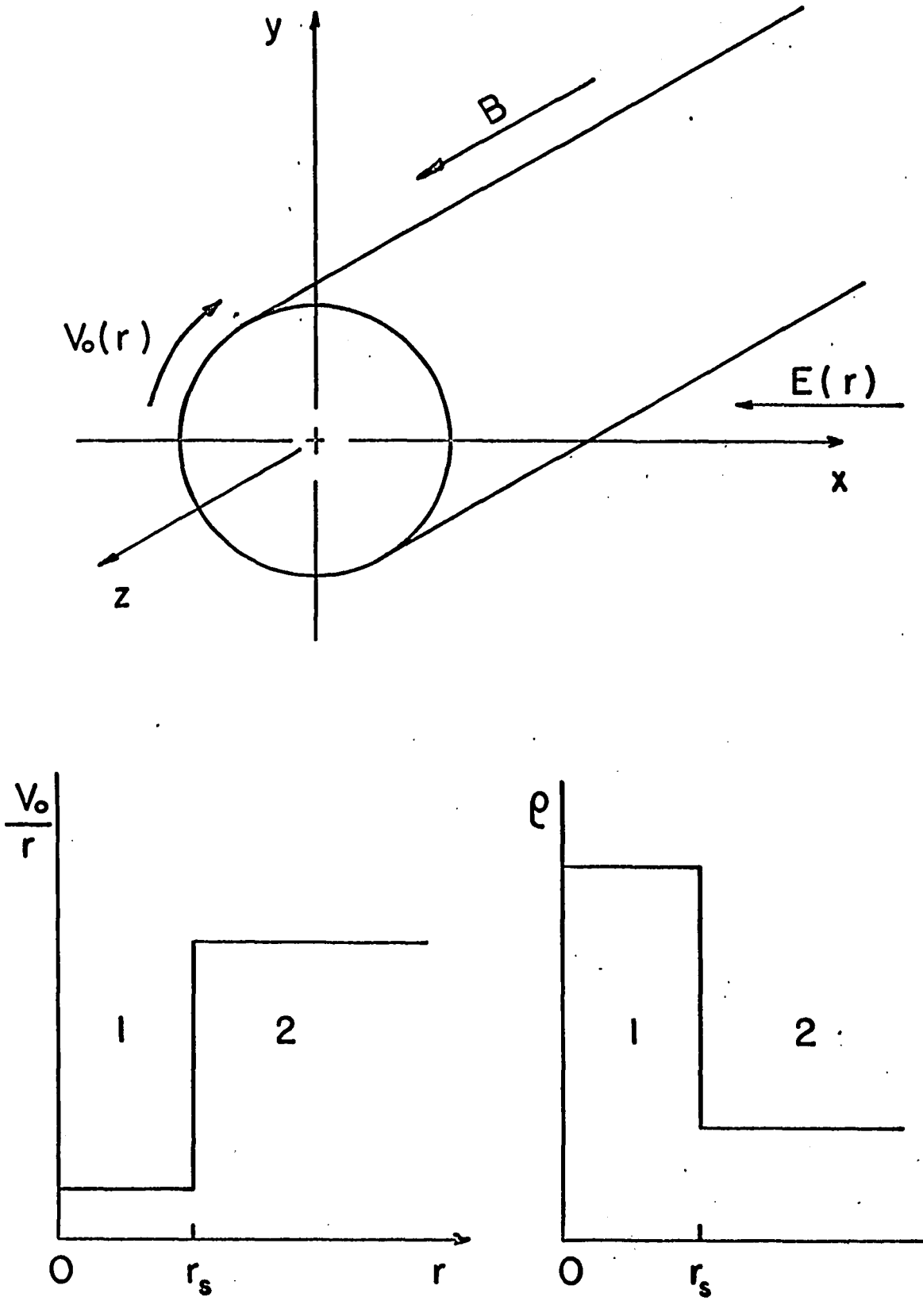

Fig. 4-2 Configuration for non-uniform electric field

The constants C_1 and D_2 will be eliminated by the establishment of a jump condition at $r = r_s$ which will lead to the characteristic equation for the frequencies. Before finding the jump condition it is necessary to show that ψ is continuous across r_s. The jump condition will be found by integrating Eq. (1) from $r_s - \epsilon$ to $r_s + \epsilon$ and the limit taken as ϵ goes to zero.

The displacement of the surface of discontinuity is represented by

$$F(r, \theta, t)$$

The condition that the plasma at the surface moves with the surface leads to

$$\frac{d}{dt} F = \frac{E_\theta}{B} \tag{5}$$

where the right hand side is the perturbed velocity in the r direction to lowest order in Larmor radius. Since the surface may be assumed to oscillate in the same way as the other variables, i.e., exp. $i(\omega t + m\theta)$ one obtains from (5) using $\frac{d}{dt} \rightarrow (\omega + \frac{m}{r} V_o)$

$$iF\left(\omega + \frac{m}{r} V_o\right) = \frac{E_\theta}{B} \tag{6}$$

or using the definition of ψ

$$\psi = iBF \tag{7}$$

which shows that ψ is continuous to lowest order at $r = r_s$.

Now Eq. (1) can be integrated to find the jump condition at r_s. Rewriting the equation one has

$$\lim_{\epsilon \to 0} \int_{r_s-\epsilon}^{r_s+\epsilon} \{ (T\psi')' + [(1-m^2)\gamma\overline{\omega} + r^2\omega^2]\rho'\psi + (1-m^2)\overline{\omega}^2\rho r\psi \} = 0 \qquad (8)$$

Terms which are bounded (in this case the last term) will vanish upon taking the limit $\epsilon \to 0$. The first and second terms will contribute to the jump condition since derivatives of functions which are discontinuous appear in these terms which makes them unbounded. After performing the integrations and going to the limit the jump condition is found to be

$$\Delta_s (T\psi') + [(1-m^2)\gamma\overline{\omega}_s + r_s^2\omega^2]\psi_s \Delta_s \rho = 0 \qquad (9)$$

where

$$\Delta_s(f) \equiv f(r_s^+) - f(r_s^-) \equiv f_2 - f_1$$

and where

$$\overline{\omega}_s \equiv \omega + \frac{m}{2r}(V_{O_1} + V_{O_2})$$

The values for ψ_1' and ψ_2' are found by differentiating Eq. (4)

$$\begin{aligned} \psi_1')_s &= C_1(m-1)r_s^{m-2} = \psi_s(m-1)r_s^{-1} \\ \psi_2')_s &= -D_2(m+1)r_s^{-m-2} = \psi_s(m+1)r_s^{-1} \end{aligned} \qquad (10)$$

where the continuity of ψ at r_s has been used. Now Eq. (10), the definition of T and the new quantities

$$\alpha_1 = \frac{\rho_1}{\rho_1+\rho_2} \ , \quad \alpha_2 = \frac{\rho_2}{\rho_1+\rho_2} \ , \quad \bar{\gamma} = \frac{\gamma}{m} \tag{11}$$

may be used in Eq.(9) to yield the equation for the characteristic frequencies

$$\omega^2 + \left\{\frac{2}{r_s}\left[(m+1)V_{O_2}\alpha_2 + (m-1)V_{O_1}\alpha_1\right] - (\alpha_2-\alpha_1)\frac{(1-m^2)}{r_s^2}\bar{\gamma}\right\}\omega$$

$$+ \frac{m(m+1)}{r_s^2}V_{O_2}^2\alpha_2 + \frac{m(m-1)}{r_s^2}V_{O_1}\alpha_1 - (\alpha_2-\alpha_1)\frac{m(1-m^2)}{2r_s^3}\bar{\gamma}(V_{O_1}+V_{O_2}) = 0 \tag{12}$$

which may be solved to give

$$\omega = -\frac{1}{r_s}\left[(m+1)V_{O_2}\alpha_2 + (m-1)V_{O_1}\alpha_1\right] + \frac{(1-m^2)}{2r_s^2}(\alpha_2-\alpha_1)\bar{\gamma}$$

$$\pm\left\{\frac{1}{r_s^2}\left[(m+1)V_{O_2}\alpha_2 + (m-1)V_{O_1}\alpha_1 - \frac{(1-m^2)}{2r_s}(\alpha_2-\alpha_1)\bar{\gamma}\right]^2\right. \tag{13}$$

$$\left. - \frac{1}{r_s^2}\left[m(m+1)V_{O_2}^2\alpha_2 + m(m-1)V_{O_1}^2\alpha_1 - \frac{m(1-m^2)}{2r_s}(\alpha_2-\alpha_1)(V_{O_1}+V_{O_2})\bar{\gamma}\right]\right\}^{\frac{1}{2}}$$

Stability requires that ω be real which yields the condition for stability

$$\left[(m+1)V_{O_2}\alpha_2 + (m-1)V_{O_1}\alpha_1 - \frac{(1-m^2)}{2r_s}(\alpha_2-\alpha_1)\bar{\gamma}\right] >$$

$$m(m+1)V_{O_2}^2\alpha_2 + m(m-1)V_{O_1}^2\alpha_1 - \frac{m(1-m^2)}{2r_s}(\alpha_2-\alpha_1)(V_{O_1}+V_{O_2})\bar{\gamma} \tag{14}$$

The physical meaning of the stability condition is seen more clearly

if Eq. (14) is rewritten

$$-m^2\alpha_1\alpha_2(V_{O_2}-V_{O_1})^2 - m(1-2\alpha_2)(V_{O_2}^2\alpha_2+V_{O_1}^2\alpha_1)+(V_{O_2}\alpha_2-V_{O_1}\alpha_1)^2$$

$$+\overline{\gamma}(\alpha_2-\alpha_1)(1-m^2)\left[\frac{m}{2r_s}(V_{O_1}+V_{O_2})-\frac{(m+1)}{r_s}V_{O_2}\alpha_2-\frac{(m-1)}{r_s}V_{O_1}\alpha_1\right. \qquad (15)$$

$$\left.+\frac{\overline{\gamma}}{4}(\alpha_2-\alpha_1)(1-m^2)\right] > 0$$

Expression (15) will be discussed below.

4.4 Discussion of Results

The first term in Eq. (15) is due to the shear in the velocity. This is the main mechanism which drives the instability. The second and third terms are due to the cylindrical geometry and do not appear in the analysis for a plane geometry. The net effect of these two terms is destabilizing and is caused by the centrifugal force which acts to push more dense plasma to a region of less dense plasma. The last term contains the FLR effects. The net effect of the FLR term is stabilizing and since it is multiplied by a factor $(1 - m^2)$ it is more stabilizing for the higher mode numbers (short wavelengths). This is the result obtained for the gravitational flute instability.[10]

4.5 Solution for Mode One

For $m = 1$, Eq. (1) degenerates to

$$(T\psi')' + r^2\omega^2\rho'\psi = 0 \qquad (16)$$

In the two regions where ρ and $\frac{V_o}{r}$ are constant, ψ must now satisfy

$$\psi'' + \frac{3}{r}\psi' = 0 \tag{17}$$

which has the solution

$$\psi = -\frac{D}{2r^2} + C \tag{18}$$

In region 2 the boundary condition that ψ vanish as r becomes infinite requires that $C = 0$, hence

$$\psi_2 = -\frac{D}{2r^2} \tag{19}$$

The boundary condition (as r goes to infinity) is the same as for $m > 1$, however in region 1, ψ is no longer required to vanish at $r = 0$. The reason for this is implicit in the physical meaning of $m = 1$ which represents an off axis displacement of the plasma column as a whole. Now it is only required that ψ be bounded at the origin. This leads to the solution in region 1:

$$\psi_1 = C \tag{20}$$

The jump condition for this case is found from Eq. (17) as

$$\Delta_s (T \psi') + r_s^2 \omega^2 \psi_s \Delta_s \rho = 0 \tag{21}$$

On substituting Eqs. (19) and (20) one finds the dispersion relation

$$\omega^2 + 4\alpha_2 \frac{V_{O_2}}{r_s}\omega + 2\alpha_2 \frac{V_{O_2}^2}{r_s^2} = 0 \tag{22}$$

This leads to the expression for the frequencies

$$\omega = -2\alpha_2 \frac{V_{O_2}}{r_s} \pm \frac{V_{O_2}}{r_s} [\alpha_2 (4\alpha_2 - 2)]^{\frac{1}{2}} \qquad (23)$$

4.6 Discussion of Results for Mode One

Notice that for this case no FLR effects appear. This is a result of the degeneracy of Eq. (1) for the case of $m=1$. The physical meaning of this lies in the fact that for the case of an off axis shift of the column as a whole the perturbed electric field is a constant in space and therefore the averaging effect of the finite particle orbits gives no contribution. Since α_2 can never be greater than $\frac{1}{2}$ for density profiles which are peaked at the center, mode one is seen to be unstable. The same result has been found by Kadomtsev[14] for the gravitational flute instability.

4.7 Numerical Calculations

To interprete FLR damping affects on the growth rate of the modes, numerical calculations were done for several hypothetical sets of parameters on the IBM 7040 computer at The City College Computation Center. A typical case is presented in Fig. 4-3. The linear growth rate, $\mathrm{Im}(\omega)$, is plotted against mode number for various values of the parameter $\overline{\gamma}$. The parameter $\overline{\gamma}$ is proportional to $r_L v_{th}$ which means $\overline{\gamma}$ is directly proportional to temperature and

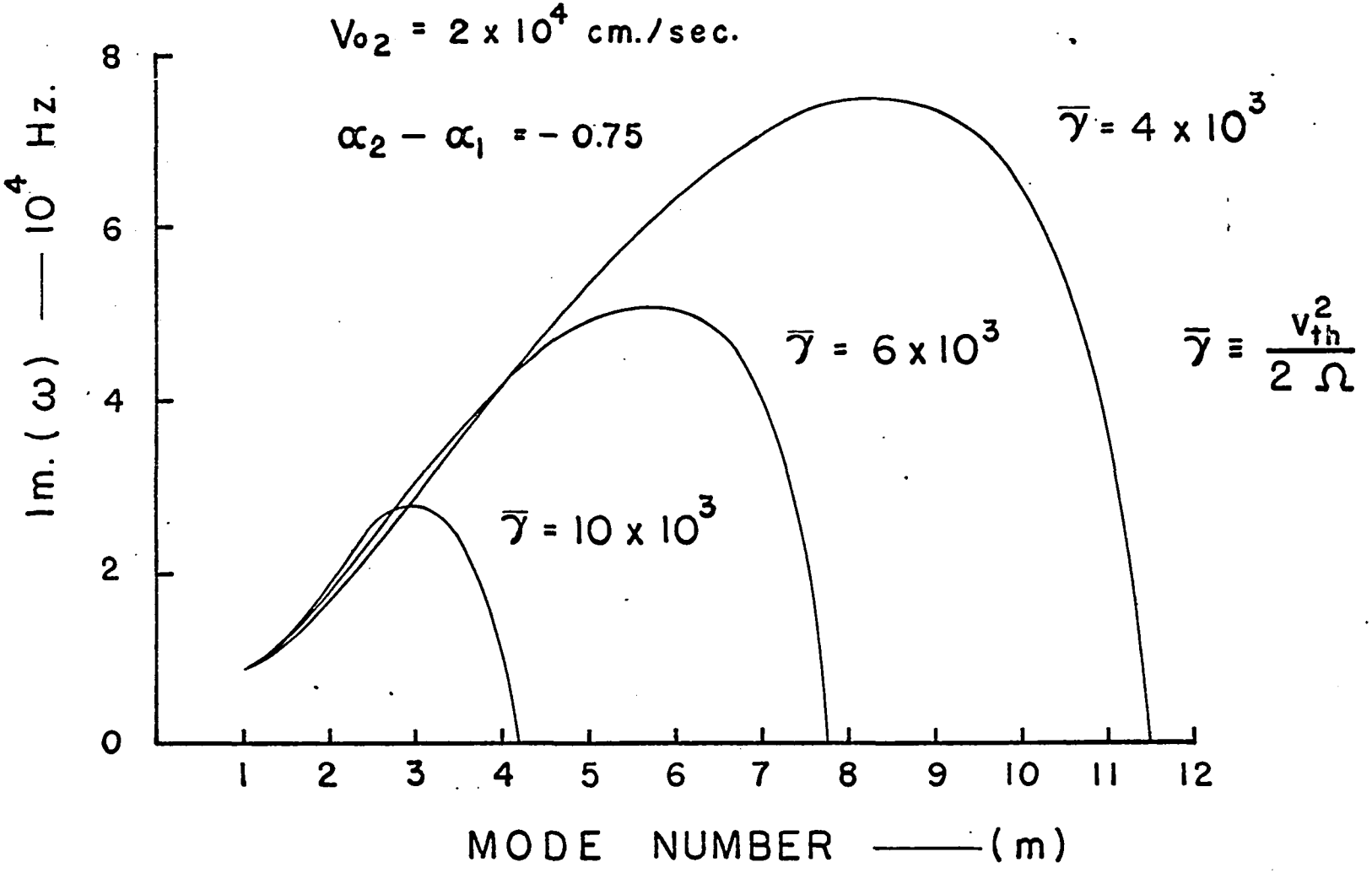

Fig. 4-3 Mode growth rates (Im. ω)

inversely proportional to magnetic field. Several effects are immediately apparent from Fig.4-3. First, the growth rate for $m=1$ is independent of $\overline{\gamma}$ which has already been noted. Second, for lower values of $\overline{\gamma}$ the growth rates of several modes are comparable indicating that more than one mode may be observed at one time. Last, it is seen that for small $\overline{\gamma}$ (large B or low T) the growth rates of higher modes become large. This is expected since for large B the Larmor radius becomes small and therefore FLR damping becomes small. also, it has been shown[16] that in the limit $\overline{\gamma} \to 0$ Eq. (1) in the case of plane geometry reduces to the equation describing the Kelvin-Helmholtz instability in an ordinary fluid. In fact when Eq.(1) is solved for the case of plane geometry and the limit taken as $\overline{\gamma} \to 0$ the solution is identical with that for the ordinary Kelvin-Helmholtz instability.[24] In this case the higher modes are known to have the largest growth rates. When examining Fig.4-3 one should take into account that the quantity $\alpha_2 - \alpha_1$ always multiplies $\overline{\gamma}$ in Eq. (13) so that if $\overline{\gamma}$ is replaced by a constant multiple of $\alpha_2 - \alpha_1$ the resulting curves will be identical to those shown.

The real part of the frequency for the same input as in Fig. 4-3 is shown in Fig. 4-4. For modes greater than mode one the non-linear variation of frequency with mode number deduced in Eq. (13) is illustrated in Fig.4-4. Here, as is the case for the imaginary part of the frequency, there is no FLR effect for mode one.

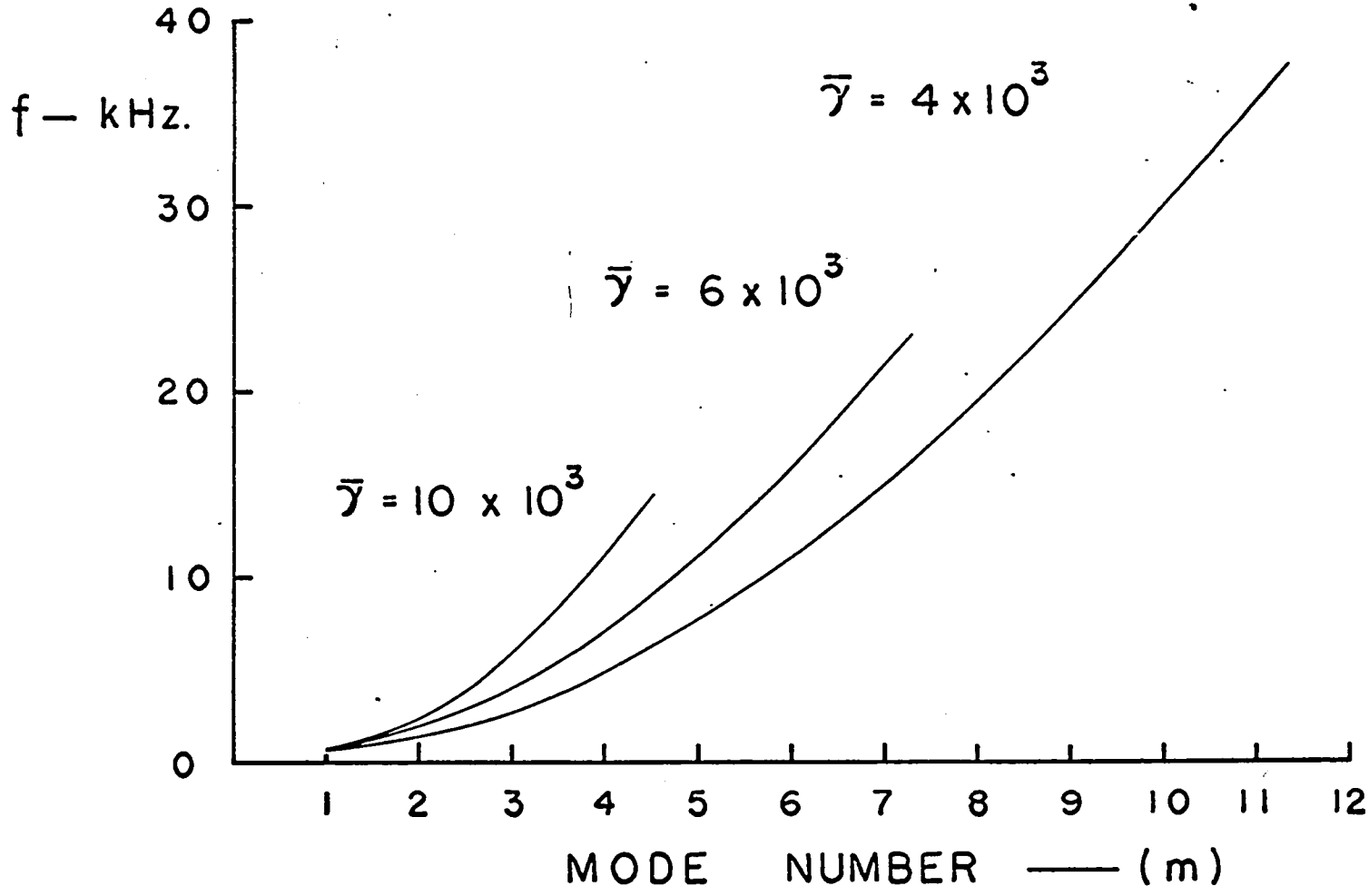

Fig. 4-4 Mode frequencies

For a given mode the frequencies are seen to increase for increasing $\overline{\gamma}$. This means that the frequency increases for decreasing magnetic field when all the other variables are held constant. Such variation is difficult to observe in a Q-machine since a change of magnetic field automatically produces a change of the other parameters so in Chapter 5 the frequencies are compared on a point by point basis.

4.8 The Eigenfunctions

More information about the flute modes can be obtained by examining the eigenfunctions, ψ. These functions are proportional to the wave amplitude by definition. In the experiment the amplitudes are actually limited by nonlinear processes. This will be discussed further in Chapter 5. The dependence of ψ on r is shown in Fig,4-5. Since ψ must vanish at the origin, the eigenfunction in region 1 must increase with a power of r while the vanishing of ψ at infinity means must decrease with an inverse power of r. The continuity of ψ at r_s means that $\psi_1 = \psi_2$ there. Notice that for the higher modes ψ peaks sharply at r_s. If r_s occurs at the edge of the column as it does in a Q-machine, then this amplitude variation is indicative of an edge oscillation. For the case when $m = 1$ the eigenfunction is constant in region 1 and does not peak at r_s, but falls off as r^{-2} for r greater than r_s. This is consistent with the physical picture of mode one given earlier.

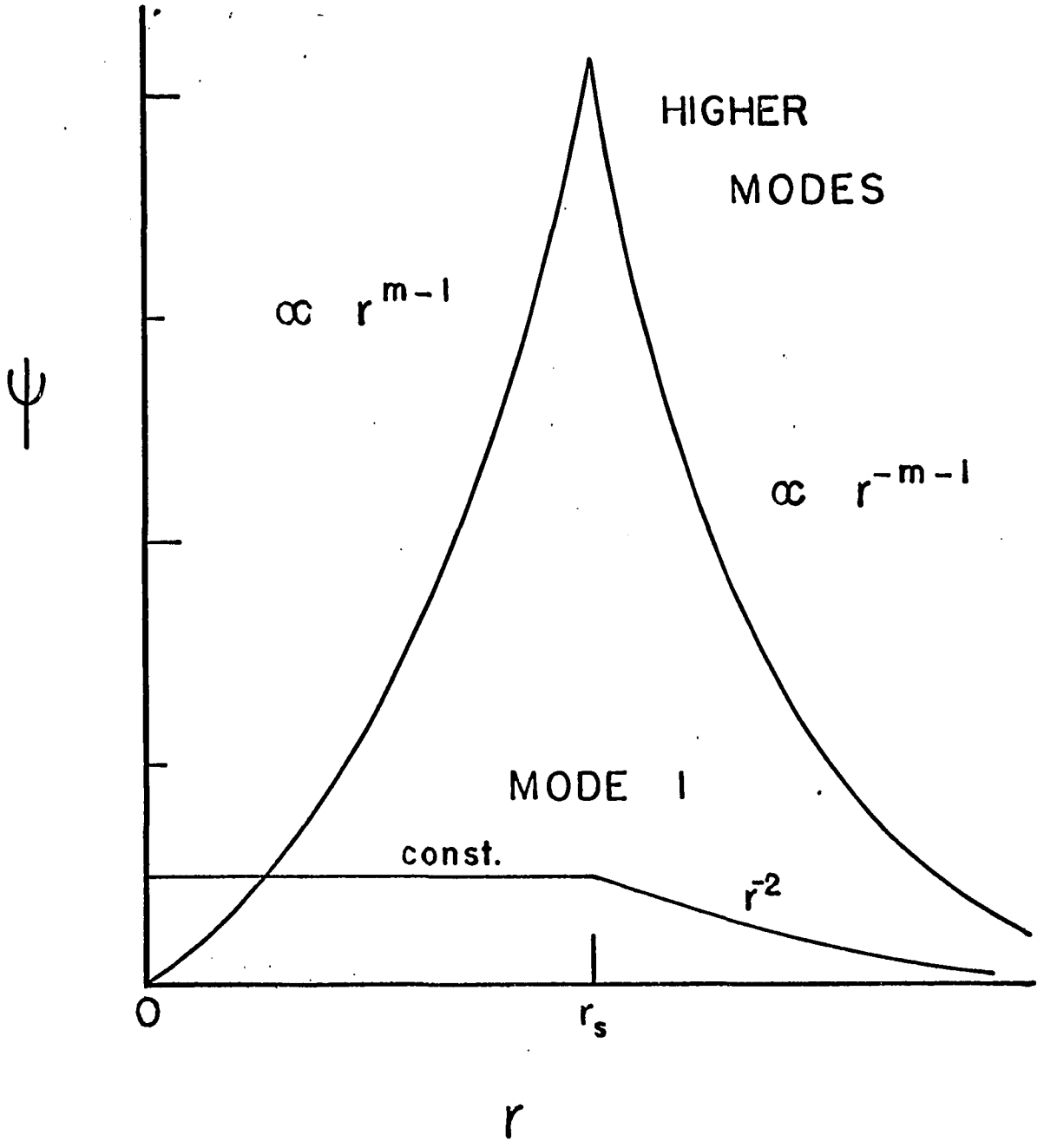

Fig. 4-5 Eigenfunction dependence on position

4.9 Three Region Solution

Now that the two region has been discussed and the main physical features of the theory have been made apparent, the experimentally interesting case of three regions is considered. Looking at the potential profiles in Fig. 3-2 it will be seen that there are three distinct slopes corresponding to three different regions where V_o is constant. In the interior of the plasma $V_o = 0$, at the edge of the column V_o is very large and then breaks into a region where V_o is relatively small. In this case there are three regions with two discontinuities leadking to three solutions of Eq. (1) and two jump conditions. The following assumptions which have been guided by the experiments have been made:

1. $\frac{m}{r} V_{O_2} \gg \omega$

2. $r_{12} \sim r_{23}$

where r_{12} is the radius of the discontinuity between regions 1 and 2 and r_{23} is the radius of the discontinuity between regions 2 and 3. The characteristic equation for the frequencies for this case is

$$\delta(m^2-1)\rho_2 \bar{\omega}_2^2 + (m-1)\rho_1 \bar{\omega}_1^2 + (m+1)\rho_3 \bar{\omega}_3^2 - \left[\omega^2 + m^2(1-m^2)\bar{\gamma}\frac{V_{O_2}}{r_{12}}\right](\rho_3 - \rho_1) = 0 \tag{24}$$

where the symbol, δ, is defined by

$$\delta = \frac{r_{23} - r_{12}}{r_{12}}$$

This dispersion relation is derived in Appendix B. It is shown that the assumption $\frac{m}{r} V_{O_2} \gg \omega$, makes the FLR correction to the real part of the frequency small. The factor δ, which multiplies the contribution from the second region, represents a weighting factor depending on the thickness of region two. If one formally sets δ equal to zero one expects to recover the two region solution. This, however, must be done before the above restriction on V_{O_2} is made, as shown in Appendix B.

4.10 Summary

In this chapter the mechanism of excitation of flute instabilities has been described. In the presence of non-uniform electric fields the instability resembles the Kelvin-Helmholtz instability of an ordinary fluid. The eigenvalue problem formulated by Rosenbluth and Simon[1] has been solved for the special case when the density and zero order drift velocity divided by r are constant in two adjacent regions and suffer a jump discontinuity on the surface of the cylinder $r=r_s$. The choice of this special case leads to a differential equation in each of the two regions for which the solution is known. These solutions are used in a jump condition at $r=r_s$ in order to solve for the frequencies. The important results are:

1. The shear in the velocity drives the instability similar to the Kelvin-Helmholtz instability of an ordinary fluid.

2. FLR effects stabilize for short wavelengths similar to the case of the gravitational flute instability.
3. Mode one has no FLR effects.
4. The eigenfunctions which are proportional to the wave amplitude peak sharply at $r = r_s$ which is characteristic of edge oscillations in Q-machines.
5. The equation for the frequencies is presented when three regions exist in the plasma. The results show that the thickness of the center region, where the velocity is high, is important in determining the frequency and stability of the different modes.

In the next chapter, the theoretical results are compared with the experimental data.

CHAPTER 5

COMPARISON OF THEORY WITH EXPERIMENT AND CONCLUSIONS

In the last chapter the differential equation for a flute mode in a non-uniform electric field was solved for the case of two distinct regions in a cylindrical plasma column and the dispersion relation for the three region case was given. The solution to the two region problem made clear the physical mechanism of the instability and the FLR effects. This solution is not applicable to experiments in a Q-machine because the plasma shows three well defined regions rather than two. Therefore in this chapter the three region solution will be compared with the experiment.

It should be noted that the assumption that $k_{\parallel}$ is zero has been used in the derivation of Eq. (1). The measurement showing that $k_{\parallel}$ is approximately zero has already been presented in Chapter 3 so that this requirement is satisfied.

5.1 Interpretation of the Data

In order to make a detailed comparison of the theory with the experiment the following parameters in Eq. (25) must first be obtained: ρ_1, ρ_2, ρ_3, V_{O_1}, V_{O_2}, V_{O_3}, δ, and $\overline{\gamma}$. The calculation of $\overline{\gamma}$ presents

no problem since it depends on the temperature which has been measured with a pyrometer and the magnetic field which has been measured with a calibrated gaussmeter. The choice of the other parameters listed above is not so straightforward and the method of choosing them will be explained with the help of Fig. 5-1. In Fig.5-1 is shown a a typical set of floating potential and density profiles for the case when the potassium was sprayed on the hot plate from one nozzle. First consider the potential profile. From this plot one calculates E_o, the zero order electric field, by taking the slope and hence the zero order E x B drift velocity, V_o, can be computed from $V_o = \frac{E_r}{B}$. It will be noticed that there are three well defined slopes in the potential profile in Fig.5-1. From the origin to the edge of the hot plate, the slope is zero. This was the case for most of the runs and indicates that the central core of the column undergoes no drift due to radial electric fields. At the edge of the hot plate there exists a small region in which the potential changes rapidly. This is caused by the change in sheath conditions from the hot plate to the relatively cool aperature limiter. In this region the electric drift is very large creating shear in the velocity at the edge of the plasma column. The third region has a milder slope than the second so there will be additional shear between these two regions.

The densities used are chosen at the center of the region over which V_o is constant. The quantity δ is calculated from the definition

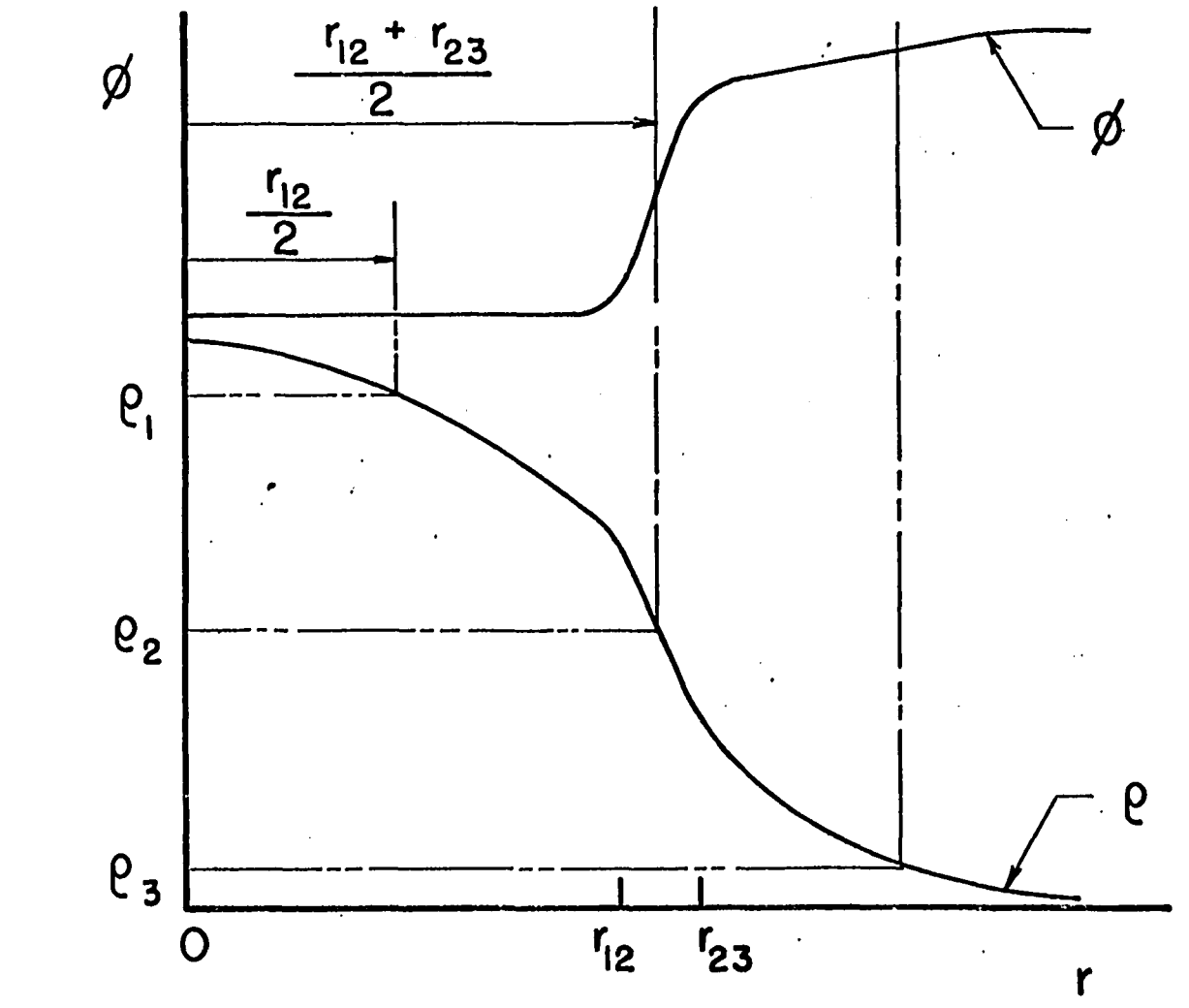

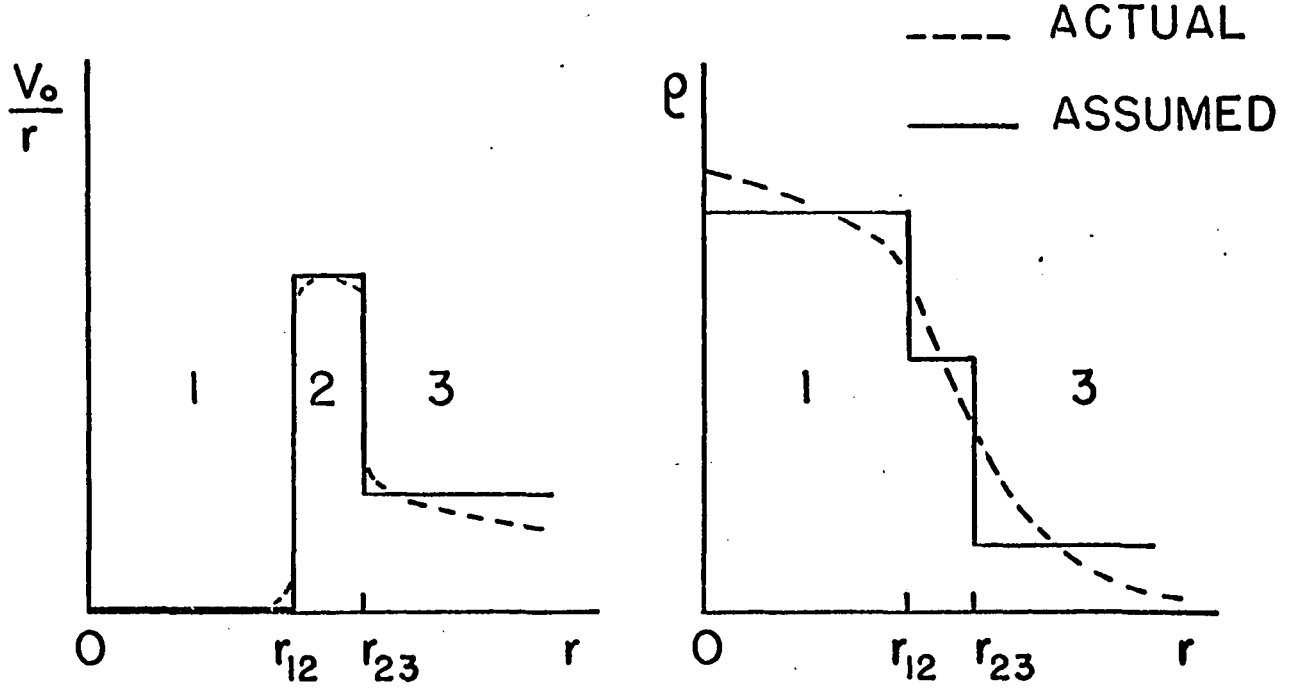

Fig. 5-1 Experimental and assumed profiles

given below Eq. (24). The respective radii are shown in Fig.5-1. The lower sketch in Fig.5-1 shows the measured variation of $\frac{V_o}{r}$ and ρ along with their assumed variations.

5.2 Comparison of the Frequencies

Using the parameters chosen as described above, the real part of the frequency can be calculated from the dispersion relation, Eq. (24), and compared with the measured values. The plot of $f_{meas.}$ vs $f_{calc.}$ (Fig. 5-2) shows good agreement. The error bars indicate the error in measuring the slopes from the potential profiles. In plotting this curve only the dominant mode on a given spectrum was used since the other modes may be subjected to non-linear phenomena such as mode locking[4] which would cause an error in the frequency. It should be noted that the factor δ which multiplies the dominant term for the real part of the frequency (Eq.(24)) represents the relative thickness of the central region.

5.3 Comparison of Mode Amplitude with Linear Growth Rates

The imaginary part of the frequency represents the linear growth rate of an unstable mode. In all cases where a mode has been observed, the calculations have shown the mode to be unstable. The growth rates of modes 3, 4, and 5 are shown in Fig. 5-3 where the calculated points have been joined by straight lines. The broken lines

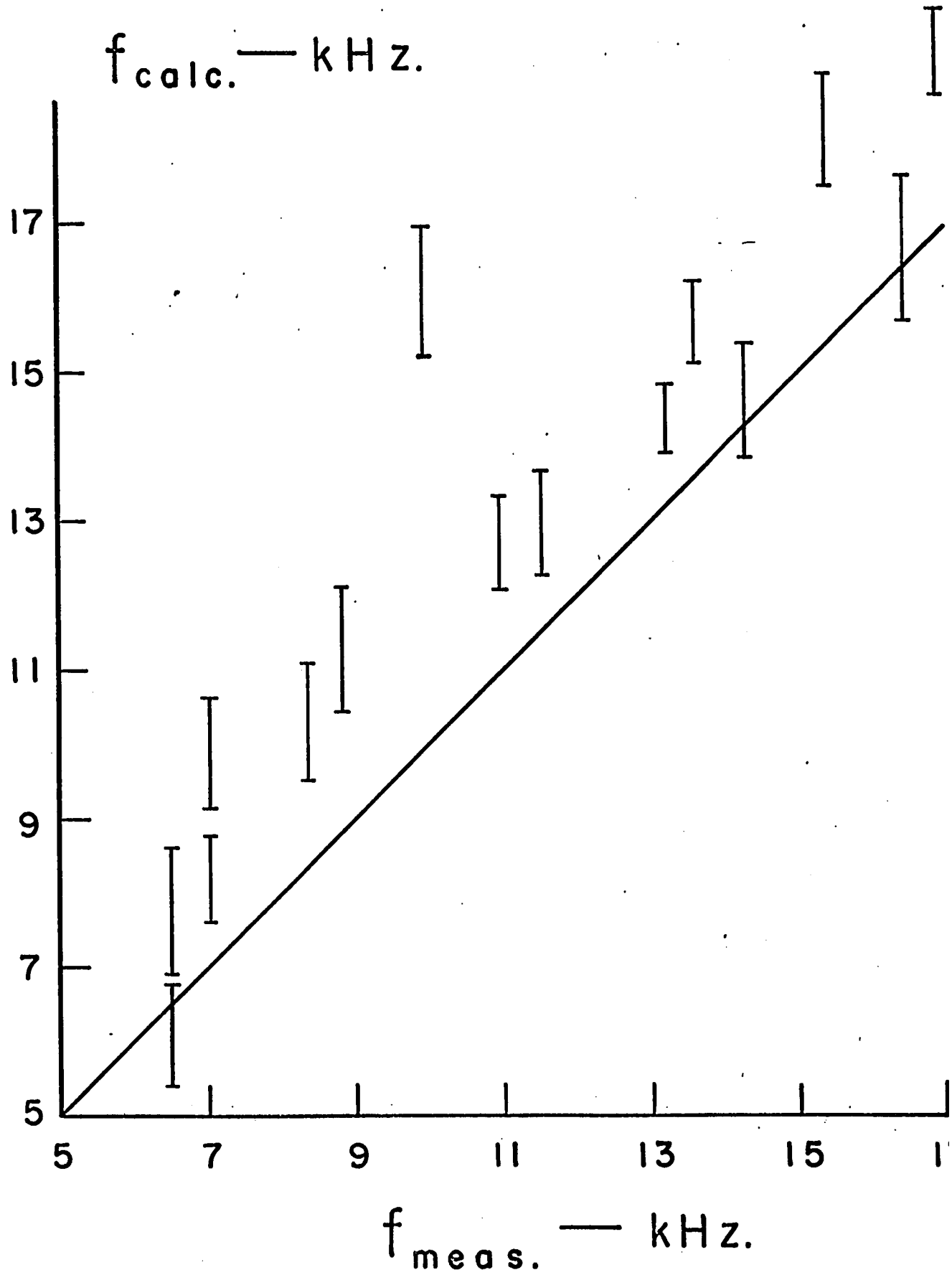

Fig. 5-2 Frequency comparison

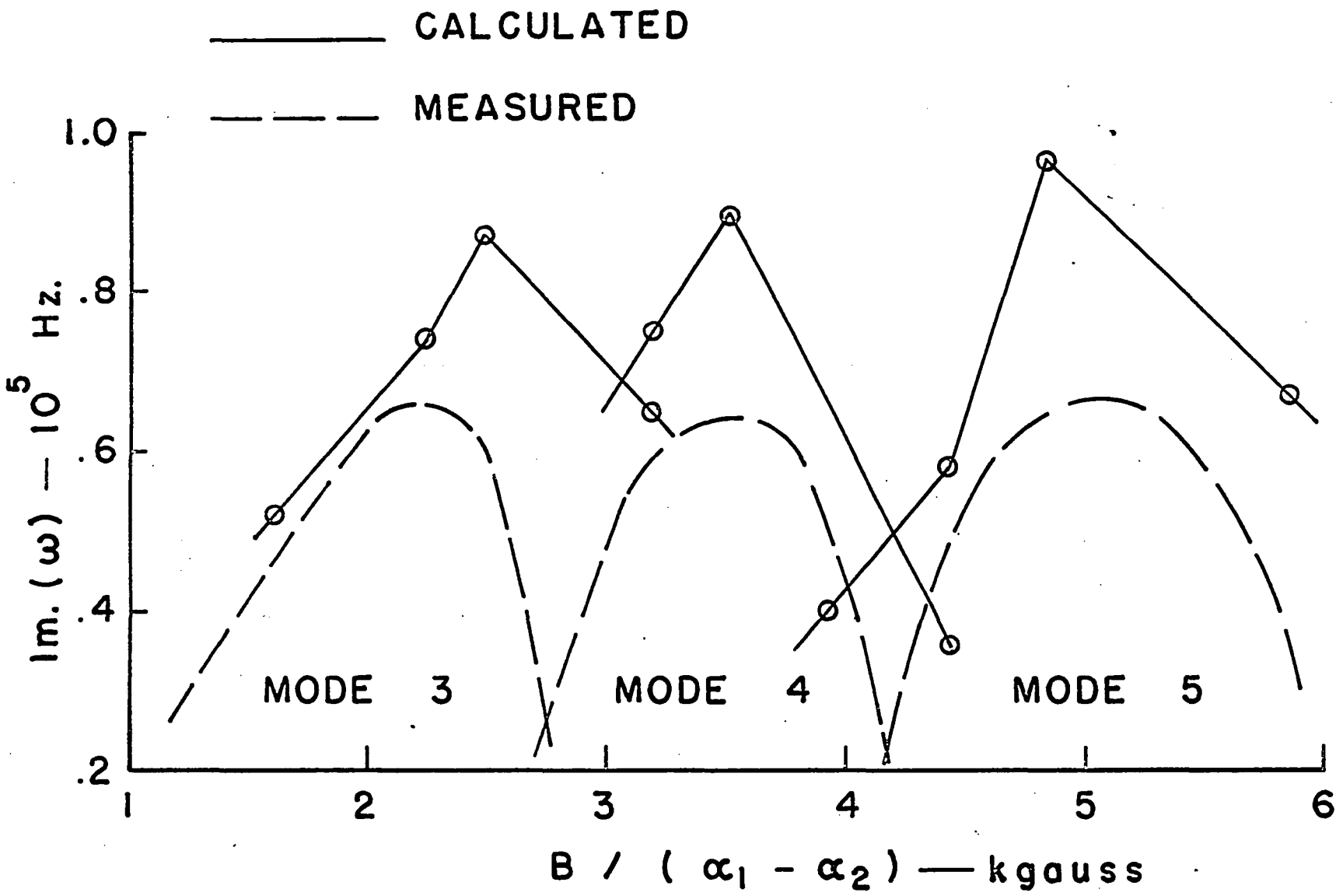

Fig. 5-3 Growth rate comparison with mode amplitude

are experimental values, Fig. 3-8, shown for comparison. Considering that the mode amplitudes are limited by nonlinear phenomena the results are good. The predicted mode transitions correspond well to the observed transitions.

The curves shown in Fig.5-3 are similar to those obtained by Hendel and Politzer,[7] but the two phenomena are different. In Ref.7 a collisional drift wave was observed where the selective mode damping is caused by ion-ion collisions. In the present experiments the density has been such that collisions may be neglected, hence FLR damping becomes important.

5.4 Mode One

It will be remembered that mode one was not observed in the experiments. According to the theory mode one has a smaller growth rate than the higher modes, and even if destabilized it would be difficult to detect. The only possibility of observing mode one is at the origin where the amplitudes of the higher modes is required to vanish, but the amplitude of mode one may be finite. Some evidence for the presence of mode one is presented below where the radial dependence of the eigenfunctions is considered.

5.5 Radial Dependence of the Wave

One further comparison which can be made between theory and experiment is that of the radial dependence of the wave. To do this one compares the eigenfunction

$$\psi = \frac{E_\theta}{\omega + \frac{m}{r} V_o}$$

which is calculated from the experimental data, to the theoretical solution for ψ. Since E_θ is essentially a measure of the wave amplitude, the relative amplitude (Fig. 3-4) calculated from the density fluctuations may be used in its place. A typical case is shown in Fig. 5-4 where the dominant mode observed was mode three. In Fig. 5-4 the points are calculated values and the curves have the proportionality shown. It is obvious from the plotted points that ψ (measured) does not vanish at the origin which is required by the boundary conditions. Neither the error due to placing the probe nor the error due to the finite length of the probe tip are large enough to explain the observed magnitude of ψ at the origin. This discrepancy occurred over the entire range of magnetic field.

The only mode which is not required to have a vanishing amplitude at the origin is mode one. The eigenfunction for mode one should be a constant in region one and should decrease like $1/r^2$ in region three. The eigenfunction predicted for mode three is

$$\psi_1 \sim r^2 , \quad \psi_3 \sim r^{-4}$$

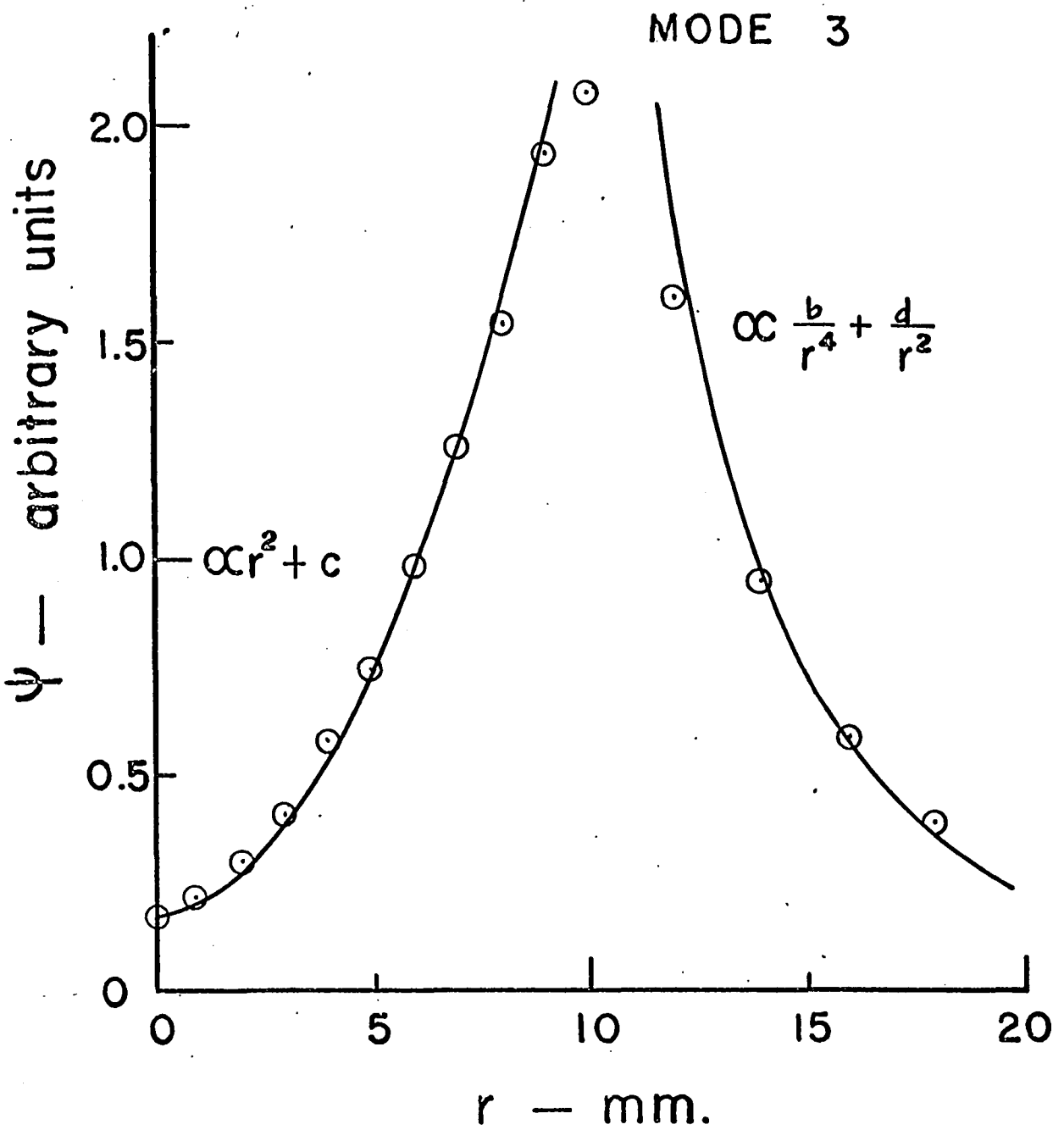

Fig. 5-4 Eigenfunction comparison

If the calculated points are considered to be a sum of contributions of modes one and three (since Eq. (1) is linear the principle of superposition holds) then subtracting out the theoretical contribution of mode one (making ψ for mode three vanish at the origin) shows that the radial dependence of the amplitude is predicted by the theory.

In this chapter the experimental work which has been performed has been compared to the theory of a flute mode in a non-uniform electric field formulated as a differential equation in the literature[1] and solved for a special case in Chapter 4. The assumptions made in solving the differential equation have been shown to approximate the conditions which obtain in a Q-machine where edge oscillations have been observed. The following comparison show agreement with the theory:

1. Frequency of the wave
2. Mode amplitude patterns
3. Radial dependence of the wave amplitude

5.6 Conclusions

The equation of Rosenbluth and Simon[1] describing a flute instability in a non-uniform electric field has been solved for the conditions ρ = constant and $\frac{V_o}{r}$ = constant in adjacent regions. The solutions satisfy easily obtainable boundary conditions at the surfaces where ρ and V_o are discontinuous. The eigenfunctions and their

corresponding eigenvalues, ω, have been found yielding the frequencies and a stability criterion which are readily compared to experiment. The assumptions made to obtain the solution approximately satisfy the experimental conditions found in a Q-machine.

The theory shows the velocity shear and centrifugal force to be destabilizing. FLR effects have been found to stabilize the higher modes which is the same result obtained for the gravitational flute instability.[12] The mode $m = 1$ has no FLR effects due to the degeneracy of Eq. (1) for this case. The radial dependence of the eigenfunctions shows the wave amplitude has a sharp peak at $r = r_s$, the surface of maximum velocity shear.

An instability characterized by a maximum relative amplitude near the maximum velocity shear has been studied in a Q-machine. The experimental data is compared with a three region solution to Eq. (1). Frequencies calculated from the theory are in agreement with those measured experimentally, linear growth rate patterns agree with the measured mode amplitude patterns and the radial dependence of the eigenfunctions compares favorably with measured values.

It should be noted that the theory has been derived from a linearized equation and should not be expected to be valid outside the linear domain. The amplitudes observed in the present work must be limited by non-linear processes since they arise from an overstability and therefore should grow without bound. The linear theory

is strictly valid only in the small time interval when the perturbation amplitude is small. While no rigorous justification exists for the interpretation of non-linear modes with a linear theory it has been recently pointed out[25] that both in experiments with plasmas[7] and ordinary fluids[24] large amplitude observations have been explained by linear theories. The present experiments fall into this category.

APPENDIX A

TWO REGION SOLUTION FOR PLANE GEOMETRY

The solution for plane geometry is found using the method given in Chapter 4 for cylindrical geometry, except now the differential equation is[1,16]

$$(T\psi')' - k^2(T - g\rho')\psi = 0$$

$$\psi = \frac{E_v}{\bar{\omega}} \quad , \qquad \bar{\omega} = \omega + kV_o \tag{A1}$$

$$T = \bar{\omega}(\rho\bar{\omega} + \gamma\rho'), \quad \gamma = \frac{k\, v_{th}^2}{2\,\Omega}$$

Here the zero order electric field acts in the x direction producing a zero order E ×B drift in the y direction. The configuration is shown in Fig. A-1. The upper figure shows the geometry and the lower figure shows the assumed density and velocity profiles. In the two regions where the density and velocity are constant Eq. (A1) becomes

$$\psi'' - k^2\psi = 0 \tag{A2}$$

with the solutions

$$\begin{aligned} \psi_1 &= Ae^{kx} \qquad x \le 0 \\ \psi_2 &= Ae^{-kx} \qquad x \ge 0 \end{aligned} \tag{A3}$$

where the subscripts indicate the region of validity of the respective solutions. The jump condition is found by integrating Eq. (A1) from $-\epsilon$ to $+\epsilon$ and going to the limit as ϵ approaches zero. The jump

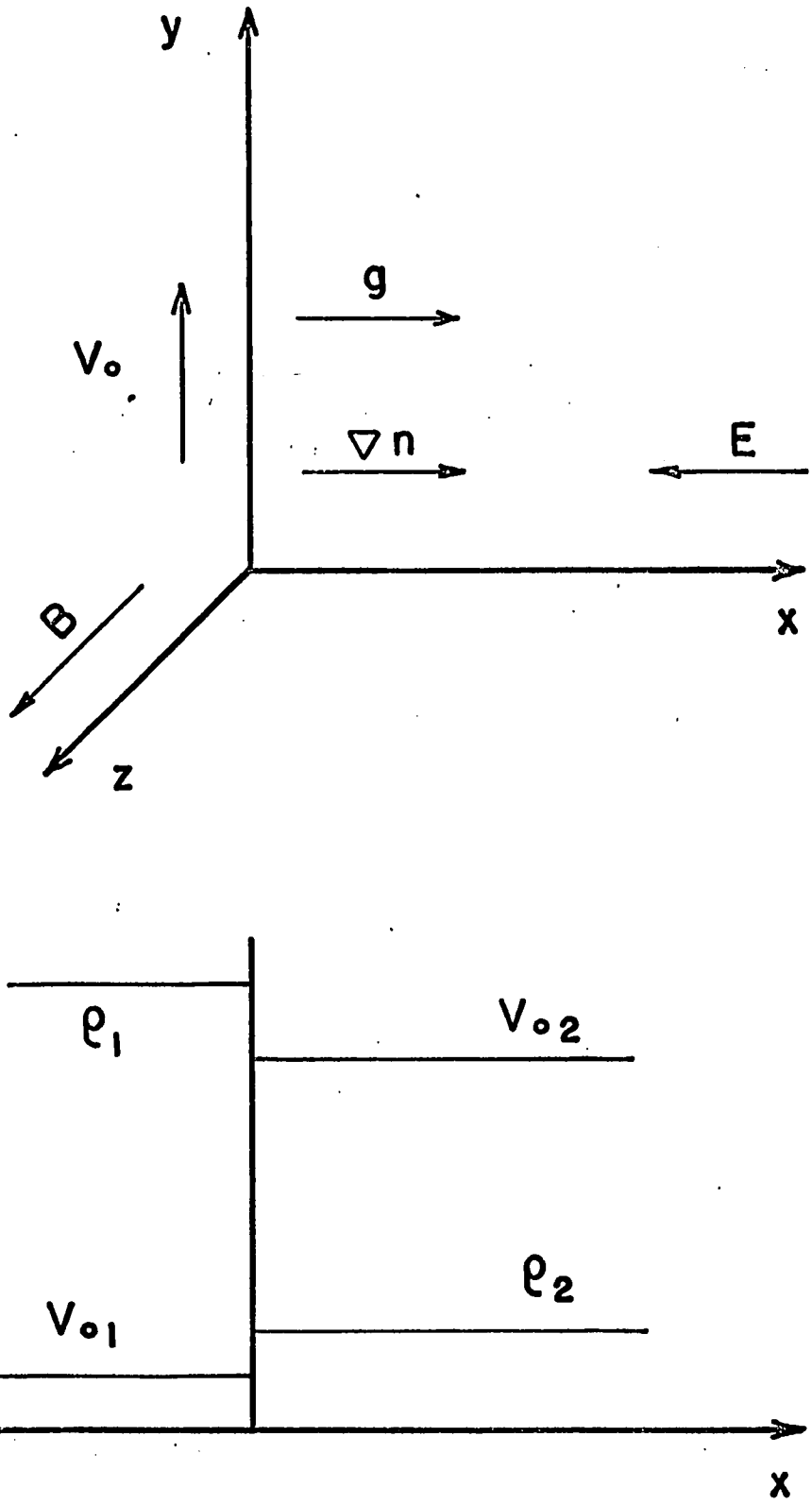

Fig. A1 Plane geometry configuration

condition for this case is

$$\Delta_s (T\psi') + (g - \varpi_s \gamma) k^2 \psi_s \Delta_s \rho = 0 \tag{A4}$$

Using the solutions (Eq. A3) in the jump condition gives the characteristic equation for the frequencies as

$$\begin{aligned} &\omega^2 + 2k\omega\left[(\alpha_2 V_{O_2} + \alpha_1 V_{O_1}) + \frac{\gamma}{2}(\alpha_2 - \alpha_2)\right] \\ &+ k^2\left[(\alpha_2 V_{O_2}^2 + \alpha_1 V_{O_1}^1) + (\alpha_2 - \alpha_1)\left(\frac{\gamma}{2}(V_{O_1} + V_{O_2}) - \frac{g}{k}\right)\right] = 0 \end{aligned} \tag{A5}$$

which can be solved for the frequencies

$$\begin{aligned} \omega = &- k\left[\alpha_1 V_{O_1} + \alpha_2 V_{O_2} + \frac{\gamma}{2}(\alpha_2 - \beta_1)\right] \\ &\pm k\left\{(\alpha_2 - \alpha_1)\left[\gamma V_{O_1}(\alpha_1 - \tfrac{1}{2}) + \gamma V_{O_2}(\alpha_2 - \tfrac{1}{2}) + \frac{g}{k}\right]\right. \\ &\left. - \alpha_1 \alpha_2 (V_{O_1} - V_{O_2})^2\right\}^{\frac{1}{2}} \end{aligned} \tag{A6}$$

The reality of the frequencies yields the stability condition

$$(\alpha_2 - \alpha_1)\left[\gamma V_{O_1}(\alpha_1 - \tfrac{1}{2}) + \gamma V_{O_2}(\alpha_2 - \tfrac{1}{2}) + \frac{g}{k}\right] - \alpha_1\alpha_2 (V_{O_1} - V_{O_2})^2 > 0 \tag{A7}$$

Except for the explicit inclusion of an effective gravitational acceleration, the major difference between Eq. (A7) and Eq. (15) is that no centrifugal effects are found, as expected. The shear in the velocity is again destabilizing and FLR effects are stabilizing. The gravity term will be either stabilizing or destabilizing depending on its direction.

It has been shown[16] that Eq. (A1) reduces to the equation for the Kelvin-Helmholtz instability of an ordinary fluid in the zero

Larmor radius limit. This is tantamount to setting $\gamma = 0$. When γ is formally set equal to zero in the equation for the frequencies, Eq. (A6), the result is

$$\omega = -k\left[\alpha_1 V_{O_1} + \alpha_2 V_{O_2}\right] \pm k\left\{(\alpha_2 - \alpha_1)\frac{g}{k} - \alpha_1\alpha_2 (V_{O_1} - V_{O_2})^2\right\}^{\frac{1}{2}} \qquad \text{(A8)}$$

This is identical with the equation given by Chandrasekhar[24] for the Kelvin-Helmholtz instability of an ordinary fluid.

APPENDIX B

THREE REGION SOLUTION

In the Q-machine there are three well defined regions over which the drift velocity is constant. The two region theory which has been presented in the text of this thesis shows all the essential features of the physical mechanisms which affect the instability, but is inadequate for comparison with the experimental results. The extension of the solution to three regions presents no formal difficulties, but the algebra is more involved.

It is desired to solve Eq. (1) for the case when there are three regions over which the density and zero order drift velocity divided by r are constant. In these regions Eq. (1) again reduces to Eq. (2), but now the solutions in the three regions are given by

$$\begin{aligned} \psi_1 &= Ar^{m-1} \\ \psi_2 &= Br^{m-1} + Cr^{-m-1} \\ \psi_3 &= Dr^{-m-1} \end{aligned} \tag{B1}$$

Instead of the jump condition, Eq. (9), one now has two jump conditions to satisfy at the interfaces between the three regions. Substitution of the above solutions into the two jump conditions for this case and using the continuity of ψ across each of the jump regions yields three equations for the three integration constants

$$2m\,\frac{C}{D}\,\rho_2\,\bar{\omega}_2^{\,2} = (m-1)\rho_2\,\bar{\omega}_2^{\,2} + (m+1)\rho_3\,\bar{\omega}_3^{\,3} - \left[\omega^2 + \frac{2m(1-m^2)}{r_{23}^2}\,\bar{\gamma}\,\bar{\omega}_{23}\right](\rho_3 - \rho_2) \quad \text{(B2)}$$

$$2m\,\frac{C}{A}\,r_{12}^{-2m}\,\rho_2\,\bar{\omega}_2^{\,2} = (m-1)\rho_2\,\bar{\omega}_2^{\,2} - (m-1)\rho_1\,\bar{\omega}_1^{\,2} + \left[\omega^2 + \frac{2m(1-m^2)}{r_{12}^2}\,\bar{\gamma}\,\bar{\omega}_{12}\right](\rho_2 - \rho_1) \quad \text{(B3)}$$

$$\frac{C}{D} = \frac{C}{Ar_{23}^{2m} + C\left(1 - \frac{r_{23}^{2m}}{r_{12}^{2m}}\right)} \quad \text{(B4)}$$

The first two equations come from the jump conditions and the third from the continuity of

$$\begin{aligned} W_o &= 2m\rho_2\,\bar{\omega}_2^{\,2} \\ W_1 &= \text{r.h.s. of Eq. (B2)} \\ W_2 &= \text{r.h.s. of Eq. (B3)} \end{aligned} \quad \text{(B5)}$$

one obtains

$$W_o W_2 = R\,W_o W_1 + (1-R)\,W_1 W_2 \quad \text{(B6)}$$

where

$$R = \left(\frac{r_{23}}{r_{12}}\right)^{2m} \approx 1 \quad \text{(B7)}$$

If $R=1$ the usual two region solution is recovered. The assumption that R is approximately equal to unity has been guided by the experimental results. Using this assumption one may write $R = 1 + \epsilon$ where ϵ is considered small compared with 1. Equation (B6) then becomes

$$W_o W_2 = (1+\epsilon)\,W_o W_1 - \epsilon\,W_1 W_2 \quad \text{(B8)}$$

Since in the experiments V_{o_2} is much larger than $\frac{\omega}{k}$ the following approximations are made:

$$1. \quad \bar{\omega}_2 \approx k V_{O_2}$$

$$2. \quad \frac{\bar{\omega}_{12}}{r_{12}^2} \approx \frac{\bar{\omega}_{23}}{r_{23}^2} \approx \frac{k V_{O_2}}{2 r_{12}^2} \approx \frac{k V_{O_2}}{2 r_{23}^2} \tag{B9}$$

$$3. \quad \bar{\omega}_2^2 >> \omega^2, \quad \bar{\omega}_1^2, \quad \bar{\omega}_3^2$$

Using approximations 1 and 2 the difference $W_2 - W_1$ is found from (B2) and (B3) as

$$W_2 - W_1 = -(m-1)\rho_1 \bar{\omega}_1^2 - (m+1)\rho_3 \bar{\omega}_3^2 + \left[\omega^2 + \frac{m(1-m^2)}{r_{12}^2}\gamma k V_{O_2}\right](\rho_3 - \rho_1) \tag{B10}$$

and using the third approximation one finds

$$\frac{W_2}{W_O} = \frac{(m-1)\rho_2 \bar{\omega}_2^2}{2m\rho_2 \bar{\omega}_2^2} + \ldots \quad \frac{m-1}{2m} \tag{B11}$$

Substituting the last two results into Eq. (B8) the dispersion relation in terms of ϵ is

$$\frac{\epsilon}{2}\left(\frac{m^2-1}{m}\right)\bar{\omega}_2^2 \rho_2 + (m-1)\rho_1 \bar{\omega}_1^2 + (m+1)\rho_3 \bar{\omega}_3^2 - \left[\omega^2 + m(1-m^2)\bar{\gamma}\,\frac{k V_{O_2}}{r_{12}^2}\right](\rho_3 - \rho_1) = 0 \tag{B12}$$

Since ϵ is small one can write

$$-\epsilon = 1 - \left(\frac{r_{23}}{r_{12}}\right)^{2m} = 1 - (1+\delta)^{2m} + \ldots \approx -2m\delta \tag{B13}$$

where δ is the relative thickness of region two and is given by

$$\delta = \frac{r_{23} - r_{12}}{r_{12}} \tag{B14}$$

so that the dispersion relation becomes

$$\delta(m^2-1)\rho_2\overline{\omega}_2^2+(m-1)\rho_1\overline{\omega}_1^2+(m+1)\rho_3\overline{\omega}_3^2 - \left[\omega^2+\frac{m^2(1-m^2)}{r_{12}^3}\overline{\gamma}\,V_{O_2}\right](\rho_3-\rho_1) = 0 \tag{B15}$$

This is the relationship from which the frequencies and growth rates used in the comparison with the experiment have been calculated.

REFERENCES

1 Rosenbluth, M.N. and A. Simon, Phys. Fluids 8, 1300 (1965).

2 D'Angelo, N. and R.W. Motley, Phys. Fluids 6, 422 (1963).

3 Buchelnikova, N.S., Soviet Physics: JETP 19, 755 (1964).

4 Lashinsky, H., Phys. Rev. Lett. 12, 121 (1964).

5 Buchelnikova, N.S., A.M. Kudryavtsev and R.A. Salimov, Soviet Physics: Tech. Phys. 10, 53 (1965).

6 Little, P.F. and P.J. Barrett, Proceedings of Conference on Quiescent Plasmas 1, 173 (Frascati: 1967).

7 Hendel, H.W., B. Coppi, F. Perkins and P. Politzer, Phys. Rev. Lett. 18, 439 (1967).

8 Hartman, C.W. and R.H. Munger, Proceedings of Conference on Quiescent Plasmas 1, 49 (Frascati: 1967).

9 Enriques, L., A.M. Levine and G.B. Righetti, Laboratory Gas Ionizzati Report LGI 68/3 (Frascati: 1968).

10 Hendel, H., American Physical Society Spring Meeting, Washington, D.C., 1967.

11 Kadomtsev, B.B., Review of Plasma Physics 2, (Consultants Bureau: New York, 1966).

12 Rosenbluth, M.N., N. Rostoker and N.A. Krall, Nucl. Fusion, Suppl., Part 1, 143 (1962).

13 Mikhailovskii, A.B., Soviet Physics: JETP 16, 364 (1963).

14 Kadomtsev,B.B., Plasma Turbulence, (Academic Press: London and New York, 1965) p.91 .

15 Schmidt, George, Physics of High Temperature Plasmas (Academic Press: New York and London, 1966).

16 Stringer, T.E. and G. Schmidt, Plasma Physics 9, 53 (1967).

17 Rynn, N. and N. D'Angelo, Rev. Sci. Instr. 31, 1326 (1960).

18 Jones, H.A. and I. Langmuir, General Electric Review 30, 408 (1927).

19 Bennett, W.H., Phys. Rev. 45, 890 (1934).

20 Chen, F.F., in Plasma Diagnostic Techniques, Huddleston,R.H. and S.L. Leonard, editors (Academic Press: New York and London, 1965).

21 Leheny, R.F., Columbia University Plasma Laboratory Report No. 29 (1966).

22 Chen, F.F., Phys. Fluids 8, 912 (1965).

23 Kruskal,M.D. and M. Schwarzchild, Proc. Roy. Soc. A233, 348 (1954).

24 Chandrasekhar, S., Hydrodynamic and Hydromagnetic Stability (Oxford University Press: London, 1961).

25 Hendel, H.W., T.K. Chu, and P.A. Politzer, Princeton Plasma Physics Laboratory Report, Matt. 586, 1968. To be published in Phys. Fluids.

VITA

Gerald I. Kent, born in New York City on December 3, 1941, is married and has no children.

He attended elementary school in the Bronx and received his Diploma from Flushing High School in June, 1958. Mr. Kent came to The City College in September of 1959 with advanced standing from Brooklyn College. While an undergraduate, he was active in both college and community service areas. Mr. Kent was a member of ASCE, Alpha Epsilon Pi Fraternity, Inter-Fraternity Council, The City College Blood Bank and was elected to Chi Epsilon Fraternity and the Lock and Key Society. He received the Bachelor of Civil Engineering degree in January of 1963.

During the summers from 1955 to 1964 Mr. Kent worked on construction projects as a surveyor and assistant supervisor. In the summer of 1965 he worked for Parsons, Brinckerhoff, Quade and Douglas Inc. on dynamic studies of structures for the SFBART system.

After receiving the Bachelor's degree Mr. Kent accepted a Research Assistantship from the City University. He became interested in plasma physics, but continued to work in the Civil Engineering Department where a program in this area was available. He received the Master of Engineering degree in June, 1964 after writing his thesis "Theoretical and Experimental Study of Plasma Currents in High Temperature Rocket Flames." Mr. Kent continued to work towards the Ph.D. degree on a full time basis and completed his dissertation in early 1968.